CONTENTS

LIST OF FIGURES

1. INTRODUCTION

This report presents the details of the governing equations, physical parameterizations, and numerical algorithms defining the version of the NCAR Community Climate Model designated CCM3. The material provides an overview of the major model components, and the way in which they interact as the numerical integration proceeds. Details on the coding implementation, along with in-depth information on running the CCM3 code, are given in a separate technical report entitled "User's Guide to NCAR CCM3" (Acker *et al.*, 1996). As before, it is our objective that this model provide NCAR and the university research community with a reliable, well documented atmospheric general circulation model. This version of the CCM incorporates significant improvements to the physics package, new capabilities such as the incorporation of a slab ocean component, and a number of enhancements to the implementation (e.g., the ability to integrate the model on parallel distributed-memory computational platforms). We believe that collectively these improvements provide the research community with a significantly improved atmospheric modeling capability.

a. Brief History

Over the last decade, the NCAR Climate and Global Dynamics (CGD) Division has provided a comprehensive, three-dimensional global atmospheric model to university and NCAR scientists for use in the analysis and understanding of global climate. Because of its widespread use, the model was designated a community tool and given the name Community Climate Model (CCM). The original versions of the NCAR Community Climate Model, CCM0A (Washington, 1982) and CCM0B (Williamson *et al.,* 1983), were based on the Australian spectral model (Bourke *et al.,* 1977; McAvaney *et al.,* 1978) and an adiabatic, inviscid version of the ECMWF spectral model (Baede *et al.,* 1979). The CCM0B implementation was constructed so that its simulated climate would match the earlier CCM0A model to within natural variability (e.g., incorporated the same set of physical parameterizations and numerical approximations), but also provided a more flexible infrastructure for conducting medium– and long–range global forecast studies. The major strength of this latter effort was that all aspects of the model were described in a series of technical notes, which included a Users' Guide (Sato *et al.,* 1983), a subroutine guide which provided a detailed description of the code (Williamson *et al.,* 1983) a detailed description of the algorithms (Williamson, 1983), and a compilation of the simulated circulation statistics (Williamson and Williamson, 1984). This development activity firmly established NCAR's commitment to provide a versatile, modular, and well–documented atmospheric general circulation model that would be suitable for climate and forecast studies by NCAR and university scientists. A more detailed discussion of the early history and philosophy of the Community Climate Model can be found in Anthes (1986).

The second generation community model, CCM1, was introduced in July of 1987, and included a number of significant changes to the model formulation which were manifested in changes to the simulated climate. Principal changes to the model included major modifications to the parameterization of radiation, a revised vertical finite-differencing technique for the dynamical core, modifications to vertical and horizontal diffusion processes, and modifications to the formulation of surface energy exchange. A number of new modeling capabilities were also introduced, including a seasonal mode in which the specified surface conditions vary with time, and an optional interactive surface hydrology which followed the formulation presented by Manabe (1969). A detailed series of technical documentation was also made available for this version (Williamson *et al.*, 1987; Bath *et al.*, 1987a; Bath *et al.*, 1987b; Williamson and Williamson, 1987; Hack *et al.*, 1989) and more completely describe this version of the CCM.

The most ambitious set of model improvements occurred with the introduction of the third generation of the Community Climate Model, CCM2, which was released in October of 1992. This version was the product of a major effort to improve the physical representation of a wide range of key climate processes, including clouds and radiation, moist convection, the planetary boundary layer, and transport. The introduction of this model also marked a new philosophy with respect to implementation. The CCM2 code was entirely restructured so as to satisfy three major objectives: much greater ease of use, which included portability across a wide range of computational platforms; conformance to a plug-compatible physics interface standard; and the incorporation of single-job multitasking capabilities.

The standard CCM2 model configuration was significantly different from its predecessor in almost every way, starting with resolution where the CCM2 employed a horizontal T42 spectral resolution (approximately 2.8 x 2.8 degree transform grid), with 18 vertical levels and a rigid lid at 2.917 mb. Principal algorithmic approaches shared with CCM1 were the use of a semi-implicit, leap frog time integration scheme; the use of the spectral transform method for treating the dry dynamics; and the use of a bi-harmonic horizontal diffusion operator. Major changes to the dynamical formalism included the use of a terrain-following hybrid vertical coordinate, and the incorporation of a shape-preserving semi-Lagrangian transport scheme (Williamson and Rasch, 1994) for advecting water vapor, as well as an arbitrary number of other scalar fields (e.g., cloud water variables, chemical constituents, etc.). Principal changes to the physics included the use of a δ-Eddington approximation to calculate solar absorption (Briegleb, 1992); the use of a Voigt line shape to more accurately treat infrared radiative cooling in the stratosphere; the inclusion of a diurnal cycle to properly account for the interactions between the radiative effects of the diurnal cycle and the surface fluxes of sensible and latent heat; the incorporation of a finite heat capacity soil/sea ice model; a more sophisticated cloud fraction parameterization and treatment of cloud optical properties (Kiehl *et al.*, , 1994); the incorporation of a sophisticated non-local treatment of boundary-layer processes

(Holtslag and Boville, 1992); the use of a simple mass flux representation of moist convection (Hack, 1994), and the optional incorporation of the Biosphere-Atmosphere Transfer Scheme (BATS) of Dickinson *et al.* (1986). As with previous versions of the model, a User's Guide (Bath *et al.,* 1992) and model description (Hack *et al.*, 1993) were provided to completely document the model formalism and implementation. Control simulation data sets were documented in Williamson (1993).

b. Overview of CCM3

The CCM3 is the fourth generation in the series of NCAR's Community Climate Model. Many aspects of the model formulation and implementation are identical to the CCM2, although there are a number of important changes that have been incorporated into the collection of parameterized physics, along with some modest changes to the dynamical formalism. Modifications to the physical representation of specific climate processes in the CCM3 have been motivated by the need to address the more serious systematic errors apparent in CCM2 simulations, as well as to make the atmospheric model more suitable for coupling to land, ocean, and sea-ice component models. Thus, an important aspect of the changes to the model atmosphere has been that they address well known systematic biases in the top-of-atmosphere and surface (to the extent that they are known) energy budgets. When compared to the CCM2, changes to the model formulation fall into five major categories: modifications to the representation of radiative transfer through both clear and cloudy atmospheric columns, modifications to hydrologic processes (i.e., in the form of changes to the atmospheric boundary layer, moist convection, and surface energy exchange), the incorporation of a sophisticated land surface model, the incorporation of an optional slab mixed-layer ocean/thermodynamic sea-ice component, and a collection of other changes to the formalism which at present do not introduce significant changes to the model climate.

Changes to the clear-sky radiation formalism include the incorporation of minor CO_2 bands trace gases (CH_4, N_2O, $CFC11$, $CFC12$) in the longwave parameterization, and the incorporation of a background aerosol (0.14 optical depth) in the shortwave parameterization. All-sky changes include improvements to the way in which cloud optical properties (effective radius and liquid water path) are diagnosed, the incorporation of the radiative properties of ice clouds, and a number of minor modifications to the diagnosis of convective and layered cloud amount. Collectively these modification substantially reduce systematic biases in the global annually averaged clear-sky and all-sky outgoing longwave radiation and absorbed solar radiation to well within observational uncertainty, while maintaining very good agreement with global observational estimates of cloud forcing. Additionally, the large warm bias in simulated July surface temperature over the Northern Hemisphere, the systematic overprediction of precipitation over warm land areas, and a large component of the stationary-wave error in CCM2, are also reduced as a result of cloud-radiation improvements.

Modifications to hydrologic processes include revisions to the major contributing parameterizations. The formulation of the atmospheric boundary layer parameterization has been revised (in collaboration with Dr. A. A. M. Holtslag of KNMI), resulting in significantly improved estimates of boundary layer height, and a substantial reduction in the overall magnitude of the hydrologic cycle. Parameterized convection has also been modified where this process is now represented using the deep moist convection formalism of Zhang and McFarlane (1995) in conjunction with the scheme developed by Hack (1994) for CCM2. This change results in an additional reduction in the magnitude of the hydrologic cycle and a smoother distribution of tropical precipitation. Surface roughness over oceans is also diagnosed as a function of surface wind speed and stability, resulting in more realistic surface flux estimates for low wind speed conditions. The combination of these changes to hydrological components results in a 13% reduction in the annually averaged global latent heat flux and the associated precipitation rate. It should be pointed out that the improvements in the radiative and hydrologic cycle characteristics of the model climate have been achieved without compromising the quality of the simulated equilibrium thermodynamic structures (one of the major strengths of the CCM2) thanks in part to the incorporation of a Sundqvist (1988) style evaporation of stratiform precipitation.

The CCM3 incorporates version 1 of the Land Surface Model (LSM) developed by Bonan (1996) which provides for the comprehensive treatment of land surface processes. This is a one-dimensional model of energy, momentum, water, and CO_2 exchange between the atmosphere and land, accounting for ecological differences among vegetation types, hydraulic and thermal differences among soil types, and allowing for multiple surface types including lakes and wetlands within a grid cell. LSM replaces the prescribed surface wetness, prescribed snow cover, and prescribed surface albedos in CCM2. It also replaces the land surface fluxes in CCM2, using instead flux parameterizations that include hydrological and ecological processes (e.g., soil water, phenology, stomatal physiology, interception of water by plants).

The fourth class of changes to the CCM2 includes the option to run CCM3 with a simple slab ocean-thermodynamic sea ice model. The model employs a spatially and temporally prescribed ocean heat flux and mixed layer depth, which ensures replication of realistic sea surface temperatures and ice distributions for the present climate. The model allows for the simplest interactive surface for the ocean and sea ice components of the climate system.

The final class of model modifications include a change to the form of the hydrostatic matrix which ensures consistency between ω and the discrete continuity equation, and a more generalized form of the gravity wave drag parameterization. In the latter case, the parameterization is configured to behave in the same way as the CCM2 parameterization of wave drag, but includes the capability to exploit more sophisticated descriptions of this process.

A detailed technical description of the Land Surface Model (Bonan, 1996) complements this technical note. A separate User's Guide (Acker *et al.,* 1996) is also available, which provides details of the code logic, flow, data structures and style, and explains how to modify and run CCM3. One of the more significant implementation differences with the earlier model is that CCM3 includes an optional message-passing configuration, allowing the model to be executed as a parallel task in distributed-memory environments. This is an example of how the Climate and Global Dynamics Division continues to invest in technical improvements to the CCM in the interest of making it easier to acquire and use in evolving computational environments. As was the case for CCM2, the code is internally documented, obviating the need for a separate technical note that describes each subroutine and common block in the model library. Thus, the Users' Guide, the land surface technical note, the present report, the actual code and a planned series of reviewed scientific publications are designed to completely document CCM3.

2. OVERVIEW OF TIME DIFFERENCING

The temporal approximations are designed around a time-splitting formalism. In this section we provide the details of the splitting and relate the various steps to the individual processes described in later sections. When describing time-split algorithms, the notational details often become very complex and cumbersome (e.g., CCM1 in Williamson *et al.*, 1987), even though each process or sub-step in isolation can be described as a straightforward centered, forward or backward process. Therefore, we do not carry the detailed notation forward throughout this report, but rather, describe each process individually with simple, local notation and relate that simple notation to the complete, and therefore complex, notation adopted in this section only.

The general prognostic equations for a generic model variable ψ can be written as

$$\frac{\partial \psi}{\partial t} = P_T\left(\psi\right) + \Gamma\left(\psi\right) + F\left(\psi\right) + P_A\left(\psi\right) \ , \tag{2.a.1}$$

where P_T represents those physical parameterizations applied as tendencies, P_A those parameterizations applied as adjustments, and Γ represents the dynamical components. The term F is an ad hoc correction to ensure conservation of atmospheric mass, water vapor, and chemical constituents if included by the dynamical processes.

We describe a basic time step assuming the unfiltered prognostic variables are known on the Gaussian grid at time $n, (\psi^n)$ and time filtered prognostic variables are known at time $n-1, \left(\overline{\psi}^{n-1}\right)$. The time step is complete after the predicted variables are available at grid points at time $n+1, \left(\psi^{n+1}\right)$, and time filtered values are available at time $n, \left(\overline{\psi}^{n}\right)$.

One complete time step proceeds as

$$\psi^- = \overline{\psi}^{n-1} + 2\Delta t P_T^n\left(\psi^-, \psi^n, \overline{\psi}^{n-1}\right) \tag{2.a.2}$$

$$\begin{cases} \hat{\psi}^+ = \psi^- + 2\Delta t \Gamma\left(\hat{\psi}^+, \psi^n, \psi^-, \overline{\psi}^{n-1}\right) & (2.a.3a) \\ \hat{\psi}^+ = L_{\lambda\varphi\eta}^n\left(\psi^-\right) & (2.a.3b) \end{cases}$$

$$\psi^+ = \hat{\psi}^+ + 2\Delta t F \tag{2.a.4}$$

$$\psi^{n+1} = P_A\left(\psi^+\right) \tag{2.a.5}$$

$$\overline{\psi}^{n} = \psi^n + \alpha\left(\overline{\psi}^{n-1} - 2\psi^n + \psi^{n+1}\right) \ . \tag{2.a.6}$$

The time filter, (2.*a*.6), was originally designed by Robert (1966) and later studied by Asselin (1972). The tendency physics (2.*a*.2) includes (in the following order) the cloud parameterization; radiative fluxes and atmospheric heating rates; update land surface properties; temperature update; surface fluxes; free atmosphere vertical diffusivities, ABL height, diffusivities and countergradient term; vertical diffusion solution; gravity wave drag; and Rayleigh friction. Note that for greater stability $(2.a.2)$ is, in general, implicit with the unknown ψ^- appearing on the right-hand side. To make the solution practical, this step is further subdivided into time split steps for each component as described in Section 4.1. The end result of step $(2.a.2)$ is the net tendency attributable to the tendency physics

$$P_T^n = \frac{\psi^- - \overline{\psi}^{n-1}}{2\Delta t} \,. \tag{2.a.7}$$

The dynamical step $(2.a.3)$ is written in two general forms, with $(2.a.3a)$ for the semi-implicit spectral transform dynamical components and $(2.a.3b)$ for the semi-Lagrangian advection of water vapor (and additional constituents). Because the tendency physics $(2.a.2)$ is formulated in terms of u and v, but the dynamics $(2.a.3a)$ is formulated in terms of vorticity and divergence (ζ and δ), it is convenient to rewrite $(2.a.3a)$ by substituting in $(2.a.2)$:

$$\hat{\psi}^+ = \overline{\psi}^{n-1} + 2\Delta t \Gamma\left(\hat{\psi}^+, \psi^n, \psi^-, \overline{\psi}^{n-1}\right) + 2\Delta t P_T^n\left(\psi^-, \psi^n, \overline{\psi}^{n-1}\right) \,. \tag{2.a.8}$$

One subtle point associated with the dynamics is that, in some minor ways, Γ explicitly depends on $\overline{\psi}^{n-1}$, as indicated in $(2.a.3a)$. In a traditional time-split approach, this dependency would be replaced with an equivalent one on ψ^-, leading to the equation

$$\hat{\psi}^+ = \psi^- + 2\Delta t \Gamma\left(\hat{\psi}^+, \psi^n, \psi^-\right) \,. \tag{2.a.9}$$

Formally, however, the approximation actually used in the model is as given in $(2.a.3a)$, which yields $(2.a.8)$. Equation $(2.a.2)$ is used only to provide the tendencies, not for a provisional forecast value entering in the dynamics.

The dynamics step $(2.a.3a)$, or more properly $(2.a.8)$, is based on a centered semi-implicit, spectral transform method. It includes a transformation from grid to spectral space during the forecast and an inverse transform to grid space of the updated variables. Horizontal diffusion is applied on η surfaces in spectral space and a partial correction to p surfaces (consisting of the leading term only) is applied locally on the return to grid space. The details of this step are presented in Section 3.

The advection of water vapor and constituents is cleanly time split, as indicated in $(2.a.3b)$. In this semi-Lagrangian step, L represents the interpolation operator applied to determine ψ^- at the departure point. The superscript n implies that the winds at time n are used to determine the departure point. Details are provided in Section 3.c.

The fixer step $(2.a.4)$ applies a change to the surface pressure and water vapor (and constituents) such that the global average of dry atmosphere mass, water vapor, and constituents are conserved in the advective process, *i.e.*,

$$\int \pi^+ dA - \int \left(\sum q^+ \Delta\hat{p}^+\right) dA = \int \overline{\pi}^{n-1} dA - \int \left(\sum q^- \Delta\overline{p}^{n-1}\right) dA \qquad (2.a.10)$$

$$\int \left(\sum q^+ \Delta p^+\right) dA = \int \left(\sum q^- \Delta\overline{p}^{n-1}\right) dA \;, \qquad (2.a.11)$$

and

$$\int \left(\sum \psi^+ (1-q^+)\Delta p^+\right) dA = \int \left(\sum \psi^- (1-q^-)\Delta p^-\right) dA \qquad (2.a.12)$$

where π is the surface pressure, q is the specific humidity and ψ is the constituent mixing ratio based on a dry atmosphere. The $\sum$ denotes an approximation to the integral by a vertical sum over the grid values, and the integral $\int (\quad) \, dA$ denotes the discrete horizontal Gaussian quadrature approximation to the integral. Details are given in Section 3.d.

The adjustment physics $(2.a.5)$ consists of a number of adjustment type sub-steps also, each applied in a time-split manner. These sub-steps are mass flux convective parameterization, large scale stable condensation, and dry convective adjustment (at the levels activated). They are detailed in Section 4.2.

Finally, the time filtering $(2.a.6)$ is applied to complete the time step. The form $(2.a.6)$ is applied to u, v, T, q and π (where π is surface pressure). To be consistent with u and v, ζ and δ must also be filtered. To minimize data motion in the code, the filter is applied in two steps to ζ and δ only:

$$\widetilde{\psi}^n = \psi^n + \alpha\left(\overline{\psi}^{n-1} - 2\psi^n\right) , \qquad (2.a.13)$$

$$\overline{\psi}^n = \widetilde{\psi}^n + \alpha\left(\psi^{n+1}\right) \; . \qquad (2.a.14)$$

In the time split steps $(2.a.2)$ through $(2.a.6)$ all prognostic variables are not always affected by an individual sub-step, and thus by implication the "before" and "after" superscript notation denotes the same variable. For example, π (or $\ln \pi$) is not affected by the tendency physics so that π^- and $\overline{\pi}^{n-1}$ can be used interchangeably. Likewise, u, v (and ζ and δ) and T are not affected by the fixers, so $(\hat{\;})^+$ and $(\;)^+$ are interchangeable for them. In addition, u, v (and ζ and δ) and π (or $\ln \pi$) are unaffected by the adjustment physics, so $(\;)^{n+1}$ and $(\;)^+$ are interchangeable for them. By implication then, $(\;)^{n+1}$ and $(\hat{\;})^+$ also become interchangeable for u and v (and ζ and δ). This notational interchangeability should be kept in mind in the discussions in subsequent sections, relating the notations used there to this overview section.

The time step is complete after $(2.a.6)$, at which point the temporal index is decremented and the calculation proceeds back to $(2.a.2)$ for the next time step. In a circular structure such as this, the program code could easily start anywhere, and the temporal index could also be decremented anywhere. In fact, the CCM3 code appears not to start with (2.a.2), but rather to finish up the previous time step by solving (2.a.4), (2.a.5), and (2.a.6) first, at which time the history of state $\left(\overline{\psi}^n\right)$ is recorded if desired. The calculation then proceeds with (2.a.2) and part of (2.a.3a), up to the completion of the spectral transform. At this point the flow of the dynamics is interrupted while the semi-Lagrangian step (2.a.3b) is performed. After this, the dynamics (2.a.3a) is completed by solving the semi-implicit equations, applying the horizontal diffusion and performing the inverse transform. This appears to be the end of the process in the code, and the temporal indices are all shifted down one. However, as mentioned earlier, the time step as described by (2.a.2) through (2.a.6) is actually completed at the beginning of the code.

3. DYNAMICS

a. Hybrid Form of Governing Equations

The hybrid vertical coordinate that has been implemented in CCM3 is described in this section. The hybrid coordinate was developed by Simmons and Strüfing (1981) in order to provide a general framework for a vertical coordinate which is terrain following at the Earth's surface, but reduces to a pressure coordinate at some point above the surface. The hybrid coordinate is more general in concept than the modified σ scheme of Sangster (1960), which is used in the GFDL SKYHI model. However, the hybrid coordinate is normally specified in such a way that the two coordinates are identical.

The following description uses the same general development as Simmons and Strüfing (1981), who based their development on the generalized vertical coordinate of Kasahara (1974). A specific form of the coordinate (the hybrid coordinate) is introduced at the latest possible point. The description here differs from Simmons and Strüfing (1981) in allowing for an upper boundary at finite height (nonzero pressure), as in the original development by Kasahara. Such an upper boundary may be required when the equations are solved using vertical finite differences.

Generalized terrain-following vertical coordinates

Deriving the primitive equations in a generalized terrain-following vertical coordinate requires only that certain basic properties of the coordinate be specified. If the surface pressure is π, then we require the generalized coordinate $\eta(p, \pi)$ to satisfy:

1. $\eta(p, \pi)$ is a monotonic function of p.

2. $\eta(\pi, \pi) = 1$

3. $\eta(0, \pi) = 0$

4. $\eta(p_t, \pi) = \eta_t$ where p_t is the top of the model.

The latter requirement provides that the top of the model will be a pressure surface, simplifying the specification of boundary conditions. In the case that $p_t = 0$, the last two requirements are identical and the system reduces to that described in Simmons and Strüfing (1981). The boundary conditions that are required to close the system are:

$$\dot{\eta}(\pi, \pi) = 0, \tag{3.a.1}$$

$$\dot{\eta}(p_t, \pi) = \omega(p_t) = 0. \tag{3.a.2}$$

Given the above description of the coordinate, the continuous system of equations can be written following Kasahara (1974) and Simmons and Strüfing (1981). The prognostic equations are:

$$\frac{\partial \zeta}{\partial t} = \mathbf{k} \cdot \nabla \times (\mathbf{n}/\cos\phi) + F_{\zeta_H}, \tag{3.a.3}$$

$$\frac{\partial \delta}{\partial t} = \nabla \cdot (\mathbf{n}/\cos\phi) - \nabla^2 (E + \Phi) + F_{\delta_H}, \tag{3.a.4}$$

$$\begin{aligned}\frac{\partial T}{\partial t} &= \frac{-1}{a\cos^2\phi}\left[\frac{\partial}{\partial\lambda}(UT) + \cos\phi\frac{\partial}{\partial\phi}(VT)\right] + T\delta - \dot{\eta}\frac{\partial T}{\partial\eta} + \frac{R}{c_p^*}\mathcal{T}\frac{\omega}{p} \\ &\quad + Q + F_{T_H} + F_{F_H}, \end{aligned} \tag{3.a.5}$$

$$\frac{\partial q}{\partial t} = \frac{-1}{a\cos^2\phi}\left[\frac{\partial}{\partial\lambda}(Uq) + \cos\phi\frac{\partial}{\partial\phi}(Vq)\right] + q\delta - \dot{\eta}\frac{\partial q}{\partial\eta} + S, \tag{3.a.6}$$

$$\frac{\partial \pi}{\partial t} = -\int_1^{\eta_t} \nabla\cdot\left(\frac{\partial p}{\partial\eta}\mathbf{V}\right) d\eta. \tag{3.a.7}$$

The notation follows standard conventions except that the virtual temperature is represented by $\mathcal{T}$ and the following terms have been introduced, with $\mathbf{n} = (n_U, n_V)$:

$$n_U = +(\zeta + f)V - \dot{\eta}\frac{\partial U}{\partial\eta} - R\frac{\mathcal{T}}{p}\frac{1}{a}\frac{\partial p}{\partial\lambda} + F_U, \tag{3.a.8}$$

$$n_V = -(\zeta + f)U - \dot{\eta}\frac{\partial V}{\partial\eta} - R\frac{\mathcal{T}}{p}\frac{\cos\phi}{a}\frac{\partial p}{\partial\phi} + F_V, \tag{3.a.9}$$

$$E = \frac{U^2 + V^2}{2\cos^2\phi}, \tag{3.a.10}$$

$$(U, V) = (u, v)\cos\phi, \tag{3.a.11}$$

$$\mathcal{T} = \left[1 + \left(\frac{R_v}{R} - 1\right)q\right]T, \tag{3.a.12}$$

$$c_p^* = \left[1 + \left(\frac{c_{p_v}}{c_p} - 1\right)q\right]c_p. \tag{3.a.13}$$

The terms F_U, F_V, Q, and S represent the sources and sinks as determined by the tendency physics for momentum (in terms of U and V), temperature, and moisture, respectively. This is discussed in the overview (Section 2) and in detail in Section 4. The terms F_{ζ_H} and F_{δ_H} represent sources due to horizontal diffusion of momentum, while F_{T_H} and F_{F_H} represent sources attributable to horizontal diffusion of temperature and a contribution from frictional heating (see sections on horizontal diffusion and horizontal diffusion correction).

In addition to the prognostic equations, three diagnostic equations are required:

$$\Phi = \Phi_s + R \int_{p(\eta)}^{p(1)} \mathcal{T} d \ln p, \tag{3.a.14}$$

$$\dot{\eta}\frac{\partial p}{\partial \eta} = -\frac{\partial p}{\partial t} - \int_{\eta_t}^{\eta} \nabla \cdot \left(\frac{\partial p}{\partial \eta}\mathbf{V} \right) d\eta, \tag{3.a.15}$$

$$\omega = \mathbf{V} \cdot \nabla p - \int_{\eta_t}^{\eta} \nabla \cdot \left(\frac{\partial p}{\partial \eta}\mathbf{V} \right) d\eta. \tag{3.a.16}$$

Note that the bounds on the vertical integrals are specified as values of η (e.g., η_t, 1) or as functions of p (e.g., p (1), which is the pressure at $\eta = 1$).

Conversion to final form

Equations $(3.a.1) - (3.a.16)$ are the complete set which must be solved by a GCM. However, in order to solve them, the function $\eta(p, \pi)$ must be specified. In advance of actually specifying $\eta(p, \pi)$, the equations will be cast in a more convenient form. Most of the changes to the equations involve simple applications of the chain rule for derivatives, in order to obtain terms that will be easy to evaluate using the predicted variables in the model. For example, terms involving horizontal derivatives of p must be converted to terms involving only $\partial p / \partial \pi$ and horizontal derivatives of π. The former can be evaluated once the function $\eta(p, \pi)$ is specified.

The vertical advection terms in $(3.a.5), (3.a.6), (3.a.8)$, and $(3.a.9)$ may be rewritten as:

$$\dot{\eta}\frac{\partial \psi}{\partial \eta} = \dot{\eta}\frac{\partial p}{\partial \eta}\frac{\partial \psi}{\partial p}, \tag{3.a.17}$$

since $\dot{\eta}\partial p / \partial \eta$ is given by (3.a.15). Similarly, the first term on the right-hand side of (3.a.15) can be expanded as

$$\frac{\partial p}{\partial t} = \frac{\partial p}{\partial \pi}\frac{\partial \pi}{\partial t}, \tag{3.a.18}$$

and $(3.a.7)$ invoked to specify $\partial \pi / \partial t$.

The integrals which appear in $(3.a.7), (3.a.15)$, and $(3.a.16)$ can be written more conveniently by expanding the kernel as

$$\nabla \cdot \left(\frac{\partial p}{\partial \eta}\mathbf{V} \right) = \mathbf{V} \cdot \nabla \left(\frac{\partial p}{\partial \eta} \right) + \frac{\partial p}{\partial \eta} \nabla \cdot \mathbf{V} . \tag{3.a.19}$$

The second term in $(3.a.19)$ is easily treated in vertical integrals, since it reduces to an integral in pressure. The first term is expanded to:

$$\begin{aligned}
\mathbf{V}\cdot\nabla\left(\frac{\partial p}{\partial\eta}\right) &= \mathbf{V}\cdot\frac{\partial}{\partial\eta}\left(\nabla p\right) \\
&= \mathbf{V}\cdot\frac{\partial}{\partial\eta}\left(\frac{\partial p}{\partial\pi}\nabla\pi\right) \\
&= \mathbf{V}\cdot\frac{\partial}{\partial\eta}\left(\frac{\partial p}{\partial\pi}\right)\nabla\pi + \mathbf{V}\cdot\frac{\partial p}{\partial\pi}\nabla\left(\frac{\partial\pi}{\partial\eta}\right) .
\end{aligned} \tag{3.a.20}$$

The second term in $(3.a.20)$ vanishes because $\partial\pi/\partial\eta = 0$, while the first term is easily treated once $\eta(p,\pi)$ is specified. Substituting $(3.a.20)$ into $(3.a.19)$, one obtains:

$$\nabla\cdot\left(\frac{\partial p}{\partial\eta}\mathbf{V}\right) = \frac{\partial}{\partial\eta}\left(\frac{\partial p}{\partial\pi}\right)\mathbf{V}\cdot\nabla\pi + \frac{\partial p}{\partial\eta}\nabla\cdot\mathbf{V} . \tag{3.a.21}$$

Using $(3.a.21)$ as the kernel of the integral in $(3.a.7), (3.a.15)$, and $(3.a.16)$, one obtains integrals of the form

$$\begin{aligned}
\int\nabla\cdot\left(\frac{\partial p}{\partial\eta}\mathbf{V}\right)d\eta &= \int\left[\frac{\partial}{\partial\eta}\left(\frac{\partial p}{\partial\pi}\right)\mathbf{V}\cdot\nabla\pi + \frac{\partial p}{\partial\eta}\nabla\cdot\mathbf{V}\right]d\eta \\
&= \int\mathbf{V}\cdot\nabla\pi d\left(\frac{\partial p}{\partial\pi}\right) + \int\delta dp.
\end{aligned} \tag{3.a.22}$$

The original primitive equations $(3.a.3)-(3.a.7)$, together with $(3.a.8)$, $(3.a.9)$, and $(3.a.14)-(3.a.16)$ can now be rewritten with the aid of $(3.a.17), (3.a.18)$, and $(3.a.22)$.

$$\frac{\partial\zeta}{\partial t} = \mathbf{k}\cdot\nabla\times\left(\mathbf{n}/\cos\phi\right) + F_{\zeta_H} , \tag{3.a.23}$$

$$\frac{\partial\delta}{\partial t} = \nabla\cdot\left(\mathbf{n}/\cos\phi\right) - \nabla^2\left(E+\Phi\right) + F_{\delta_H} , \tag{3.a.24}$$

$$\begin{aligned}
\frac{\partial T}{\partial t} = \frac{-1}{a\cos^2\phi}\left[\frac{\partial}{\partial\lambda}(UT) + \cos\phi\frac{\partial}{\partial\phi}(VT)\right] + T\delta - \dot{\eta}\frac{\partial p}{\partial\eta}\frac{\partial T}{\partial p} + \frac{R}{c_p^*}T\frac{\omega}{p} \\
+ Q + F_{T_H} + F_{F_H}
\end{aligned} \tag{3.a.25}$$

$$\frac{\partial q}{\partial t} = \frac{-1}{a\cos^2\phi}\left[\frac{\partial}{\partial\lambda}(Uq) + \cos\phi\frac{\partial}{\partial\phi}(Vq)\right] + q\delta - \dot{\eta}\frac{\partial p}{\partial\eta}\frac{\partial q}{\partial p} + S, \tag{3.a.26}$$

$$\frac{\partial \pi}{\partial t} = - \int_{(\eta_t)}^{(1)} \mathbf{V} \cdot \nabla \pi d \left(\frac{\partial p}{\partial \pi} \right) - \int_{p(\eta_t)}^{p(1)} \delta dp, \tag{3.a.27}$$

$$n_U = +(\zeta + f)V - \dot{\eta} \frac{\partial p}{\partial \eta} \frac{\partial U}{\partial p} - R \frac{\mathcal{T}}{a} \frac{1}{p} \frac{\partial p}{\partial \pi} \frac{\partial \pi}{\partial \lambda} + F_U, \tag{3.a.28}$$

$$n_V = -(\zeta + f)U - \dot{\eta} \frac{\partial p}{\partial \eta} \frac{\partial V}{\partial p} - R \frac{\mathcal{T} \cos \phi}{a} \frac{1}{p} \frac{\partial p}{\partial \pi} \frac{\partial \pi}{\partial \phi} + F_V, \tag{3.a.29}$$

$$\Phi = \Phi_s + R \int_{p(\eta)}^{p(1)} \mathcal{T} d \ln p, \tag{3.a.30}$$

$$\begin{aligned} \dot{\eta} \frac{\partial p}{\partial \eta} = \frac{\partial p}{\partial \pi} & \left[\int_{(\eta_t)}^{(1)} \mathbf{V} \cdot \nabla \pi d \left(\frac{\partial p}{\partial \pi} \right) + \int_{p(\eta_t)}^{p(1)} \delta dp \right] \\ & - \int_{(\eta_t)}^{(\eta)} \mathbf{V} \cdot \nabla \pi d \left(\frac{\partial p}{\partial \pi} \right) - \int_{p(\eta_t)}^{p(\eta)} \delta dp, \end{aligned} \tag{3.a.31}$$

$$\omega = \frac{\partial p}{\partial \pi} \mathbf{V} \cdot \nabla \pi - \int_{(\eta_t)}^{(\eta)} \mathbf{V} \cdot \nabla \pi d \left(\frac{\partial p}{\partial \pi} \right) - \int_{p(\eta_t)}^{p(\eta)} \delta dp. \tag{3.a.32}$$

Once $\eta(p, \pi)$ is specified, then $\partial p / \partial \pi$ can be determined and $(3.a.23) - (3.a.32)$ can be solved in a GCM.

In the actual definition of the hybrid coordinate, it is not necessary to specify $\eta(p, \pi)$ explicitly, since $(3.a.23) - (3.a.32)$ only requires that p and $\partial p / \partial \pi$ be determined. It is sufficient to specify $p(\eta, \pi)$ and to let η be defined implicitly. This will be done in a later section. In the case that $p(\eta, \pi) = \sigma \pi$ and $\eta_t = 0$, $(3.a.23) - (3.a.32)$ can be reduced to the set of equations solved by CCM1.

Continuous equations using $\partial \ln(\pi) / \partial t$

In practice, the solutions generated by solving the above equations are excessively noisy. This problem appears to arise from aliasing problems in the hydrostatic equation $(3.a.30)$. The $\ln p$ integral introduces a high order nonlinearity which enters directly into the divergence equation $(3.a.24)$. Large gravity waves are generated in the vicinity of steep orography, such as in the Pacific Ocean west of the Andes.

The equations given above, using π as a prognostic variable, may be easily converted to equations using $\Pi = \ln(\pi)$, resulting in the hydrostatic equation becoming only quadratically nonlinear except for moisture contributions to virtual temperature. Since the spectral transform method will be used to solve the equations, gradients will be obtained during the transform from wave to grid space. Outside of the prognostic equation for Π, all terms involving $\nabla\pi$ will then appear as $\pi\nabla\Pi$.

Equations (3.a.23) – (3.a.32) become:

$$\frac{\partial\zeta}{\partial t} = \mathbf{k}\cdot\nabla\times(\mathbf{n}/\cos\phi) + F_{\zeta_H}, \tag{3.a.33}$$

$$\frac{\partial\delta}{\partial t} = \nabla\cdot(\mathbf{n}/\cos\phi) - \nabla^2\left(E+\Phi\right) + F_{\delta_H}, \tag{3.a.34}$$

$$\begin{aligned}\frac{\partial T}{\partial t} &= \frac{-1}{a\cos^2\phi}\left[\frac{\partial}{\partial\lambda}(UT) + \cos\phi\frac{\partial}{\partial\phi}(VT)\right] + T\delta - \dot{\eta}\frac{\partial p}{\partial\eta}\frac{\partial T}{\partial p} + \frac{R}{c_p^*}\mathcal{T}\frac{\omega}{p}\\ &\quad + Q + F_{T_H} + F_{F_H},\end{aligned} \tag{3.a.35}$$

$$\frac{\partial q}{\partial t} = \frac{-1}{a\cos^2\phi}\left[\frac{\partial}{\partial\lambda}(Uq) + \cos\phi\frac{\partial}{\partial\phi}(Vq)\right] + q\delta - \dot{\eta}\frac{\partial p}{\partial\eta}\frac{\partial q}{\partial p} + S, \tag{3.a.36}$$

$$\frac{\partial\Pi}{\partial t} = -\int_{(\eta_t)}^{(1)}\mathbf{V}\cdot\nabla\Pi d\left(\frac{\partial p}{\partial\pi}\right) - \frac{1}{\pi}\int_{p(\eta_t)}^{p(1)}\delta dp, \tag{3.a.37}$$

$$n_U = +(\zeta+f)V - \dot{\eta}\frac{\partial p}{\partial\eta}\frac{\partial U}{\partial p} - R\frac{\mathcal{T}}{a}\frac{\pi}{p}\frac{\partial p}{\partial\pi}\frac{\partial\Pi}{\partial\lambda} + F_U, \tag{3.a.38}$$

$$n_V = -(\zeta+f)U - \dot{\eta}\frac{\partial p}{\partial\eta}\frac{\partial V}{\partial p} - R\frac{\mathcal{T}\cos\phi}{a}\frac{\pi}{p}\frac{\partial p}{\partial\pi}\frac{\partial\Pi}{\partial\phi} + F_V, \tag{3.a.39}$$

$$\Phi = \Phi_s + R\int_{p(\eta)}^{p(1)}\mathcal{T}d\ln p, \tag{3.a.40}$$

$$\begin{aligned}\dot{\eta}\frac{\partial p}{\partial\eta} &= \frac{\partial p}{\partial\pi}\left[\int_{(\eta_t)}^{(1)}\pi\mathbf{V}\cdot\nabla\Pi d\left(\frac{\partial p}{\partial\pi}\right) + \int_{p(\eta_t)}^{p(1)}\delta dp\right]\\ &\quad - \int_{(\eta_t)}^{(\eta)}\pi\mathbf{V}\cdot\nabla\Pi d\left(\frac{\partial p}{\partial\pi}\right) - \int_{p(\eta_t)}^{p(\eta)}\delta dp,\end{aligned} \tag{3.a.41}$$

$$\omega = \frac{\partial p}{\partial\pi}\pi\mathbf{V}\cdot\nabla\Pi - \int_{(\eta_t)}^{(\eta)}\pi\mathbf{V}\cdot\nabla\Pi d\left(\frac{\partial p}{\partial\pi}\right) - \int_{p(\eta_t)}^{p(\eta)}\delta dp. \tag{3.a.42}$$

The above equations reduce to the standard σ equations used in CCM1 if $\eta = \sigma$ and $\eta_t = 0$. (Note that in this case $\partial p/\partial\pi = p/\pi = \sigma$.)

Semi-implicit formulation

The model described by (3.a.33) – (3.a.42), without the horizontal diffusion terms, together with boundary conditions (3.a.1) and (3.a.2), is integrated in time using the semi-implicit leapfrog scheme described below. The semi-implicit form of the time differencing will be applied to (3.a.34) and (3.a.35) without the horizontal diffusion sources, and to (3.a.37). In order to derive the semi-implicit form, one must linearize these equations about a reference state. Isolating the terms that will have their linear parts treated implicitly, the prognostic equations (3.a.33), (3.a.34), and (3.a.37) may be rewritten as:

$$\frac{\partial \delta}{\partial t} = -R\mathcal{T}\nabla^2 \ln p - \nabla^2\Phi + X_1, \tag{3.a.43}$$

$$\frac{\partial T}{\partial t} = +\frac{R}{c_p^*}\mathcal{T}\frac{\omega}{p} - \dot{\eta}\frac{\partial p}{\partial \eta}\frac{\partial T}{\partial p} + Y_1, \tag{3.a.44}$$

$$\frac{\partial \Pi}{\partial t} = -\frac{1}{\pi}\int_{p(\eta_t)}^{p(1)} \delta dp + Z_1, \tag{3.a.45}$$

where X_1, Y_1, Z_1 are the remaining nonlinear terms not explicitly written in (3.a.43) – (3.a.45). The terms involving Φ and ω may be expanded into vertical integrals using (3.a.40) and (3.a.42), while the $\nabla^2 \ln p$ term can be converted to $\nabla^2\Pi$, giving:

$$\frac{\partial \delta}{\partial t} = -RT\frac{\pi}{p}\frac{\partial p}{\partial \pi}\nabla^2\Pi - R\nabla^2\int_{p(\eta)}^{p(1)} T d\ln p \; + X_2, \tag{3.a.46}$$

$$\frac{\partial T}{\partial t} = -\frac{R}{c_p}\frac{T}{p}\int_{p(\eta_t)}^{p(\eta)} \delta dp - \left[\frac{\partial p}{\partial \pi}\int_{p(\eta_t)}^{p(1)} \delta dp - \int_{p(\eta_t)}^{p(\eta)} \delta dp\right]\frac{\partial T}{\partial p} + Y_2, \tag{3.a.47}$$

$$\frac{\partial \Pi}{\partial t} = -\frac{1}{\pi}\int_{p(\eta_t)}^{p(1)} \delta dp + Z_2. \tag{3.a.48}$$

Once again, only terms that will be linearized have been explicitly represented in (3.a.46) – (3.a.48), and the remaining terms are included in X_2, Y_2, and Z_2. Anticipating the linearization, $\mathcal{T}$ and c_p^* have been replaced by T and c_p in (3.a.46) and (3.a.47). Furthermore, the virtual temperature corrections are included with the other nonlinear terms.

In order to linearize (3.a.46) – (3.a.48), one specifies a reference state for temperature and pressure, then expands the equations about the reference state:

$$T = T^r + T', \tag{3.a.49}$$

$$\pi = \pi^r + \pi', \tag{3.a.50}$$

$$p = p^r(\eta, \pi^r) + p'. \tag{3.a.51}$$

In the special case that $p(\eta, \pi) = \sigma\pi$, (3.a.46) – (3.a.48) can be converted into equations involving only $\Pi = \ln \pi$ instead of p, and (3.a.50) and (3.a.51) are not required. This is a major difference between the hybrid coordinate scheme being developed here and the σ coordinate scheme in CCM1.

Expanding (3.a.46) – (3.a.48) about the reference state (3.a.49) – (3.a.51) and retaining only the linear terms explicitly, one obtains:

$$\frac{\partial \delta}{\partial t} = -R\nabla^2 \left[T^r \frac{\pi^r}{p^r} \left(\frac{\partial p}{\partial \pi} \right)^r \Pi + \int_{p^r(\eta)}^{p^r(1)} T' d \ln p^r + \int_{p'(\eta)}^{p'(1)} \frac{T^r}{p^r} dp' \right] + X_3, \qquad (3.a.52)$$

$$\frac{\partial T}{\partial t} = -\frac{R}{c_p} \frac{T^r}{p^r} \int_{p^r(\eta_t)}^{p^r(\eta)} \delta dp^r - \left[\left(\frac{\partial p}{\partial \pi} \right)^r \int_{p^r(\eta_t)}^{p^r(1)} \delta dp^r - \int_{p^r(\eta_t)}^{p^r(\eta)} \delta dp^r \right] \frac{\partial T^r}{\partial p^r} + Y_3, (3.a.53)$$

$$\frac{\partial \Pi}{\partial t} = -\frac{1}{\pi^r} \int_{p^r(\eta_t)}^{p^r(1)} \delta dp^r + Z_3. \qquad (3.a.54)$$

The semi-implicit time differencing scheme treats the linear terms in (3.a.52) – (3.a.54) by averaging in time. The last integral in (3.a.52) is reduced to purely linear form by the relation

$$dp' = \pi' d \left(\frac{\partial p}{\partial \pi} \right)^r + x\,. \qquad (3.a.55)$$

In the hybrid coordinate described below, p is a linear function of π, so x above is zero.

We will assume that centered differences are to be used for the nonlinear terms, and the linear terms are to be treated implicitly by averaging the previous and next time steps. Finite differences are used in the vertical, and are described in the following sections. At this stage only some very general properties of the finite difference representation must be specified. A layering structure is assumed in which field values are predicted on K layer midpoints denoted by an integer index, η_k (see Figure 1). The interface between η_k and η_{k+1} is denoted by a half-integer index, $\eta_{k+1/2}$. The model top is at $\eta_{1/2} = \eta_t$, and the Earth's surface is at $\eta_{K+1/2} = 1$. It is further assumed that vertical integrals may be written as a matrix (of order K) times a column vector representing the values of a field at the η_k grid points in the vertical. The column vectors representing a vertical column of grid points will be denoted by underbars, the matrices will be denoted by bold-faced capital letters, and superscript T will denote the vector transpose.

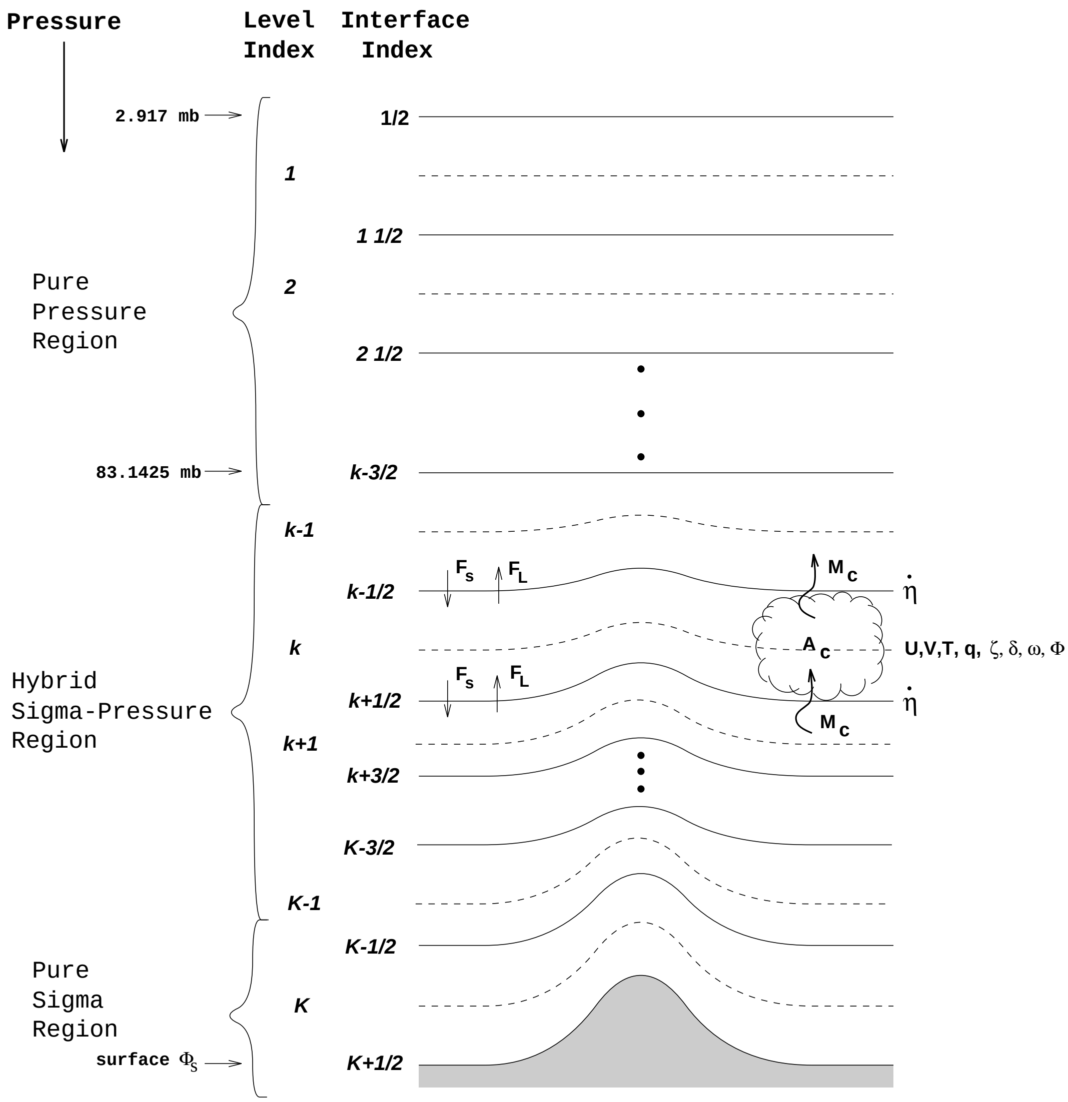

Figure 1. Vertical level structure of CCM

The finite difference forms of $(3.a.52) - (3.a.54)$ may then be written down as:

$$
\begin{aligned}
\underline{\delta}^{n+1} &= \underline{\delta}^{n-1} + 2\Delta t \underline{X}^n \\
&- 2\Delta t R \underline{b}^r \nabla^2 \left(\frac{\Pi^{n-1} + \Pi^{n+1}}{2} - \Pi^n \right) \\
&- 2\Delta t R \mathbf{H}^r \nabla^2 \left(\frac{(\underline{T}')^{n-1} + (\underline{T}')^{n+1}}{2} - (\underline{T}')^n \right) \\
&- 2\Delta t R \underline{h}^r \nabla^2 \left(\frac{\Pi^{n-1} + \Pi^{n+1}}{2} - \Pi^n \right), \qquad (3.a.56)
\end{aligned}
$$

$$\underline{T}^{n+1} = \underline{T}^{n-1} + 2\Delta t \underline{Y}^n - 2\Delta t \mathbf{D}^r \left(\frac{\underline{\delta}^{n-1} + \underline{\delta}^{n+1}}{2} - \underline{\delta}^n \right), \tag{3.a.57}$$

$$\Pi^{n+1} = \Pi^{n-1} + 2\Delta t Z^n - 2\Delta t \left(\frac{\underline{\delta}^{n-1} + \underline{\delta}^{n+1}}{2} - \underline{\delta}^n \right)^T \frac{1}{\Pi^r} \underline{\Delta p}^r, \tag{3.a.58}$$

where $()^n$ denotes a time varying value at time step n. The quantities $\underline{X}^n, \underline{Y}^n$, and Z^n are defined so as to complete the right-hand sides of $(3.a.43) - (3.a.45)$. The components of $\underline{\Delta p}^r$ are given by $\Delta p_k^r = p_{k+\frac{1}{2}}^r - p_{k-\frac{1}{2}}^r$. This definition of the vertical difference operator Δ will be used in subsequent equations. The reference matrices $\mathbf{H}^r$ and $\mathbf{D}^r$, and the reference column vectors $\underline{b}^r$ and $\underline{h}^r$, depend on the precise specification of the vertical coordinate and will be defined later.

Energy conservation

We shall impose a requirement on the vertical finite differences of the model that they conserve the global integral of total energy *in the absence of sources and sinks.* We need to derive equations for kinetic and internal energy in order to impose this constraint. The momentum equations (more painfully, the vorticity and divergence equations) without the F_U, F_V, F_{ζ_H} and F_{δ_H} contributions, can be combined with the continuity equation

$$\frac{\partial}{\partial t}\left(\frac{\partial p}{\partial \eta}\right) + \nabla \cdot \left(\frac{\partial p}{\partial \eta}\mathbf{V}\right) + \frac{\partial}{\partial \eta}\left(\frac{\partial p}{\partial \eta}\dot{\eta}\right) = 0 \tag{3.a.59}$$

to give an equation for the rate of change of kinetic energy:

$$\frac{\partial}{\partial t}\left(\frac{\partial p}{\partial \eta}E\right) = -\nabla \cdot \left(\frac{\partial p}{\partial \eta}E\mathbf{V}\right) - \frac{\partial}{\partial \eta}\left(\frac{\partial p}{\partial \eta}E\dot{\eta}\right) - \frac{R\mathcal{T}}{p}\frac{\partial p}{\partial \eta}\mathbf{V}\cdot\nabla p - \frac{\partial p}{\partial \eta}\mathbf{V}\cdot\nabla\Phi\,. \tag{3.a.60}$$

The first two terms on the right-hand side of $(3.a.60)$ are transport terms. The horizontal integral of the first (horizontal) transport term should be zero, and it is relatively straightforward to construct horizontal finite difference schemes that ensure this. For spectral models, the integral of the horizontal transport term will not vanish in general, but we shall ignore this problem.

The vertical integral of the second (vertical) transport term on the right-hand side of $(3.a.60)$ should vanish. Since this term is obtained from the vertical advection terms for momentum, which will be finite differenced, we can construct a finite difference operator that will ensure that the vertical integral vanishes.

The vertical advection terms are the product of a vertical velocity $(\dot{\eta}\partial p/\partial\eta)$ and the vertical derivative of a field $(\partial\psi/\partial p)$. The vertical velocity is defined in terms of vertical integrals of fields (3.a.41), which are naturally taken to interfaces. The vertical derivatives are also naturally taken to interfaces, so the product is formed there, and then adjacent interface values of the products are averaged to give a midpoint value. It is the definition of the average that must be correct in order to conserve kinetic energy under vertical advection in (3.a.60). The derivation will be omitted here, the resulting vertical advection terms are of the form:

$$\left(\dot{\eta}\frac{\partial p}{\partial\eta}\frac{\partial\psi}{\partial p}\right)_k = \frac{1}{2\Delta p_k}\left[\left(\dot{\eta}\frac{\partial p}{\partial\eta}\right)_{k+1/2}(\psi_{k+1}-\psi_k) + \left(\dot{\eta}\frac{\partial p}{\partial\eta}\right)_{k-1/2}(\psi_k-\psi_{k-1})\right], \quad (3.a.61)$$

$$\Delta p_k = p_{k+1/2} - p_{k-1/2}. \quad (3.a.62)$$

The choice of definitions for the vertical velocity at interfaces is not crucial to the energy conservation (although not completely arbitrary), and we shall defer its definition until later. The vertical advection of temperature is not required to use (3.a.61) in order to conserve mass or energy. Other constraints can be imposed that result in different forms for temperature advection, but we will simply use (3.a.61) in the system described below.

The last two terms in (3.a.60) contain the conversion between kinetic and internal (potential) energy and the form drag. Neglecting the transport terms, under assumption that global integrals will be taken, noting that $\nabla p = \frac{\pi}{p}\frac{\partial p}{\partial\pi}\nabla\Pi$, and substituting for the geopotential using (3.a.40), (3.a.60) can be written as:

$$\frac{\partial}{\partial t}\left(\frac{\partial p}{\partial\eta}E\right) = -R\mathcal{T}\frac{\partial p}{\partial\eta}\mathbf{V}\cdot\left(\frac{\pi}{p}\frac{\partial p}{\partial\pi}\nabla\Pi\right)$$
$$-\frac{\partial p}{\partial\eta}\mathbf{V}\cdot\nabla\Phi_s - \frac{\partial p}{\partial\eta}\mathbf{V}\cdot\nabla\int_{p(\eta)}^{p(1)} R\mathcal{T}\,d\ln p + \ldots \quad (3.a.63)$$

The second term on the right-hand side of (3.a.63) is a source (form drag) term that can be neglected as we are only interested in internal conservation properties. The last term on the right-hand side of (3.a.63) can be rewritten as

$$\frac{\partial p}{\partial\eta}\mathbf{V}\cdot\nabla\int_{p(\eta)}^{p(1)} R\mathcal{T}\,d\ln p = \nabla\cdot\left\{\frac{\partial p}{\partial\eta}\mathbf{V}\int_{p(\eta)}^{p(1)} R\mathcal{T}\,d\ln p\right\}$$

$$-\nabla\cdot\left(\frac{\partial p}{\partial\eta}\mathbf{V}\right)\int_{p(\eta)}^{p(1)}R\mathcal{T}d\ln p\,. \qquad (3.a.64)$$

The global integral of the first term on the right-hand side of (3.a.64) is obviously zero, so that (3.a.63) can now be written as:

$$\frac{\partial}{\partial t}\left(\frac{\partial p}{\partial\eta}E\right)=-R\mathcal{T}\frac{\partial p}{\partial\eta}\mathbf{V}\cdot\left(\frac{\pi}{p}\frac{\partial p}{\partial\pi}\nabla\Pi\right)$$
$$+\nabla\cdot\left(\frac{\partial p}{\partial\eta}\mathbf{V}\right)\int_{p(\eta)}^{p(1)}R\mathcal{T}d\ln p+... \qquad (3.a.65)$$

We now turn to the internal energy equation, obtained by combining the thermodynamic equation (3.a.35), without the Q, F_{T_H}, and F_{F_H} terms, and the continuity equation (3.a.59):

$$\frac{\partial}{\partial t}\left(\frac{\partial p}{\partial\eta}c_p^*T\right)=-\nabla\cdot\left(\frac{\partial p}{\partial\eta}c_p^*T\mathbf{V}\right)-\frac{\partial}{\partial\eta}\left(\frac{\partial p}{\partial\eta}c_p^*T\dot{\eta}\right)$$
$$+R\mathcal{T}\frac{\partial p}{\partial\eta}\frac{\omega}{p}\,. \qquad (3.a.66)$$

As in (3.a.60), the first two terms on the right-hand side are advection terms that can be neglected under global integrals. Using (3.a.16), (3.a.66) can be written as:

$$\frac{\partial}{\partial t}\left(\frac{\partial p}{\partial\eta}c_p^*T\right)=R\mathcal{T}\frac{\partial p}{\partial\eta}\mathbf{V}\cdot\left(\frac{\pi}{p}\frac{\partial p}{\partial\pi}\nabla\Pi\right)$$
$$-R\mathcal{T}\frac{\partial p}{\partial\eta}\frac{1}{p}\int_{\eta_t}^{\eta}\nabla\cdot\left(\frac{\partial p}{\partial\eta}\mathbf{V}\right)d\eta+... \qquad (3.a.67)$$

The rate of change of total energy due to internal processes is obtained by adding (3.a.65) and (3.a.67) and must vanish. The first terms on the right-hand side of (3.a.65) and (3.a.67) obviously cancel in the continuous form. When the equations are discretized in the vertical, the terms will still cancel, providing that the same definition is used for $(1/p\ \partial p/\partial\pi)_k$ in the nonlinear terms of the vorticity and divergence equations (3.a.38) and (3.a.39), and in the ω term of (3.a.35) and (3.a.42).

The second terms on the right-hand side of (3.a.65) and (3.a.67) must also cancel in the global mean. This cancellation is enforced locally in the horizontal on the column integrals of (3.a.65) and (3.a.67), so that we require:

$$\int_{\eta_t}^{1}\left\{\nabla\cdot\left(\frac{\partial p}{\partial\eta}\mathbf{V}\right)\int_{p(\eta)}^{p(1)}R\mathcal{T}d\ln p\right\}d\eta$$
$$=\int_{\eta_t}^{1}\left\{R\mathcal{T}\frac{\partial p}{\partial\eta}\frac{1}{p}\int_{\eta_t}^{\eta}\nabla\cdot\left(\frac{\partial p}{\partial\eta'}\mathbf{V}\right)d\eta'\right\}d\eta. \qquad (3.a.68)$$

The inner integral on the left-hand side of ($3.a.68$) is derived from the hydrostatic equation ($3.a.40$), which we shall approximate as

$$\Phi_k = \Phi_s + R \sum_{\ell=k}^{K} H_{k\ell} \mathcal{T}_\ell,$$

$$= \Phi_s + R \sum_{\ell=1}^{K} H_{k\ell} \mathcal{T}_\ell, \tag{3.a.69}$$

$$\underline{\Phi} = \Phi_s \underline{1} + R \mathbf{H} \underline{\mathcal{T}}, \tag{3.a.70}$$

where $H_{k\ell} = 0$ for $\ell < k$. The quantity $\underline{1}$ is defined to be the unit vector. The inner integral on the right-hand side of ($3.a.68$) is derived from the vertical velocity equation ($3.a.42$), which we shall approximate as

$$\left(\frac{\omega}{p}\right)_k = \left(\frac{\pi}{p}\frac{\partial p}{\partial \pi}\right)_k \mathbf{V}_k \cdot \nabla \Pi$$

$$- \sum_{\ell=1}^{K} C_{k\ell} \left[\delta_\ell \Delta p_\ell + \pi \left(\mathbf{V}_\ell \cdot \nabla \Pi\right) \Delta \left(\frac{\partial p}{\partial \pi}\right)_\ell \right], \tag{3.a.71}$$

where $C_{k\ell} = 0$ for $\ell > k$, and $C_{k\ell}$ is included as an approximation to $1/p_k$ for $\ell \leq k$ and the symbol Δ is similarly defined as in ($3.a.62$). $C_{k\ell}$ will be determined so that ω is consistent with the discrete continuity equation following Williamson and Olson (1994). Using ($3.a.69$) and ($3.a.71$), the finite difference analog of ($3.a.68$) is

$$\sum_{k=1}^{K} \left\{ \frac{1}{\Delta \eta_k} \left[\delta_k \Delta p_k + \pi \left(\mathbf{V}_k \cdot \nabla \Pi\right) \Delta \left(\frac{\partial p}{\partial \pi}\right)_k \right] R \sum_{\ell=1}^{K} H_{k\ell} \mathcal{T}_\ell \right\} \Delta \eta_k$$

$$= \sum_{k=1}^{K} \left\{ R \mathcal{T}_k \frac{\Delta p_k}{\Delta \eta_k} \sum_{\ell=1}^{K} C_{k\ell} \left[\delta_\ell \Delta p_\ell + \pi \left(\mathbf{V}_\ell \cdot \nabla \Pi\right) \Delta \left(\frac{\partial p}{\partial \pi}\right)_\ell \right] \right\} \Delta \eta_k, \tag{3.a.72}$$

where we have used the relation $\nabla \cdot \mathbf{V}(\partial p/\partial \eta)_k = [\delta_k \Delta p_k + \pi \left(\mathbf{V}_k \cdot \nabla \Pi\right) \Delta \left(\partial p/\partial \pi\right)_k]/\Delta \eta_k$ (see $3.a.22$). We can now combine the sums in ($3.a.72$) and simplify to give

$$\sum_{k=1}^{K} \sum_{\ell=1}^{K} \left\{ \left[\delta_k \Delta p_k + \pi \left(\mathbf{V}_k \cdot \nabla \Pi\right) \Delta \left(\frac{\partial p}{\partial \pi}\right)_k \right] H_{k\ell} \mathcal{T}_\ell \right\}$$

$$= \sum_{k=1}^{K} \sum_{\ell=1}^{K} \left\{ \left[\delta_\ell \Delta p_\ell + \pi \left(\mathbf{V}_\ell \cdot \nabla \Pi\right) \Delta \left(\frac{\partial p}{\partial \pi}\right)_\ell \right] \Delta p_k C_{k\ell} \mathcal{T}_k \right\}. \tag{3.a.73}$$

Interchanging the indexes on the left-hand side of ($3.a.73$) will obviously result in identical expressions if we require that

$$H_{k\ell} = C_{\ell k} \Delta p_\ell. \tag{3.a.74}$$

Given the definitions of vertical integrals in (3.a.70) and (3.a.71) and of vertical advection in (3.a.61) and (3.a.62) the model will conserve energy as long as we require that **C** and **H** satisfy (3.a.74). We are, of course, still neglecting lack of conservation due to the truncation of the horizontal spherical harmonic expansions.

Horizontal diffusion

CCM3 contains a horizontal diffusion term for T, ζ, and δ to prevent spectral blocking and to provide reasonable kinetic energy spectra. The horizontal diffusion operator in CCM3 is also used to ensure that the CFL condition is not violated in the upper layers of the model. The horizontal diffusion is a linear ∇^2 form on η surfaces in the top three levels of the model and a linear ∇^4 form with a partial correction to pressure surfaces for temperature elsewhere. The ∇^2 diffusion near the model top is used as a simple sponge to absorb vertically propagating planetary wave energy and also to control the strength of the stratospheric winter jets. The ∇^2 diffusion coefficient has a vertical variation which has been tuned to give reasonable Northern and Southern Hemisphere polar night jets.

In the top three model levels, the ∇^2 form of the horizontal diffusion is given by

$$F_{\zeta_H} = K^{(2)} \left[\nabla^2 (\zeta + f) + 2 (\zeta + f) / a^2\right], \tag{3.a.75}$$

$$F_{\delta_H} = K^{(2)} \left[\nabla^2 \delta + 2(\delta / a^2)\right], \tag{3.a.76}$$

$$F_{T_H} = K^{(2)} \nabla^2 T. \tag{3.a.77}$$

Since these terms are linear, they are easily calculated in spectral space. The undifferentiated correction term is added to the vorticity and divergence diffusion operators to prevent damping of uniform ($n = 1$) rotations (Orszag, 1974; Bourke *et al.*, 1977). The ∇^2 form of the horizontal diffusion is applied *only* to pressure surfaces in the standard model configuration.

The horizontal diffusion operator is better applied to pressure surfaces than to terrain-following surfaces (applying the operator on isentropic surfaces would be still better). Although the governing system of equations derived above is designed to reduce to pressure surfaces above some level, problems can still occur from diffusion along the lower surfaces. Partial correction to pressure surfaces of harmonic horizontal diffusion

$(\partial\xi/\partial t = K\nabla^2\xi)$ can be included using the relations:

$$\begin{aligned} \nabla_p\xi &= \nabla_\eta\xi - p\frac{\partial\xi}{\partial p}\nabla_\eta \ln p \\ \nabla_p^2\xi &= \nabla_\eta^2\xi - p\frac{\partial\xi}{\partial p}\nabla_\eta^2 \ln p - 2\nabla_\eta\left(\frac{\partial\xi}{\partial p}\right)\cdot\nabla_\eta p + \frac{\partial^2\xi}{\partial^2 p}\nabla_\eta^2 p\,. \end{aligned} \tag{3.a.78}$$

Retaining only the first two terms above gives a correction to the η surface diffusion which involves only a vertical derivative and the Laplacian of log surface pressure,

$$\nabla_p^2\xi = \nabla_\eta^2\xi - \pi\frac{\partial\xi}{\partial p}\frac{\partial p}{\partial\pi}\nabla^2\Pi + \ldots \tag{3.a.79}$$

Similarly, biharmonic diffusion can be partially corrected to pressure surfaces as:

$$\nabla_p^4\xi = \nabla_\eta^4\xi - \pi\frac{\partial\xi}{\partial p}\frac{\partial p}{\partial\pi}\nabla^4\Pi + \ldots \tag{3.a.80}$$

The bi-harmonic ∇^4 form of the diffusion operator is applied at all other levels (generally throughout the troposphere) as

$$F_{\zeta_H} = -K^{(4)}\left[\nabla^4(\zeta+f) - (\zeta+f)\left(2/a^2\right)^2\right], \tag{3.a.81}$$

$$F_{\delta_H} = -K^{(4)}\left[\nabla^4\delta - \delta(2/a^2)^2\right], \tag{3.a.82}$$

$$F_{T_H} = -K^{(4)}\left[\nabla^4 T - \pi\frac{\partial T}{\partial p}\frac{\partial p}{\partial\pi}\nabla^4\Pi\right]. \tag{3.a.83}$$

The second term in F_{T_H} consists of the leading term in the transformation of the ∇^4 operator to pressure surfaces. It is included to offset partially a spurious diffusion of T over mountains. As with the ∇^2 form, the ∇^4 operator can be conveniently calculated in spectral space. The correction term is then completed after transformation of T and $\nabla^4\Pi$ back to grid–point space. As with the ∇^2 form, an undifferentiated term is added to the vorticity and divergence diffusion operators to prevent damping of uniform rotations.

Finite difference equations

It will be assumed that the governing equations will be solved using the spectral method in the horizontal, so that only the vertical and time differences are presented here. The schematic dynamics term Γ in equation $(2.a.3a)$ includes horizontal diffusion of $T, (\zeta+f)$, and δ. Only T has the leading term correction to pressure surfaces. Thus, equations that include the terms in this time split sub-step are of the form

$$\frac{\partial \psi}{\partial t} = \mathrm{Dyn}\,(\psi) - (-1)^i K^{(2i)} \nabla^{2i}_{\eta} \psi \,, \tag{3.a.84}$$

for $(\zeta + f)$ and δ, and

$$\frac{\partial T}{\partial t} = \mathrm{Dyn}\,(T) - (-1)^i K^{(2i)} \left\{ \nabla^{2i}_{\eta} T - \pi \frac{\partial T}{\partial p} \frac{\partial p}{\partial \pi} \nabla^{2i} \Pi \right\} \,, \tag{3.a.85}$$

where $i = 1$ in the top few model levels and $i = 2$ elsewhere (generally within the troposphere). These equations are further subdivided into time split components:

$$\psi^{n+1} = \psi^{n-1} + 2\Delta t \ \mathrm{Dyn}\left(\psi^{n+1}, \psi^{n}, \psi^{n-1}\right) \,, \tag{3.a.86}$$

$$\psi^{*} = \psi^{n+1} - 2\Delta t \ (-1)^i K^{(2i)} \nabla^{2i}_{\eta} \left(\psi^{*n+1}\right) \,, \tag{3.a.87}$$

$$\hat{\psi}^{n+1} = \psi^{*} \,, \tag{3.a.88}$$

for $(\zeta + f)$ and δ, and

$$T^{n+1} = T^{n-1} + 2\Delta t \ \mathrm{Dyn}\left(T^{n+1}, T^{n}, T^{n-1}\right) \,, \tag{3.a.89}$$

$$T^{*} = T^{n+1} - 2\Delta t \ \left(-1\right)^i K^{(2i)} \nabla^{2i} \eta \left(T^{*}\right) \,, \tag{3.a.90}$$

$$\hat{T}^{n+1} = T^{*} + 2\Delta t \ \left(-1\right)^i K^{(2i)} \pi \frac{\partial T^{*}}{\partial p} \frac{\partial p}{\partial \pi} \nabla^{2i} \, \Pi \,, \tag{3.a.91}$$

for T, where in the standard model i only takes the value 2 in (3.a.91). The first step from $(\ )^{n-1}$ to $(\ )^{n+1}$ includes the transformation to spectral coefficients. The second step from $(\ )^{n+1}$ to $(\hat{\ })^{n+1}$ for δ and ζ , or $(\ )^{n+1}$ to $(\ )^{*}$ for T, is done on the spectral coefficients, and the final step from $(\ )^{*}$ to $(\hat{\ })^{n+1}$ for T is done after the inverse transform to the grid point representation.

The following finite-difference description details only the forecast given by (3.a.86) and (3.a.89). In what follows we use $(\ )^{n-1}$ instead of $\overline{(\ )}^{n-1}$ from (2.a.8). This notation is convenient for discussing the dynamical equations in isolation. The finite-difference form of the forecast equation for water vapor will be presented later in Section 3c. The general structure of the complete finite difference equations is determined by the semi-implicit time differencing and the energy conservation properties described above. In order to complete the specification of the finite differencing, we require a definition of the vertical coordinate. The actual specification of the generalized vertical coordinate takes advantage of the structure of the equations (3.a.33)$-$(3.a.42). The equations can be finite-differenced in the vertical and, in time, without having to know the value of η anywhere. The quantities that must be known are p and $\partial p/\partial \pi$ at the grid points. Therefore the coordinate is defined implicitly through the relation:

$$p(\eta, \pi) = A(\eta)p_0 + B(\eta)\pi \,, \tag{3.a.92}$$

which gives

$$\frac{\partial p}{\partial \pi} = B(\eta) \,. \tag{3.a.93}$$

A set of levels η_k may be specified by specifying A_k and B_k, such that $\eta_k \equiv A_k + B_k$, and difference forms of (3.a.33) – (3.a.42) may be derived.

The finite difference forms of the Dyn operator (3.a.33) – (3.a.42), including semi-implicit time integration are:

$$\underline{\zeta}^{n+1} = \underline{\zeta}^{n-1} + 2\Delta t \mathbf{k} \cdot \nabla \times \left(\underline{\mathbf{n}}^n / \cos\phi \right) , \tag{3.a.94}$$

$$\begin{aligned}
\underline{\delta}^{n+1} &= \underline{\delta}^{n-1} + 2\Delta t \left[\nabla \cdot \left(\underline{\mathbf{n}}^n / \cos\phi \right) - \nabla^2 \left(\underline{E}^n + \Phi_s \underline{1} + R\mathbf{H}^n (\underline{T}^{'})^n \right) \right] \\
&\quad - 2\Delta t R \mathbf{H}^r \nabla^2 \left(\frac{(\underline{T}')^{n-1} + (\underline{T}')^{n+1}}{2} - (\underline{T}')^n \right) \\
&\quad - 2\Delta t R \left(\underline{b}^r + \underline{h}^r \right) \nabla^2 \left(\frac{\Pi^{n-1} + \Pi^{n+1}}{2} - \Pi^n \right) ,
\end{aligned} \tag{3.a.95}$$

$$\begin{aligned}
(\underline{T}^{'})^{n+1} &= (\underline{T}^{'})^{n-1} - 2\Delta t \left[\frac{1}{a \cos^2\phi} \frac{\partial}{\partial \lambda} \left(\underline{UT'} \right)^n + \frac{1}{a \cos\phi} \frac{\partial}{\partial \phi} \left(\underline{VT'} \right)^n - \underline{\Gamma}^n \right] \\
&\quad - 2\Delta t \mathbf{D}^r \left(\frac{\underline{\delta}^{n-1} + \underline{\delta}^{n+1}}{2} - \underline{\delta}^n \right) ,
\end{aligned} \tag{3.a.96}$$

$$\begin{aligned}
\Pi^{n+1} &= \Pi^{n-1} - 2\Delta t \frac{1}{\pi^n} \left(\left(\underline{\delta}^n \right)^T \underline{\Delta p}^n + \left(\underline{\mathbf{V}}^n \right)^T \nabla \Pi^n \pi^n \underline{\Delta B} \right) \\
&\quad - 2\Delta t \left(\frac{\underline{\delta}^{n-1} + \underline{\delta}^{n+1}}{2} - \underline{\delta}^n \right)^T \frac{1}{\pi^r} \underline{\Delta p}^r ,
\end{aligned} \tag{3.a.97}$$

$$\begin{aligned}
(n_U)_k &= (\zeta_k + f) V_k - R\mathcal{T}_k \left(\frac{1}{p} \frac{\partial p}{\partial \pi} \right)_k \pi \frac{1}{a} \frac{\partial \Pi}{\partial \lambda} \\
&\quad - \frac{1}{2\Delta p_k} \left[\left(\dot{\eta} \frac{\partial p}{\partial \eta} \right)_{k+1/2} (U_{k+1} - U_k) + \left(\dot{\eta} \frac{\partial p}{\partial \eta} \right)_{k-1/2} (U_k - U_{k-1}) \right] \\
&\quad + (F_U)_k \ ,
\end{aligned} \tag{3.a.98}$$

$$(n_V)_k = - (\zeta_k + f) U_k - R\mathcal{T}_k \left(\frac{1}{p} \frac{\partial p}{\partial \pi} \right)_k \pi \frac{\cos\phi}{a} \frac{\partial \Pi}{\partial \phi}$$

$$
- \frac{1}{2\Delta p_k}\left[\left(\dot{\eta}\frac{\partial p}{\partial \eta}\right)_{k+1/2}(V_{k+1}-V_k)+\left(\dot{\eta}\frac{\partial p}{\partial \eta}\right)_{k-1/2}(V_k-V_{k-1})\right] \tag{3.a.99}
$$
$$
+ (F_V)_k \ ,
$$

$$
\Gamma_k = T'_k\delta_k + \frac{R\mathcal{T}_k}{(c_p^*)_k}\left(\frac{\omega}{p}\right)_k - Q
$$
$$
- \frac{1}{2\Delta p_k}\left[\left(\dot{\eta}\frac{\partial p}{\partial \eta}\right)_{k+1/2}(T_{k+1}-T_k)+\left(\dot{\eta}\frac{\partial p}{\partial \eta}\right)_{k-1/2}(T_k-T_{k-1})\right], \tag{3.a.100}
$$

$$
E_k = (u_k)^2 + (v_k)^2 \,, \tag{3.a.101}
$$

$$
\frac{R\mathcal{T}_k}{(c_p^*)_k} = \frac{R}{c_p}\left(\frac{T_k^r + \mathcal{T}'_k}{1+\left(\frac{c_{p_v}}{c_p}-1\right)q_k}\right), \tag{3.a.102}
$$

$$
\left(\dot{\eta}\frac{\partial p}{\partial \eta}\right)_{k+1/2} = B_{k+1/2}\sum_{\ell=1}^{K}\left[\delta_\ell \Delta p_\ell + \mathbf{V}_\ell \cdot \pi\nabla\Pi\Delta B_\ell\right]
$$
$$
- \sum_{\ell=1}^{k}\left[\delta_\ell \Delta p_\ell + \mathbf{V}_\ell \cdot \pi\nabla\Pi\Delta B_\ell\right], \tag{3.a.103}
$$

$$
\left(\frac{\omega}{p}\right)_k = \left(\frac{1}{p}\frac{\partial p}{\partial \pi}\right)_k \mathbf{V}_k \cdot \pi\nabla\Pi
$$
$$
- \sum_{\ell=1}^{k} C_{k\ell}\left[\delta_\ell \Delta p_\ell + \mathbf{V}_\ell \cdot \pi\nabla\Pi\Delta B_\ell\right], \tag{3.a.104}
$$

$$
C_{k\ell} = \begin{cases} \frac{1}{p_k} & \text{for } \ell < k \\ \frac{1}{2p_k} & \text{for } \ell = k \end{cases}, \tag{3.a.105}
$$

$$
H_{k\ell} = C_{\ell k}\Delta p_\ell, \tag{3.a.106}
$$

$$
D_{k\ell}^r = \Delta p_\ell^r \frac{R}{c_p} T_k^r C_{\ell k}^r
$$
$$
+ \frac{\Delta p_\ell^r}{2\Delta p_k^r}\left(T_k^r - T_{k-1}^r\right)\left(\epsilon_{k\ell+1} - B_{k-1/2}\right)
$$

$$+\frac{\Delta p_\ell^r}{2\Delta p_k^r}\left(T_{k+1}^r - T_k^r\right)\left(\epsilon_{k\ell} - B_{k+1/2}\right), \tag{3.a.107}$$

$$\frac{\epsilon_{k\ell}}{R} = \begin{cases} 1, & \ell \le k \\ 0, & \ell > k, \end{cases} \tag{3.a.108}$$

where notation such as $\left(\underline{UT'}\right)^n$ denotes a column vector with components $\left(U_k T_k'\right)^n$. In order to complete the system, it remains to specify the reference vector $\underline{h}^r$, together with the term $(1/p\,\partial p/\partial\pi)$, which results from the pressure gradient terms and also appears in the semi-implicit reference vector $\underline{b}^r$:

$$\left(\frac{1}{p}\frac{\partial p}{\partial \pi}\right)_k = \left(\frac{1}{p}\right)_k \left(\frac{\partial p}{\partial \pi}\right)_k = \frac{B_k}{p_k}, \tag{3.a.109}$$

$$\underline{b}^r = \underline{T}^r, \tag{3.a.110}$$

$$\underline{h}^r = 0. \tag{3.a.111}$$

The matrices $\mathbf{C}^n$ and $\mathbf{H}^n$ (*i.e.*, with components $C_{k\ell}$ and $H_{k\ell}$) must be evaluated at each time step and each point in the horizontal. It is more efficient computationally to substitute the definitions of these matrices into (3.a.95) and (3.a.104) at the cost of some loss of generality in the code. The finite difference equations have been written in the form (3.a.94) – (3.a.111) because this form is quite general. For example, the equations solved by Simmons and Strüfing (1981) at ECMWF can be obtained by changing only the vectors and hydrostatic matrix defined by (3.a.108) – (3.a.111).

b. Spectral Transform

The spectral transform method is used in the horizontal exactly as in CCM1. As shown earlier, the vertical and temporal aspects of the model are represented by finite–difference approximations. The horizontal aspects are treated by the spectral–transform method, which is described in this section. Thus, at certain points in the integration, the prognostic variables $(\zeta + f), \delta, T,$ and Π are represented in terms of coefficients of a truncated series of spherical harmonic functions, while at other points they are given by grid–point values on a corresponding Gaussian grid. In general, physical parameterizations and nonlinear operations are carried out in grid–point space. Horizontal derivatives and linear operations are performed in spectral space. Externally, the model appears to the user to be a grid–point model, as far as data required and produced by it. Similarly, since all nonlinear parameterizations are developed and carried out in grid–point space, the model also appears as a grid–point model for the incorporation of physical parameterizations, and the user need not be too concerned with the spectral aspects. For users interested in diagnosing the balance of terms in the evolution equations, however, the details are important and care must be taken to understand which terms have been spectrally truncated and which have not. The algebra involved in the spectral transformations has been presented in several publications (Daley *et al.,* 1976; Bourke *et al.,* 1977; Machenhauer, 1979). In this report, we present only the details relevant to the model code; for more details and general philosophy, the reader is referred to these earlier papers.

Spectral algorithm overview

The horizontal representation of an arbitrary variable ψ consists of a truncated series of spherical harmonic functions,

$$\psi(\lambda,\mu) = \sum_{m=-M}^{M} \sum_{n=|m|}^{\mathcal{N}(m)} \psi_n^m P_n^m(\mu) e^{im\lambda}, \tag{3.b.1}$$

where $\mu = \sin\phi$, M is the highest Fourier wavenumber included in the east–west representation, and $\mathcal{N}(m)$ is the highest degree of the associated Legendre polynomials for longitudinal wavenumber m. The properties of the spherical harmonic functions used in the representation can be found in the review by Machenhauer (1979). The model is coded for a general pentagonal truncation, illustrated in Figure 2, defined by three parameters: M, K, and N, where M is defined above, K is the highest degree of the associated Legendre polynomials, and N is the highest degree of the Legendre polynomials for $m = 0$. The common truncations are subsets of this pentagonal case:

$$\begin{aligned} \text{Triangular} &: M = N = K, \\ \text{Rhomboidal} &: K = N + M, \\ \text{Trapezoidal} &: N = K > M. \end{aligned} \tag{3.b.2}$$

The quantity $\mathcal{N}(m)$ in (3.b.1) represents an arbitrary limit on the two-dimensional wavenumber n, and for the pentagonal truncation described above is simply given by $\mathcal{N}(m) = \min(N + |m|, K)$.

The associated Legendre polynomials used in the model are normalized such that

$$\int_{-1}^{1} [P_n^m(\mu)]^2 \, d\mu = 1. \tag{3.b.3}$$

With this normalization, the Coriolis parameter f is

$$f = \frac{\Omega}{\sqrt{0.375}} P_1^o, \tag{3.b.4}$$

which is required for the absolute vorticity.

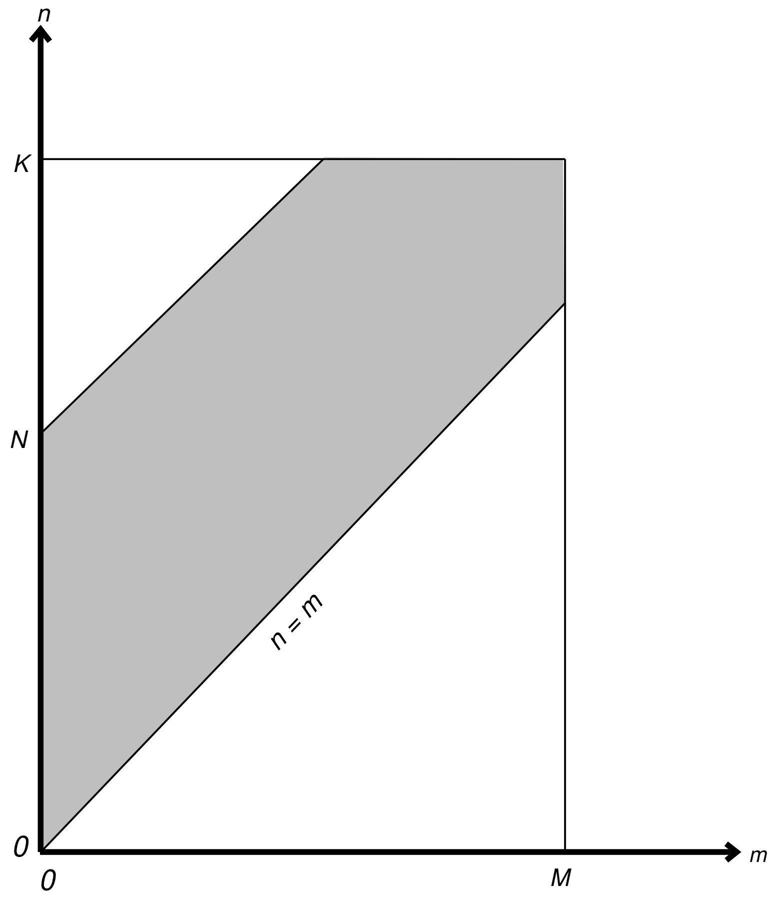

Figure 2. Pentagonal truncation parameters

The coefficients of the spectral representation (3.b.1) are given by

$$\psi_n^m = \int_{-1}^{1} \frac{1}{2\pi} \int_0^{2\pi} \psi(\lambda, \mu) e^{-im\lambda} d\lambda P_n^m(\mu) d\mu. \tag{3.b.5}$$

The inner integral represents a Fourier transform,

$$\psi^m(\mu) = \frac{1}{2\pi} \int_0^{2\pi} \psi(\lambda, \mu) e^{-im\lambda} d\lambda, \tag{3.b.6}$$

which is performed by a Fast Fourier Transform (FFT) subroutine. The outer integral is performed via Gaussian quadrature,

$$\psi_n^m = \sum_{j=1}^{J} \psi^m(\mu_j) P_n^m(\mu_j) w_j, \tag{3.b.7}$$

where μ_j denotes the Gaussian grid points in the meridional direction, w_j the Gaussian weight at point μ_j, and J the number of Gaussian grid points from pole to pole. The Gaussian grid points (μ_j) are given by the roots of the Legendre polynomial $P_J(\mu)$, and the corresponding weights are given by

$$w_j = \frac{2(1-\mu_j^2)}{\left[J\ P_{J-1}(\mu_j)\right]^2}. \tag{3.b.8}$$

The weights themselves satisfy

$$\sum_{j=1}^{J} w_j = 2.0\ . \tag{3.b.9}$$

The Gaussian grid used for the north–south transformation is generally chosen to allow un-aliased computations of quadratic terms only. In this case, the number of Gaussian latitudes J must satisfy

$$J \geq (2N + K + M + 1)/2 \quad \text{for} \ \ \mathrm{M} \leq 2(\mathrm{K}-\mathrm{N}), \tag{3.b.10}$$

$$J \geq (3K + 1)/2 \qquad\qquad \text{for} \ \ \mathrm{M} \geq 2(\mathrm{K}-\mathrm{N}). \tag{3.b.11}$$

For the common truncations, these become

$$J \geq (3K + 1)/2 \qquad\qquad \text{for triangular and trapezoidal,} \tag{3.b.12}$$

$$J \geq (3N + 2M + 1)/2 \qquad \text{for rhomboidal.} \tag{3.b.13}$$

In order to allow exact Fourier transform of quadratic terms, the number of points P in the east–west direction must satisfy

$$P \geq 3M + 1 \quad . \tag{3.b.14}$$

The actual values of J and P are often not set equal to the lower limit in order to allow use of more efficient transform programs.

Although in the next section of this model description, we continue to indicate the Gaussian quadrature as a sum from pole to pole, the code actually deals with the symmetric and antisymmetric components of variables and accumulates the sums from equator to pole only. The model requires an even number of latitudes to easily use the symmetry conditions. This may be slightly inefficient for some spectral resolutions. We define a new index, which goes from $-I$ at the point next to the south pole to $+I$ at the point next to the north pole and not including 0 (there are no points at the equator or pole in the Gaussian grid), *i.e.*, let $I = J/2$ and $i = j - J/2$ for $j \geq J/2+1$ and $i = j - J/2 - 1$ for $j \leq J/2$; then the summation in (3.*b*.7) can be rewritten as

$$\psi_n^m = \sum_{\substack{i=-I \\ i\neq 0}}^{I} \psi^m(\mu_i) P_n^m(\mu_i) w_i. \tag{3.b.15}$$

The symmetric (even) and antisymmetric (odd) components of ψ^m are defined by

$$
\begin{aligned}
(\psi_E)_i^m &= \frac{1}{2}\left(\psi_i^m + \psi_{-i}^m\right) , \\
(\psi_O)_i^m &= \frac{1}{2}\left(\psi_i^m - \psi_{-i}^m\right) .
\end{aligned}
\tag{3.b.16}
$$

Since w_i is symmetric about the equator, (3.b.15) can be rewritten to give formulas for the coefficients of even and odd spherical harmonics:

$$
\psi_n^m = \begin{cases} \sum\limits_{i=1}^{I} (\psi_E)_i^m (\mu_i) P_n^m(\mu_i) 2w_i & \text{for } n-m \text{ even} , \\ \\ \sum\limits_{i=1}^{I} (\psi_O)_i^m (\mu_i) P_n^m(\mu_i) 2w_i & \text{for } n-m \text{ odd} . \end{cases}
\tag{3.b.17}
$$

The model uses the spectral transform method (Machenhauer, 1979) for all nonlinear terms. However, the model can be thought of as starting from grid–point values at time t (consistent with the spectral representation) and producing a forecast of the grid–point values at time $t + \Delta t$ (again, consistent with the spectral resolution). The forecast procedure involves computation of the nonlinear terms including physical parameterizations at grid points; transformation via Gaussian quadrature of the nonlinear terms from grid–point space to spectral space; computation of the spectral coefficients of the prognostic variables at time $t + \Delta t$ (with the implied spectral truncation to the model resolution); and transformation back to grid–point space. The details of the equations involved in the various transformations are given in the next section.

Combination of terms

In order to describe the transformation to spectral space, for each equation we first group together all undifferentiated explicit terms, all explicit terms with longitudinal derivatives, and all explicit terms with meridional derivatives appearing in the Dyn operator. Thus, the vorticity equation (3.a.94) is rewritten

$$
\underline{(\zeta + f)}^{n+1} = \underline{V} + \frac{1}{a(1-\mu^2)}\left[\frac{\partial}{\partial \lambda}(\underline{V}_\lambda) - (1-\mu^2)\frac{\partial}{\partial \mu}(\underline{V}_\mu)\right] ,
\tag{3.b.18}
$$

where the explicit forms of the vectors $\underline{V}$, $\underline{V}_\lambda$, and $\underline{V}_\mu$ are given in Appendix A [(A1)–(A3).] The divergence equation (3.a.95) is

$$\underline{\delta}^{n+1} = \underline{D} + \frac{1}{a(1-\mu^2)}\left[\frac{\partial}{\partial\lambda}(\underline{D}_\lambda) + (1-\mu^2)\frac{\partial}{\partial\mu}(\underline{D}_\mu)\right] - \nabla^2 \underline{D}_\nabla$$
$$- \Delta t \nabla^2 (R\mathbf{H}^r \underline{T}'^{\,n+1} + R\,(\underline{b}^r + \underline{h}^r)\,\Pi^{n+1}). \tag{3.b.19}$$

The mean component of the temperature is not included in the next–to–last term since the Laplacian of it is zero. The thermodynamic equation (3.a.96) is

$$\underline{T}'^{\,n+1} = \underline{T} - \frac{1}{a(1-\mu^2)}\left[\frac{\partial}{\partial\lambda}(\underline{T}_\lambda) + (1-\mu^2)\frac{\partial}{\partial\mu}(\underline{T}_\mu)\right] - \Delta t \mathbf{D}^r\,\underline{\delta}^{n+1}. \tag{3.b.20}$$

The surface–pressure tendency (3.a.97) is

$$\Pi^{n+1} = PS - \frac{\Delta t}{\pi^r}\left(\underline{\Delta p}^r\right)^T \underline{\delta}^{n+1}. \tag{3.b.21}$$

The grouped explicit terms in (3.b.19)–(3.b.21) are all given in Appendix A [(A4)–(A11)].

Transformation to spectral space

Formally, Equations (3.b.18) – (3.b.21) are transformed to spectral space by performing the operations indicated in (3.b.22) to each term. We see that the equations basically contain three types of terms, for example, in the vorticity equation the undifferentiated term $\underline{V}$, the longitudinally differentiated term $\underline{V}_\lambda$, and the meridionally differentiated term $\underline{V}_\mu$. All terms in the original equations were grouped into one of these terms on the Gaussian grid so that they could be transformed at once.

Transformation of the undifferentiated term is obtained by straightforward application of (3.b.5) – (3.b.7),

$$\{\underline{V}\}_n^m = \sum_{j=1}^{J} \underline{V}^m(\mu_j) P_n^m(\mu_j) w_j, \tag{3.b.22}$$

where $\underline{V}^m(\mu_j)$ is the Fourier coefficient of $\underline{V}$ with wavenumber m at the Gaussian grid line μ_j. The longitudinally differentiated term is handled by integration by parts, using the cyclic boundary conditions,

$$\left\{\frac{\partial}{\partial\lambda}(\underline{V}_\lambda)\right\}^m = \frac{1}{2\pi}\int_o^{2\pi} \frac{\partial \underline{V}_\lambda}{\partial\lambda} e^{-im\lambda} d\lambda,$$
$$= im\frac{1}{2\pi}\int_o^{2\pi} \underline{V}_\lambda e^{-im\lambda} d\lambda, \tag{3.b.23}$$

so that the Fourier transform is performed first, then the differentiation is carried out in spectral space. The transformation to spherical harmonic space then follows (3.b.25):

$$\left\{ \frac{1}{a(1-\mu^2)} \frac{\partial}{\partial \lambda} (\underline{V}_\lambda) \right\}_n^m = im \sum_{j=1}^{J} \underline{V}_\lambda^m(\mu_j) \frac{P_n^m(\mu_j)}{a(1-\mu_j^2)} w_j, \tag{3.b.24}$$

where $\underline{V}_\lambda^m(\mu_j)$ is the Fourier coefficient of $\underline{V}_\lambda$ with wavenumber m at the Gaussian grid line μ_j.

The latitudinally differentiated term is handled by integration by parts using zero boundary conditions at the poles:

$$\begin{aligned} \left\{ \frac{1}{a(1-\mu^2)} (1-\mu^2) \frac{\partial}{\partial \mu} (\underline{V}_\mu) \right\}_n^m &= \int_{-1}^{1} \frac{1}{a(1-\mu^2)} (1-\mu^2) \frac{\partial}{\partial \mu} (\underline{V}_\mu)^m P_n^m d\mu, \\ &= -\int_{-1}^{1} \frac{1}{a(1-\mu^2)} (\underline{V}_\mu)^m (1-\mu^2) \frac{dP_n^m}{d\mu} d\mu. \end{aligned} \tag{3.b.25}$$

Defining the derivative of the associated Legendre polynomial by

$$H_n^m = (1-\mu^2) \frac{dP_n^m}{d\mu}, \tag{3.b.26}$$

(3.b.28) can be written

$$\left\{ \frac{1}{a(1-\mu^2)} (1-\mu^2) \frac{\partial}{\partial \mu} (\underline{V}_\mu) \right\}_n^m = -\sum_{j=1}^{J} (\underline{V}_\mu)^m \frac{H_n^m(\mu_j)}{a(1-\mu_j^2)} w_j. \tag{3.b.27}$$

Similarly, the ∇^2 operator in the divergence equation can be converted to spectral space by sequential integration by parts and then application of the relationship

$$\nabla^2 P_n^m(\mu) e^{im\lambda} = \frac{-n(n+1)}{a^2} P_n^m(\mu) e^{im\lambda}, \tag{3.b.28}$$

to each spherical harmonic function individually so that

$$\{\nabla^2 \underline{D}_\nabla\}_n^m = \frac{-n(n+1)}{a^2} \sum_{j=1}^{J} \underline{D}_\nabla^m(\mu_j) P_n^m(\mu_j) w_j, \tag{3.b.29}$$

where $\underline{D}_\nabla^m(\mu)$ is the Fourier coefficient of the original grid variable $\underline{D}_\nabla$.

Solution of semi–implicit equations

The prognostic equations can be converted to spectral form by summation over the Gaussian grid using (3.b.22), (3.b.24), and (3.b.27). The resulting equation for absolute vorticity is

$$\underline{(\zeta + f)}_n^m = \underline{VS}_n^m, \tag{3.b.30}$$

where $\underline{(\zeta + f)}_n^m$ denotes a spherical harmonic coefficient of $\underline{(\zeta + f)}^{n+1}$, and the form of $\underline{VS}_n^m$, as a summation over the Gaussian grid, is given in Appendix A (A12).

The spectral form of the divergence equation (3.b.19) becomes

$$\underline{\delta}_n^m = \underline{DS}_n^m + \Delta t \frac{n(n+1)}{a^2} \left[R\mathbf{H}^r \underline{T}'^m_n + R\left(\underline{b}^r + \underline{h}^r\right) \Pi_n^m \right], \tag{3.b.31}$$

where $\underline{\delta}_n^m$, $\underline{T}'^m_n$, and Π_n^m are spectral coefficients of $\underline{\delta}^{n+1}$, $\underline{T}'^{n+1}$, and Π^{n+1}. The Laplacian of the total temperature in (3.b.19) is replaced by the equivalent Laplacian of the perturbation temperature in (3.b.31). $\underline{DS}_n^m$ is given in Appendix A (A13). The spectral thermodynamic equation is

$$\underline{T}'^m_n = \underline{TS}_n^m - \Delta t \mathbf{D}^r \underline{\delta}_n^m, \tag{3.b.32}$$

with $\underline{TS}_n^m$ defined in Appendix A (A14), while the surface pressure equation is

$$\Pi_n^m = PS_n^m - \underline{\delta}_n^m \left(\underline{\Delta p}^r\right)^T \frac{\Delta t}{\pi^r} \tag{3.b.33}$$

where PS_n^m is also given in Appendix A (A15).

Equation (3.b.30) for vorticity is explicit and complete at this point. However, the remaining equations (3.b.31)–(3.b.33) are coupled. They are solved by eliminating all variables except $\underline{\delta}_n^m$:

$$\mathbf{A}_n \underline{\delta}_n^m = \underline{DS}_n^m + \Delta t \frac{n(n+1)}{a^2} \left[R\mathbf{H}^r (\underline{TS})_n^m + R\left(\underline{b}^r + \underline{h}^r\right) (PS)_n^m \right], \tag{3.b.34}$$

where

$$\mathbf{A}_n = \mathbf{I} + \Delta t^2 \frac{n(n+1)}{a^2} \left[R\mathbf{H}^r \mathbf{D}^r + R\left(\underline{b}^r + \underline{h}^r\right) \left(\left(\underline{\Delta p}^r\right)^T \frac{1}{\pi^r} \right) \right], \tag{3.b.35}$$

which is simply a set of K simultaneous equations for the coefficients with given wavenumbers (m, n) at each level and is solved by inverting $\mathbf{A}_n$. In order to prevent the accumulation of round–off error in the global mean divergence (which if exactly zero initially, should remain exactly zero) $(\mathbf{A}_o)^{-1}$ is set to the null matrix rather than the identity, and the formal application of (3.b.34) then always guarantees $\underline{\delta}_o^o = 0$. Once δ_n^m is known, $\underline{T}'^m_n$ and Π_n^m can be computed from (3.b.32) and (3.b.33), respectively, and all prognostic variables are known at time $n+1$ as spherical harmonic coefficients. Note that the mean component $\underline{T}'^o_o$ is not necessarily zero since the perturbations are taken with respect to a specified $\underline{T}^r$.

Horizontal diffusion

As mentioned earlier, the horizontal diffusion in (3.a.87) and (3.a.90) is computed implicitly via time splitting after the transformations into spectral space and solution of the semi-implicit equations. In the following, the ζ and δ equations have a similar form, so we write only the δ equation:

$$(\delta^*)_n^m = \left(\delta^{n+1}\right)_n^m - (-1)^i \, 2\Delta t K^{(2i)} \left[\nabla^{2i} (\delta^*)_n^m - (-1)^i (\delta^*)_n^m \left(2/a^2\right)^i \right], \tag{3.b.36}$$

$$(T^*)_n^m = \left(T^{n+1}\right)_n^m - (-1)^i \, 2\Delta t K^{(2i)} \left[\nabla^{2i} (T^*)_n^m \right] . \tag{3.b.37}$$

The extra term is present in (3.b.36), (3.b.40) and (3.b.42) to prevent damping of uniform rotations. The solutions are just

$$(\delta^*)_n^m = K_n^{(2i)} (\delta) \left(\delta^{n+1}\right)_n^m , \tag{3.b.38}$$

$$(T^*)_n^m = K_n^{(2i)} (T) \left(T^{n+1}\right)_n^m , \tag{3.b.39}$$

$$K_n^{(2)} (\delta) = \left\{1 + 2\Delta t D_n K^{(2)} \left[\left(\frac{n\,(n+1)}{a^2}\right) - \frac{2}{a^2}\right]\right\}^{-1} , \tag{3.b.40}$$

$$K_n^{(2)} (T) = \left\{1 + 2\Delta t D_n K^{(2)} \left(\frac{n\,(n+1)}{a^2}\right)\right\}^{-1} , \tag{3.b.41}$$

$$K_n^{(4)} (\delta) = \left\{1 + 2\Delta t D_n K^{(4)} \left[\left(\frac{n\,(n+1)}{a^2}\right)^2 - \frac{4}{a^4}\right]\right\}^{-1} , \tag{3.b.42}$$

$$K_n^{(4)} (T) = \left\{1 + 2\Delta t D_n K^{(4)} \left(\frac{n\,(n+1)}{a^2}\right)^2\right\}^{-1} . \tag{3.b.43}$$

$K_n^{(2)} (\delta)$ and $K_n^{(4)} (\delta)$ are both set to 1 for $n = 0$. The quantity D_n represents the "Courant number limiter", normally set to 1. However, D_n is modified to ensure that the CFL criterion is not violated in selected upper levels of the model. If the maximum wind speed in any of these upper levels is sufficiently large, then $D_n = 1000$ in that level for all $n > n_c$, where $n_c = a\Delta t \big/ \max|\mathbf{V}|$. This condition is applied whenever the wind speed is large enough that $n_c < K$, the truncation parameter in (3.b.2), and temporarily reduces the effective resolution of the model in the affected levels. The number of levels at which this "Courant number limiter" may be applied is user-selectable, but it is only used in the top level of the 18 level CCM3 control runs.

The diffusion of T is not complete at this stage. In order to make the partial correction from η to p in (3.a.81) local, it is not included until grid–point values are available. This requires that $\nabla^4\Pi$ also be transformed from spectral to grid–point space. The values of the coefficients $K^{(2)}$ and $K^{(4)}$ for the standard T42 resolution are $2.5 \times 10^5 \mathrm{m}^2\mathrm{sec}^{-1}$ and $1.0 \times 10^{16} \mathrm{m}^4\mathrm{sec}^{-1}$, respectively.

Initial divergence damping

Occasionally, with poorly balanced initial conditions, the model exhibits numerical instability during the beginning of an integration because of excessive noise in the solution. Therefore, an optional divergence damping is included in the model to be applied over the first few days. The damping has an initial e-folding time of Δt and linearly decreases to

0 over a specified number of days, t_D, usually set to be 2. The damping is computed implicitly via time splitting after the horizontal diffusion.

$$r = \max\left[\frac{1}{\Delta t}(t_D - t)/t_D,\ 0\right] \tag{3.b.44}$$

$$(\delta^*)_n^m = \frac{1}{1+2\Delta t r}(\delta^*)_n^m \tag{3.b.45}$$

Transformation from spectral to physical space

After the prognostic variables are completed at time $n+1$ in spectral space $\left(\underline{(\zeta+f)^*}\right)_n^m$, $(\underline{\delta^*})_n^m$, $(\underline{T^*})_n^m$, $\left(\Pi^{n+1}\right)_n^m$, they are transformed to grid space. For a variable ψ, the transformation is given by

$$\psi(\lambda,\mu) = \sum_{m=-M}^{M}\left[\sum_{n=|m|}^{\mathcal{N}(m)} \psi_n^m P_n^m(\mu)\right] e^{im\lambda}. \tag{3.b.46}$$

The inner sum is done essentially as a vector product over n, and the outer is again performed by an FFT subroutine. The term needed for the remainder of the diffusion terms, $\nabla^4\Pi$, is calculated from

$$\nabla^4\Pi^{n+1} = \sum_{m=-M}^{M}\left[\sum_{n=|m|}^{\mathcal{N}(m)}\left(\frac{n(n+1)}{a^2}\right)^2\left(\Pi^{n+1}\right)_n^m P_n^m(\mu)\right] e^{im\lambda}. \tag{3.b.47}$$

In addition, the derivatives of Π are needed on the grid for the terms involving $\nabla\Pi$ and $\mathbf{V}\cdot\nabla\Pi$,

$$\mathbf{V}\cdot\nabla\Pi = \frac{U}{a(1-\mu^2)}\frac{\partial\Pi}{\partial\lambda} + \frac{V}{a(1-\mu^2)}(1-\mu^2)\frac{\partial\Pi}{\partial\mu}. \tag{3.b.48}$$

These required derivatives are given by

$$\frac{\partial\Pi}{\partial\lambda} = \sum_{m=-M}^{M} im\left[\sum_{n=|m|}^{\mathcal{N}(m)} \Pi_n^m P_n^m(\mu)\right] e^{im\lambda}, \tag{3.b.49}$$

and using (3.b.26),

$$(1-\mu^2)\frac{\partial\Pi}{\partial\mu} = \sum_{m=-M}^{M}\left[\sum_{n=|m|}^{\mathcal{N}(m)} \Pi_n^m H_n^m(\mu)\right] e^{im\lambda}, \tag{3.b.50}$$

which involve basically the same operations as (3.b.47). The other variables needed on the grid are U and V. These can be computed directly from the absolute vorticity and divergence coefficients using the relations

$$(\zeta+f)_n^m = -\frac{n(n+1)}{a^2}\psi_n^m + f_n^m, \tag{3.b.49}$$

$$\delta_n^m = -\frac{n(n+1)}{a^2}\chi_n^m, \tag{3.b.52}$$

in which the only nonzero f_n^m is $f_1^o = \Omega/\sqrt{.375}$, and

$$U = \frac{1}{a}\frac{\partial\chi}{\partial\lambda} - \frac{(1-\mu^2)}{a}\frac{\partial\psi}{\partial\mu}, \tag{3.b.53}$$

$$V = \frac{1}{a}\frac{\partial\psi}{\partial\lambda} + \frac{(1-\mu^2)}{a}\frac{\partial\chi}{\partial\mu}. \tag{3.b.54}$$

Thus, the direct transformation is

$$U = -\sum_{m=-M}^{M} a \sum_{n=|m|}^{\mathcal{N}(m)} \left[\frac{im}{n(n+1)}\delta_n^m P_n^m(\mu) - \frac{1}{n(n+1)}(\zeta+f)_n^m H_n^m(\mu)\right] e^{im\lambda}$$

$$-\frac{a}{2}\frac{\Omega}{\sqrt{0.375}}H_1^o, \tag{3.b.53}$$

$$V = -\sum_{m=-M}^{M} a \sum_{n=|m|}^{\mathcal{N}(m)} \left[\frac{im}{n(n+1)}(\zeta+f)_n^m P_n^m(\mu) + \frac{1}{n(n+1)}\delta_n^m H_n^m(\mu)\right] e^{im\lambda}. \tag{3.b.56}$$

The horizontal diffusion tendencies are also transformed back to grid space. The spectral coefficients for the horizontal diffusion tendencies follow from (3.b.36) and (3.b.37):

$$F_{T_H}(T^*)_n^m = (-1)^{i+1} K^{2i}\left[\nabla^{2i}(T^*)\right]_n^m, \tag{3.b.57}$$

$$F_{\zeta_H}\left((\zeta+f)^*\right)_n^m = (-1)^{i+1} K^{2i}\left\{\nabla^{2i}(\zeta+f)^* - (-1)^i(\zeta+f)^*\left(2/a^2\right)^i\right\}, \tag{3.b.58}$$

$$F_{\delta_H}(\delta^*)_n^m = (-1) K^{2i}\left\{\nabla^{2i}(\delta^*) - (-1)^i\delta^*\left(2/a^2\right)^i\right\}, \tag{3.b.59}$$

using $i = 1$ or 2 as appropriate for the ∇^2 or ∇^4 forms. These coefficients are transformed to grid space following (3.b.1) for the T term and (3.b.55) and (3.b.56) for vorticity and divergence. Thus, the vorticity and divergence diffusion tendencies are converted to equivalent U and V diffusion tendencies.

Horizontal diffusion correction

After grid–point values are calculated, frictional heating rates are determined from the momentum diffusion tendencies and are added to the temperature, and the partial correction of the ∇^4 diffusion from η to p surfaces is applied to T. The frictional heating rate is calculated from the kinetic energy tendency produced by the momentum diffusion

$$F_{F_H} = -u^{n-1}F_{u_H}(u^*)/c_p^* - v^{n-1}F_{v_H}(v^*)/c_p^*, \tag{3.b.60}$$

where F_{u_H}, and F_{v_H} are the momentum equivalent diffusion tendencies, determined from F_{ζ_H} and F_{δ_H} just as U and V are determined from ζ and δ, and

$$c_p^* = c_p \left[1 + \left(\frac{c_{p_v}}{c_p} - 1 \right) q^{n+1} \right] . \tag{3.b.61}$$

These heating rates are then combined with the correction,

$$\hat{T}_k^{n+1} = T_k^* + (2\Delta t F_{F_H})_k + 2\Delta t \left(\pi B \frac{\partial T^*}{\partial p} \right)_k K^{(4)} \nabla^4 \Pi^{n+1}. \tag{3.b.62}$$

The vertical derivatives of T^* (where the * notation is dropped for convenience) are defined by

$$\begin{aligned} \left(\pi B \frac{\partial T}{\partial p} \right)_1 &= \frac{\pi}{2\Delta p_1} \left[B_{1+\frac{1}{2}} (T_2 - T_1) \right] , \\ \left(\pi B \frac{\partial T}{\partial p} \right)_k &= \frac{\pi}{2\Delta p_k} \left[B_{k+\frac{1}{2}} (T_{k+1} - T_k) + B_{k-\frac{1}{2}} (T_k - T_{k-1}) \right] , \\ \left(\pi B \frac{\partial T}{\partial p} \right)_K &= \frac{\pi}{2\Delta p_K} \left[B_{K-\frac{1}{2}} (T_K - T_{K-1}) \right] . \end{aligned} \tag{3.b.63}$$

The corrections are added to the diffusion tendencies calculated earlier (3.b.57) to give the total temperature tendency for diagnostic purposes:

$$\hat{F}_{T_H}(T^*)_k = F_{T_H}(T^*)_k + (2\Delta t F_{F_H})_k + 2\Delta t B_k \left(\pi \frac{\partial T^*}{\partial p} \right)_k K^{(4)} \nabla^4 \Pi^{n+1}. \tag{3.b.64}$$

c. Semi-Lagrangian Transport

The forecast equation for water vapor specific humidity and constituent mixing ratio in the η system is from (3.a.36) excluding sources and sinks.

$$\frac{dq}{dt} = \frac{\partial q}{\partial t} + \mathbf{V} \cdot \nabla q + \dot{\eta} \frac{\partial p}{\partial \eta} \frac{\partial q}{\partial p} = 0 \tag{3.c.1}$$

or

$$\frac{dq}{dt} = \frac{\partial q}{\partial t} + \mathbf{V} \cdot \nabla q + \dot{\eta} \frac{\partial q}{\partial \eta} = 0. \tag{3.c.2}$$

Equation (3.c.2) is more economical for the semi-Lagrangian vertical advection, as $\Delta\eta$ does not vary in the horizontal, while Δp does. Written in this form, the η advection equations look exactly like the σ equations.

These are the necessary equations for the time split subset (2.a.3b). For simplicity, in this section we will use the notation adopted in the previous section, *i.e.*, $(\ )^{n-1}$ for

$(\ )^-$ of (2.a.3b) and $(\ )^{n+1}$ for $(\hat{\ })^+$. Thus, the tendency sources have already been added to the time level labeled $(n-1)$ here. The semi-Lagrangian advection step (2.a.3b) is further subdivided into horizontal and vertical advection sub-steps, which, in an Eulerian form, would be written

$$q^* = q^{n-1} + 2\Delta t\,(\mathbf{V}\cdot\nabla q)^n \tag{3.c.3}$$

and

$$q^{n+1} = q^* + 2\Delta t\left(\dot{\eta}\frac{\partial q}{\partial n}\right)^n . \tag{3.c.4}$$

In the semi-Lagrangian form used here, the general form is

$$q^* = \mathrm{L}_{\lambda\varphi}\left(q^{n-1}\right), \tag{3.c.5}$$

$$q^{n+1} = \mathrm{L}_{\eta}\left(q^*\right). \tag{3.c.6}$$

Equation (3.c.5) represents the horizontal interpolation of q^{n-1} at the departure point calculated assuming $\dot{\eta}=0$. Equation (3.c.6) represents the vertical interpolation of q^* at the departure point, assuming $\mathbf{V}=0$.

The horizontal departure points are found by first iterating for the mid-point of the trajectory, using winds at time n, and a first guess as the location of the mid-point of the previous time step

$$\lambda_M^{k+1} = \lambda_A - \Delta t u^n\left(\lambda_M^k, \varphi_M^k\right)/a\cos\varphi_M^k, \tag{3.c.7}$$

$$\varphi_M^{k+1} = \varphi_A - \Delta t v^n\left(\lambda_M^k, \varphi_M^k\right)/a, \tag{3.c.8}$$

where subscript A denotes the arrival (Gaussian grid) point and subscript M the midpoint of the trajectory. The velocity components at $\left(\lambda_M^k, \varphi_M^k\right)$ are determined by Lagrange cubic interpolation. For economic reasons, the equivalent Hermite cubic interpolant with cubic derivative estimates is used at some places in this code. The equations will be presented later.

Once the iteration of (3.c.7) and (3.c.8) is complete, the departure point is given by

$$\lambda_D = \lambda_A - 2\Delta t u^n\left(\lambda_M, \varphi_M\right)/a\cos\varphi_M, \tag{3.c.9}$$

$$\varphi_D = \lambda_A - 2\Delta t v^n\left(\lambda_M, \varphi_M\right)/a, \tag{3.c.10}$$

where the subscript D denotes the departure point.

The form given by (3.c.7) – (3.c.10) is inaccurate near the poles and thus is only used for arrival points equatorward of 70° latitude. Poleward of 70° we transform to a local geodesic coordinate for the calculation at each arrival point. The local geodesic coordinate is essentially a rotated spherical coordinate system whose equator goes through the arrival point. Details are provided in Williamson and Rasch (1989). The transformed system is rotated about the axis through $\left(\lambda_A - \frac{\pi}{2}, 0\right)$ and $\left(\lambda_A + \frac{\pi}{2}, 0\right)$, by an angle φ_A so the equator goes through (λ_A, φ_A). The longitude of the transformed system is chosen to be zero at the arrival point. If the local geodesic system is denoted by (λ', φ'), with velocities (u', v'), the two systems are related by

$$\sin\phi' = \sin\phi\cos\phi_A - \cos\phi\sin\phi_A\cos\left(\lambda_A - \lambda\right), \tag{3.c.11}$$

$$\sin\phi = \sin\phi'\cos\phi_A + \cos\phi'\sin\imath_A\cos\lambda' \ , \tag{3.c.12}$$

$$\sin\lambda'\cos\phi' = -\sin\left(\lambda_A - \lambda\right)\cos\phi \ , \tag{3.c.13}$$

$$\begin{aligned} v'\cos\phi' &= v\left[\cos\phi\cos\phi_A + \sin\phi\sin\phi_A\cos\left(\lambda_A - \lambda\right)\right] \\ &\quad - u\sin\phi_A\sin\left(\lambda_A - \lambda\right), \end{aligned} \tag{3.c.14}$$

$$u'\cos\lambda' - v'\sin\lambda'\sin\phi' = u\cos\left(\lambda_A - \lambda\right) + v\sin\phi\sin\left(\lambda_A - \lambda\right) \ . \tag{3.c.15}$$

The calculation of the departure point in the local geodesic system is identical to $(3.c.7)$–$(3.c.10)$ with all variables carrying a prime. The equations can be simplified by noting that $(\lambda'_A, \varphi'_A) = (0,0)$ by design and $u'(\lambda'_A, \varphi'_A) = u(\lambda_A, \varphi_A)$ and $v'(\lambda'_A, \varphi'_A) = v(\lambda_A, \varphi_A)$. The interpolations are always done in global spherical coordinates.

The interpolants are most easily defined on the interval $0 \le \theta \le 1$. Define

$$\theta = \left(x_D - x_i\right) / \left(x_{i+1} - x_i\right), \tag{3.c.16}$$

where x is either λ or φ and the departure point x_D falls within the interval (x_i, x_{i+1}). Following (23) of Rasch and Williamson (1990) with $r_i = 3$ the Hermite cubic interpolant is given by

$$\begin{aligned} q_D &= q_{i+1}\left[3 - 2\theta\right]\theta^2 - d_{i+1}\left[h_i\theta^2\left(1-\theta\right)\right] \\ &\quad + q_i\left[3 - 2\left(1-\theta\right)\right]\left(1-\theta\right)^2 + d_i\left[h_i\theta\left(1-\theta\right)^2\right] \end{aligned} \tag{3.c.17}$$

where q_i is the value at the grid point x_i, d_i is the derivative estimate given below, and $h_i = x_{i+1} - x_i$.

Following (3.2.12) and (3.2.13) of Hildebrand (1956), the Lagrangian cubic polynomial interpolant used for the velocity interpolation, is given by

$$f_D = \sum_{j=-1}^{2} \ell_j\left(x_D\right) f_{i+j} \tag{3.c.18}$$

where

$$\ell_j(x_D) = \frac{(x_D - x_{i-1})\dots(x_D - x_{i+j-1})(x_D - x_{i+j+1})\dots(x_D - x_{i+2})}{(x_{i+j} - x_{i-1})\dots(x_{i+j} - x_{i+j-1})(x_{i+j} - x_{i+j+1})\dots(x_{i+j} - x_{i+2})} \tag{3.c.19}$$

where f can represent either u or v, or their counterparts in the geodesic coordinate system.

The derivative approximations used in (3.c.17) for q are obtained by differentiating (3.c.18) with respect to x_D, replacing f by q and evaluating the result at x_D equal x_i and x_{i+1}. With these derivative estimates, the Hermite cubic interpolant (3.c.17) is equivalent to the Lagrangian (3.c.18). If we denote the four point stencil $(x_{i-1}, x_i, x_{i+1}, x_{i+2})$ by $(x_1, x_2, x_3, x_4,)$ the cubic derivative estimates are

$$\begin{aligned} d_2 = &\left[\frac{(x_2 - x_3)(x_2 - x_4)}{(x_1 - x_2)(x_1 - x_3)(x_1 - x_4)}\right] q_1 \\ &- \left[\frac{1}{(x_1 - x_2)} - \frac{1}{(x_2 - x_3)} - \frac{1}{(x_2 - x_4)}\right] q_2 \\ &+ \left[\frac{(x_2 - x_1)(x_2 - x_4)}{(x_1 - x_3)(x_2 - x_3)(x_3 - x_4)}\right] q_3 \\ &- \left[\frac{(x_2 - x_1)(x_2 - x_3)}{(x_1 - x_4)(x_2 - x_4)(x_3 - x_4)}\right] q_4 \end{aligned} \tag{3.c.20}$$

and

$$\begin{aligned} d_3 = &\left[\frac{(x_3 - x_2)(x_3 - x_4)}{(x_1 - x_2)(x_1 - x_3)(x_1 - x_4)}\right] q_1 \\ &- \left[\frac{(x_3 - x_1)(x_3 - x_4)}{(x_1 - x_2)(x_2 - x_3)(x_2 - x_4)}\right] q_2 \\ &- \left[\frac{1}{(x_1 - x_3)} + \frac{1}{(x_2 - x_3)} - \frac{1}{(x_3 - x_4)}\right] q_3 \\ &- \left[\frac{(x_3 - x_1)(x_3 - x_2)}{(x_1 - x_4)(x_2 - x_4)(x_3 - x_4)}\right] q_4 \end{aligned} \tag{3.c.21}$$

The two dimensional (λ, φ) interpolant is obtained as a tensor product application of the one-dimensional interpolants, with λ interpolations done first. Assume the departure point falls in the grid box $(\lambda_i, \lambda_{i+1})$ and $(\varphi_i, \varphi_{i+1})$. Four λ interpolations are performed to find q values at $(\lambda_D, \varphi_{j-1}), (\lambda_D, \varphi_j), (\lambda_D, \varphi_{j+1})$, and $(\lambda_D, \varphi_{j+2})$. This is followed by one interpolation in φ using these four values to obtain the value at (λ_D, φ_D).

Cyclic continuity is used in longitude. In latitude, the grid is extended to include a pole point (row) and one row across the pole. The pole row is set equal to the average of the row next to the pole for q and to wavenumber 1 components for u and v. The row across the pole is filled with the values from the first row below the pole shifted π in longitude for q and minus the value shifted by π in longitude for u and v.

Once the departure point is known, the constituent value of $q^* = q_D^{n-1}$ is obtained as indicated in (3.c.5) by Hermite cubic interpolation (3.c.17), with cubic derivative estimates (3.c.18) and (3.c.19) modified to satisfy the Sufficient Condition for Monotonicity with C° continuity (SCMO) described below. Define $\Delta_i q$ by

$$\Delta_i q = \frac{q_{i+1} - q_i}{x_{i+1} - x_i} \ . \tag{3.c.28}$$

First, if $\Delta_i q = 0$ then

$$d_i = d_{i+1} = 0 \ . \tag{3.c.29}$$

Then, if either

$$0 \leq \frac{d_i}{\Delta_i q} \leq 3 \tag{3.c.30}$$

or

$$0 \leq \frac{d_{i+1}}{\Delta_i q} \leq 3 \tag{3.c.31}$$

is violated, d_i or d_{i+1} is brought to the appropriate bound of the relationship. These conditions ensure that the Hermite cubic interpolant is monotonic in the interval $[x_i, x_{i+1}]$.

The horizontal semi-Lagrangian sub-step (3.c.5) is followed by the vertical step (3.c.6). The vertical velocity $\dot{\eta}$ is obtained from that diagnosed in the dynamical calculations (3.a.93) by

$$(\dot{\eta})_{k+\frac{1}{2}} = \left(\dot{\eta}\,\frac{\partial p}{\partial \eta}\right)_{k+\frac{1}{2}} \Bigg/ \left(\frac{p_{k+1} - p_k}{\eta_{k+1} - \eta_k}\right), \tag{3.c.32}$$

with $\eta_k = A_k + B_k$. Note, this is the only place that the model actually requires an explicit specification of η. The mid-point of the vertical trajectory is found by iteration

$$\eta_M^{k+1} = \eta_A - \Delta t \dot{\eta}^n \left(\eta_M^k\right) . \tag{3.c.33}$$

Note, the arrival point η_A is a mid-level point where q is carried, while the $\dot{\eta}$ used for the interpolation to mid-points is at interfaces. We restrict η_M by

$$\eta_1 \leq \eta_M \leq \eta_K, \tag{3.c.34}$$

which is equivalent to assuming that q is constant from the surface to the first model level and above the top q level. Once the mid-point is determined, the departure point is calculated from

$$\eta_D = \eta_A - 2\Delta t \dot{\eta}^n \left(\eta_M\right), \tag{3.c.35}$$

with the restriction

$$\eta_1 \leq \eta_D \leq \eta_K . \tag{3.c.36}$$

The appropriate values of $\dot{\eta}$ and q are determined by interpolation (3.c.17), with the derivative estimates given by (3.c.18) and (3.c.19) for $i = 2$ to $K - 1$. At the top and bottom we assume a zero derivative (which is consistent with (3.c.34) and (3.c.36)), $d_i = 0$ for the interval $k = 1$, and $\delta_{i+1} = 0$ for the interval $k = K - 1$. The estimate at the interior end of the first and last grid intervals is determined from an uncentered cubic approximation; that is d_{i+1} at the $k = 1$ interval is equal to d_i from the $k = 2$ interval, and d_i at the $k = K - 1$ interval is equal to d_{i+1} at the $k = K - 2$ interval. The monotonic conditions (3.c.30) to (3.c.31) are applied to the q derivative estimates.

d. Mass fixers

The fixers which ensure conservation (2.a.4) are applied to the dry atmospheric mass, water vapor specific humidity and constituent mixing ratios. For water vapor and atmospheric mass the desired discrete relations, following Williamson and Olson (1994) are

$$\int\limits_2 \pi^+ - \int\limits_3 q^+ \Delta p^+ = \mathbf{P}, \tag{3.d.1}$$

$$\int\limits_3 q^+ \Delta p^+ = \int\limits_3 q^- \Delta p^-, \tag{3.d.2}$$

where $\mathbf{P}$ is the dry mass of the atmosphere. From the definition of the vertical coordinate,

$$\Delta p = p_0 \Delta A + \pi \Delta B, \tag{3.d.3}$$

and the integral $\int\limits_2$ denotes the normal Gaussian quadrature while $\int\limits_3$ includes a vertical sum followed by Gaussian quadrature. The actual fixers are chosen to have the form

$$\pi^+ (\lambda, \varphi) = \mathbf{M} \hat{\pi}^+ (\lambda, \varphi) , \tag{3.d.4}$$

preserving the horizontal gradient of Π, which was calculated earlier during the inverse spectral transform, and

$$q^+ (\lambda, \varphi, \eta) = \hat{q}^+ + \alpha \eta \hat{q}^+ |\hat{q}^+ - q^-| . \tag{3.d.5}$$

In (3.d.4) and (3.d.5) the ($\hat{}$) denotes the provisional value before adjustment. The form (3.d.5) forces the arbitrary corrections to be small when the mixing ratio is small and when the change made to the mixing ratio by the advection is small. In addition, the η factor is included to make the changes approximately proportional to mass per unit volume (Rasch et al., 1995). Satisfying (3.d.1) and (3.d.2) gives

$$\alpha = \frac{\int\limits_3 q^- \Delta p^- - \int\limits_3 \hat{q}^+ p_0 \Delta A - M \int\limits_3 \hat{q}^+ \hat{\pi}^+ \Delta B}{\int\limits_3 \eta \hat{q}^+ |\hat{q}^+ - q^-| \, p_0 \Delta A + M \int\limits_3 \eta \hat{q}^+ |\hat{q}^+ - q^-| \hat{\pi}^+ \Delta B} \tag{3.d.6}$$

and

$$\mathbf{M} = \left(\mathbf{P} + \int\limits_3 q^- \Delta p^- \right) \Big/ \int\limits_2 \hat{\pi}^+ \; . \tag{3.d.7}$$

Note that water vapor and dry mass are corrected simultaneously. Additional advected constituents are treated as mixing ratios normalized by the mass of dry air. This choice was made so that as the water vapor of a parcel changed, the constituent mixing ratios would not change. Thus the fixers which ensure conservation involve the dry mass of the atmosphere rather than the moist mass as in the case of the specific humidity above. Let χ denote the mixing ratio of constituents, then the desired relationship for conservation is

$$\int\limits_3 \chi^+ (1 - q^+) \Delta p^+ = \int\limits_3 \chi^- (1 - q^-) \Delta p^- \tag{3.d.8}$$

Following Rasch et al. (1995) the change made by the fixer is the same form as (3.d.5)

$$\chi^+ (\lambda, \varphi, \eta) = \hat{\chi}^+ + \alpha_\chi \eta \hat{\chi}^+ |\hat{\chi}^+ - \chi^-| \tag{3.d.9}$$

Substituting (3.d.9) into (3.d.8) and using (3.d.4) through (3.d.7) gives

$$\alpha_\chi = \frac{\int\limits_3 \chi^- (1 - q^-) \Delta p^- - \int\limits_{A,B} \hat{\chi}^+ (1 - \hat{q}^+) \Delta \hat{p}^+ + \alpha \int\limits_{A,B} \hat{\chi}^+ \eta \hat{q}^+ |\hat{q}^+ - q^-| \Delta p}{\int\limits_{A,B} \eta \hat{\chi}^+ |\hat{\chi}^+ - \chi^-| (1 - \hat{q}^+) \Delta p - \alpha \int\limits_{A,B} \eta \hat{\chi}^+ |\hat{\chi}^+ - \chi^-| \eta \hat{q}^+ |\hat{q}^+ - q^-| \Delta p} \tag{3.d.10}$$

where the following shorthand notation is adopted

$$\int\limits_{A,B} (\quad) \Delta p = \int\limits_3 (\quad) p_0 \Delta A + M \int\limits_3 (\quad) p_s \Delta B \tag{3.d.11}$$

4. MODEL PHYSICS

4.1 Tendency Physics

As discussed earlier, the tendency physics include (in the following order) the parameterization of cloud amount; the evaluation of radiative fluxes and atmospheric heating rates; the evaluation of surface fluxes; update land surface properties; evaluation of free atmosphere vertical diffusivities, diagnosis of the PBL height, PBL diffusivities and non-local transport term followed by the vertical diffusion solution; evaluation of gravity wave drag tendencies; and Rayleigh friction. Note that for greater stability the formulation of many of these processes is implicit, and the time step is further sub-divided into time split steps for each component to make the solution of the tendency terms more practical. The final result of the evaluation of these processes is the net tendency attributable to the tendency physics as shown in ($2.a.7$). Also note that we use the more conventional p_s notation for surface pressure (as opposed to π) for the following model physics discussion.

a. Cloud Parameterization

Cloud amount (or cloud fraction), and the associated optical properties, are evaluated via a diagnostic method in CCM3. Although the basic approach is similar to what was employed in the CCM2, the specific techniques represent some of the more significant changes to the collection of model physics. The diagnosis of cloud fraction represents a generalization of the scheme introduced by Slingo (1987), and depends on relative humidity, vertical velocity, atmospheric stability, and the convective mass flux associated with parameterized moist convection (sections 4g and 4h). Three types of cloud are diagnosed by the scheme: convective cloud, layered cloud, and low-level marine stratus. Some of the major changes from Slingo (1987) are: clouds are allowed to form in any model layer, except the layer nearest the surface; low-level frontal clouds occur for all $\omega < \omega_c$ (where ω_c is an arbitrary threshold); the relative humidity thresholds for mid- and upper-level layered clouds are functions of atmospheric stability; and convective cloud amount is determined from the rate of convective overturning (as opposed to convective precipitation rate). The minimum convective cloud fraction requirement of 20% employed in the CCM2 has been removed.

Total column convective cloud amount is diagnosed from the presence and strength of moist convective activity. In particular, it is a function of the column averaged convective mass flux diagnosed by the moist convective parameterization (e.g., along the lines of Xu and Krueger, 1991) where

$$\overline{A}_{\rm conv} = 0.035 \ln(1.0 + \overline{M_c}) \; , \qquad (4.a.1)$$

where the vertically averaged convective mass flux $\overline{M_c}$ is given by

$$\overline{M_c} = \int_{p_T}^{p_s} m_c(p)dp / \int_{p_T}^{p_s} dp \ , \tag{4.a.1.1}$$

$m_c(p)$ is in units of mb/day, and $\overline{A}_{\rm conv}$ is not allowed to exceed 80%. The convective cloud amount in each model layer is assumed to be randomly overlapped within the convectively active region, the bounds of which are provided by the moist convection parameterization. Thus, the total cloud fraction in (4.a.1) is distributed in the vertical according to

$$A_{\rm conv} = 1.0 - (1.0 - \overline{A}_{\rm conv})^{1/N}, \tag{4.a.2}$$

where N is the number of model levels within the convectively active region. For the subsequent cloud fraction calculation, the large scale relative humidity within the grid box is adjusted to account for the assumption that the fraction of convective cloud, $\overline{A}_{\rm conv}$, is saturated. The specific humidity grid value itself is unchanged. Thus, the adjusted large scale relative humidity, $RH^{'}$, is given by

$$RH^{'} = \frac{RH - A_{\rm conv}}{1 - A_{\rm conv}} \ , \tag{4.a.3}$$

where RH is the actual grid box relative humidity. The remaining cloud types are diagnosed on the basis of $RH^{'}$. Frontal and tropical low cloud fraction, *i.e.,* clouds occurring below 750 mb, are diagnosed according to

$$A_c = \begin{cases} 0 & \omega > \omega_c \\ \left(\frac{\omega_c - \omega}{\omega_c}\right)\left(\frac{RH^{'} - RH^{low}_{min}}{1 - RH^{low}_{min}}\right)^2 & 0 \le \omega \le \omega_c \\ \left(\frac{RH^{'} - RH^{low}_{min}}{1 - RH^{low}_{min}}\right)^2 & \omega < 0 \end{cases} \tag{4.a.4}$$

while stratus associated with low-level inversions is determined from

$$A_c = \begin{cases} 0 & RH^{'} < 0.6 \\ (-6.67\frac{\partial\theta}{\partial p} - 0.667)\times & (1 - \frac{0.9 - RH^{'}}{0.3}) \times (\frac{P-750}{150}) \\ & 0.6 \le RH^{'} \le 0.9 \quad \text{and} \\ & \frac{\partial\theta}{\partial p} < -0.125, 750 \le p \le 900 \\ (-6.67\frac{\partial\theta}{\partial p} - 0.667)\times & (\frac{P-750}{150})\, RH^{'} > 0.9 \quad \text{and} \\ & \frac{\partial\theta}{\partial p} < -0.125 \end{cases} \tag{4.a.5}$$

where $\frac{\partial\theta}{\partial p}$ is the maximum inversion strength and $RH^{'}$ is the adjusted layer relative humidity given by (4.a.3). The pressure factor, $(\frac{P-750}{150})$, accounts for the transition from marine stratus clouds that occur in the presence of low level inversions to trade cumulus clouds that can occur for higher level inversions. The parameter ω_c is set to

50 mb/day, allowing low level clouds to form under weak subsidence conditions. The parameter RH_{min}^{low}, the relative humidity threshold for low cloud formation, is assumed to be 0.9 (*i.e.*, 90%) over open ocean, and 0.8 over land. This distinction is made to account for enhanced cloud drop nucleation (*i.e.*, at lower relative humidities) that can occur over CCN rich land areas.

Middle and upper level cloud is defined to occur between 750 mb and the uppermost model level (which relaxes an earlier constraint that clouds form only in the troposphere). Mid- and high-level stratified (or layered) cloud amount is determined from the relation

$$A_c = \left[max \left(0 \, , \, \frac{RH' - RH_{\mathrm{lim}}}{1 - RH_{\mathrm{lim}}} \right) \right]^2 , \tag{4.a.7}$$

$$RH_{\mathrm{lim}} = .999 - (1 - RH_{min}^{high}) \left[1 - \frac{N^2}{3.5 \times 10^{-4}} \right] , \tag{4.a.8}$$

where N^2 is the square of the Brunt-Väisällä frequency:

$$N^2 = -\frac{g^2 \rho}{\theta} \frac{\partial \theta}{\partial p} . \tag{4.a.9}$$

Note that the ratio $N^2 / 3.5 \times 10^{-4}$ is not allowed to exceed 1. The parameter RH_{min}^{high}, the relative humidity threshold for mid-level and high cloud formation, is assumed to be 0.9 (*i.e.*, 90%). The cloud cover in any layer is finally defined as

$$A_c = (1.0 - A_{conv}) A_c + A_{conv} \, , \tag{4.a.10}$$

where A_c is not allowed to exceed 0.999.

As in the CCM2, cloud optical properties in the CCM3 are accounted for using the Slingo (1989) parameterization for liquid water droplet clouds. This scheme relates the extinction optical depth, the single-scattering albedo, and the asymmetry parameter to the cloud liquid water path and cloud drop effective radius (see Section 4b). The latter two microphysical cloud properties were statically specified in the CCM2. In particular, in-cloud liquid water paths were evaluated from a prescribed, meridionally and height varying, but time independent, cloud liquid water density profile, $\rho_\ell(z)$. which was analytically determined on the basis of a meridionally specified liquid water scale height (e.g., see Kiehl et al., 1994; Kiehl, 1991). The cloud drop effective radius was simply specified to be 10μm for all clouds. The CCM3 continues to diagnose cloud optical properties, but relaxes the rigid CCM2 framework. CCM3 employs the same exponentially decaying vertical profile for in-cloud water concentration

$$\rho_\ell = \rho_\ell^0 e^{(-z/h_\ell)} . \tag{4.a.11}$$

where the reference value ρ_ℓ^0 is equal to 0.21 g m^{-3}. Instead of specifying a zonally symmetric meridional dependence for the cloud water scale height, h_ℓ, it is locally diagnosed as a function of the vertically integrated water vapor (precipitable water)

$$h_\ell = 700 \ln \left(1.0 + \frac{1}{g} \int_{p_T}^{p_s} q dp \right) . \tag{4.a.12}$$

The cloud water path is then determined by integrating the liquid water concentration using

$$\mathrm{CWP} = \int \rho_\ell dz, \tag{4.a.13}$$

which can be analytically evaluated for an arbitrary layer k as

$$\mathrm{CWP}\,(k) = \rho_\ell^0 h_\ell \left[e^{-z_{k+\frac{1}{2}}/h_\ell} - e^{-z_{k-\frac{1}{2}}/h_\ell} \right], \tag{4.a.14}$$

where $z_{k+\frac{1}{2}}$ and $z_{k-\frac{1}{2}}$ are the heights of the k^{th} layer interfaces.

Observational studies have shown a distinct difference between maritime and continental effective cloud drop size, r_e, for warm clouds. For this reason, the CCM3 differentiates between the cloud drop effective radius for clouds diagnosed over maritime and continental regimes (Kiehl, 1994). Over the ocean, the cloud drop effective radius for liquid water clouds, $r_{e\ell}$, is specified to be 10μm, as in the CCM2. Over land masses $r_{e\ell}$ is determined using

$$r_{e\ell} = \begin{cases} 5\ \mu\mathrm{m} & T > -10°C \\ 5 - 5\left(\frac{T+10}{20}\right)\mu\mathrm{m} & -30°C \le T \le -10°C \\ r_{ei} & T < -30°C \end{cases} \tag{4.a.14.1}$$

An ice particle effective radius, r_{ei}, is also diagnosed by CCM3, which at the moment amounts to a specification of ice radius as a function of normalized pressure

$$r_{ei} = \begin{cases} 10\ \mu\mathrm{m} & p/p_s > p_I^{high} \\ r_{ei}^{max} - (r_{ei}^{max} - r_{ei}^{min}) \left[\frac{(p/p_s) - p_I^{high}}{p_I^{high} - p_I^{low}} \right] \mu\mathrm{m} & p/p_s \le p_I^{high} \end{cases} \tag{4.a.15.1}$$

where $r_{ei}^{max} = 30\mu$m, $r_{ei}^{min} = 10\mu$m, $p_I^{high} = 0.4$, and $p_I^{low} = 0.0$. The fraction of the total cloud water in the form of ice particles is then determined using

$$f_{ice} = \begin{cases} 0 & T > -10°C \\ -0.05\,(T + 10) & -30°C \le T \le -10°C \\ 1 & T < -30°C \end{cases} \tag{4.a.16.1}$$

Finally, for diagnostic purposes, the CCM3 calculates three levels of cloud fraction, assuming random overlap. These diagnostics, denoted as low, middle, and high cloud, are bounded by the pressure levels p_s to 700 mb, 700 mb to 400 mb, and 400 mb to the model top.

b. Parameterization of Radiation

Diurnal cycle

In the standard configuration, both the longwave and shortwave heating rates are evaluated every model hour as discussed in the following sections. Between hourly evaluations, the longwave and shortwave fluxes and heating rates are held constant. The surface radiative fluxes are also fixed between hourly calculations.

The insolation at the top of the model atmosphere is given by

$$S_I = S_0 \epsilon \cos\zeta, \tag{4.b.1}$$

where S_0 is the solar constant, ζ is the solar zenith angle, and ϵ is the eccentricity factor (square of the ratio of mean to actual distance that depends on the time of year). We represent the annual and diurnal cycle of solar insolation with a repeatable solar year of exactly 365 days and with a mean solar day of exactly 24 hours, respectively. The repeatable solar year does not allow for leap years. The expressions defining the annual and diurnal variation of solar insolation are given by:

$$\cos\zeta = \sin\phi \sin\delta - \cos\phi \cos\delta \cos(2\pi t_{\mathrm{local}})$$

$$\epsilon = 1.000110 + .034221 \cos\theta_0 + .001280 \sin\theta_0 + .000719 \cos 2\theta_0 + .000077 \sin 2\theta_0$$

$$\delta = .006918 - .399912 \cos\theta_0 + .070257 \sin\theta_0 - .006758 \cos 2\theta_0 +$$

$$.000907 \sin 2\theta_0 - .002697 \cos 3\theta_0 + .001480 \sin 3\theta_0$$

where

$$\theta_0 = \frac{2\pi d}{365} (\text{mean orbit angle})$$

and

$$d = \text{calendar day of year} (= 0,\ \text{for January 1 and 364 for December 31})$$

$$\phi = \text{latitude in radians}$$

$$\delta = \text{solar declination in radians}$$

$$t_{\mathrm{local}} = \text{calendar day with local time (ranges from 0.0 to 365.0)}.$$

Note that the calendar day d varies continuously throughout the repeatable year and is updated every model time step.

The expression for $\cos\zeta$ was taken from Sellers (1965, p.15), while the expressions for ϵ and δ were obtained from Paltridge and Platt (1976), pages 57 and 63, respectively. The eccentricity factor ϵ is appropriate for the current earth orbit and, according to Paltridge and Platt (1976), is accurate to better than 10^{-4}. Maximum eccentricity factor (the orbit point closest to the sun (perhelion)) occurs about January 3 (calendar day 2.0), and minimum ϵ (the orbit point farthest from the sun (aphelion)) occurs about July 5 (calendar day 185).

The declination δ (the angle between the celestial equator and the sun) is appropriate for the present earth obliquity of about $23\frac{1}{2}°$. The declination expression above is accurate to better than $3'$ of arc (Paltridge and Platt, 1976); since the change in declination in 24 hours is never greater than $30'$ of arc, (and remembering that the disc of the sun itself subtends an angle of $\sim 30'$ of arc), the above expression is quite an adequate approximation. Minimum declination δ occurs on about December 22 (calendar day 355.0), and maximum declination δ occurs on about June 21 (calendar day 172.0).

It does not seem necessary to compute solar insolation more accurately (for example, accounting for equation of time changes in the solar day during the year, or accounting for long-term secular changes in orbit) for two reasons: (1) the solar insolation given above multiplies approximate factors dealing with the scattering and absorption in the model's atmosphere/surface system (for example, the surface albedos in the model are not known to an accuracy of better than 1–2% of solar insolation (Briegleb *et al.*, 1986), and (2) for multi-year model runs, it is desirable when looking at interannual variability that the solar insolation repeat precisely every year in order to eliminate this source of variation. The loss (in a run of larger than 4 years) of the leap year day seems an acceptable approximation since this loss would only amount to 5 days after a 20-year run, for example.

The local time ($t_{\rm local}$) in the expression for $\cos\zeta$ depends on the calendar day as well as model longitude:

$$t_{\rm local} = d + \frac{\lambda}{360°}, \tag{4.b.2}$$

where λ = model longitude in degrees starting from Greenwich running eastward. This would mean, for example, that a model calendar day d having no fraction (such as 182.00) would refer to local midnight at Greenwich, and to local noon at the date line (180° longitude).

Solar radiation

The δ-Eddington approximation of Joseph, Wiscombe, and Weinman (1976) and also Coakley, Cess and Yurevich, (1983) has been adopted and is described in Briegleb (1992). This approximation has been shown to simulate quite well the effects of multiple scattering.

The solar spectrum is divided into 18 discrete spectral intervals (7 for O_3, 1 for the visible, 7 for H_2O, and 3 for CO_2). The CCM3 model atmosphere consists of a discrete vertical set of horizontally homogeneous layers within which radiative heating rates are to be specified (see Figure 1). Each of these layers is considered to be a homogeneous combination of several radiatively active constituents. Solar irradiance, as well as surface reflectivity for direct and diffuse radiation in each spectral interval, are specified, as well as the cosine of the solar zenith angle.

The method involves evaluating the δ-Eddington solution for the reflectivity and transmissivity for each layer in the vertical. The layers are then combined together, accounting for multiple scattering between layers, which allows evaluation of upward and downward spectral fluxes at each interface boundary between layers. This procedure is repeated for all spectral intervals to accumulate broad band fluxes, from which the heating rate can be evaluated from flux differences across each layer.

The δ-Eddington approximation allows for gaseous absorption by O_3, CO_2, O_2, and H_2O. Molecular scattering and cloud water droplet scattering/absorption are included. A summary of the spectral intervals and the absorption/scattering data used in the formulation is given in Briegleb (1992).

For cloud scattering and absorption, the radiative parameterization of Slingo [1989] for liquid water droplet clouds is employed. In this parameterization, the optical properties of the cloud droplets are represented in terms of the prescribed cloud water path (CWP in units of kg m^{-2}, see 4.a.11–14) and effective radius, $r_e = \int r^3 n(r)dr / \int r^2 n(r)dr$, where $n(r)$ is the cloud drop size distribution over radius r.

Cloud radiative properties explicitly account for the phase of water. For shortwave radiation we use the following generalization of the expression used by Slingo (1989) for liquid water clouds. The cloud liquid optical properties, for each spectral interval, (extinction optical depth, single scattering albedo, asymmetry parameter and forward scattering parameter) are defined as,

$$\tau_l^c = CWP \left[a_l^i + \frac{b_l^i}{r_{el}} \right] (1 - f_{ice}) \tag{4.b.3}$$

$$\omega_l^c = 1 - c_l^i - d_l^i r_{el} \tag{4.b.4}$$

$$g_l^c = e_l^i + f_l^i r_{el} \tag{4.b.5}$$

$$f_l^c = \left(g_l^i\right)^2 \tag{4.b.6}$$

where superscript i denotes spectral interval. The spectral intervals and coefficients for liquid water are defined in Briegleb (1993). The radiative properties of ice cloud are defined by,

$$\tau_i^c = CWP \left[a_i^i + \frac{b_i^i}{r_{ei}} \right] f_{ice} \tag{4.b.7}$$

$$\omega_i^c = 1 - c_i^i - d_i^i r_{ei} \quad (4.b.8)$$

$$g_i^c = e_i^i + f_i^i r_{ei} \quad (4.b.9)$$

$$f_i^c = \left(g_i^i\right)^2 \quad (4.b.10)$$

where the subscript i denotes ice radiative properties. The values for the coefficients $a - f$ are based on the results of Ebert and Curry (1992) and are listed in Table 4.1 for the four pseudo-spectral intervals (.25-.69 μm, .69-1.19 μm, 1.19-2.38 μm, and 2.38-4.00 μm) employed in the CCM3 shortwave radiation model. Note that when $0 < f_{ice} < 1$, then the combination of these expression in (4.b.11 - 4.b.14) represent the radiative properties for a mixed phase cloud.

TABLE 4.1: Cloud ice radiative coefficients

Interval	a	b	c	d
1	3.448×10^{-3}	2.431	1.0×1.0^{-5}	0
2	3.448×10^{-3}	2.431	1.1×10^{-4}	1.405×10^{-5}
3	3.448×10^{-3}	2.431	1.861×10^{-2}	8.328×10^{-4}
4	3.448×10^{-3}	2.431	0.46658	2.05×10^{-5}

Partial cloudiness and cloud overlap radiative effects are represented in the following manner. A parameterization that gives results approximately equal to the random overlap assumption, *without* the computational cost of calculating the spectrum of cloud cases and which gives the proper limits of zero cloud cover and complete cloud cover in a single layer, is utilized. The cloud extinction optical depth (τ_c) for each layer is modified as: $\tau_c' = \tau_c A_c^{\frac{3}{2}}$ and A_c is the fractional cloud cover in the layer; the power $\frac{3}{2}$ was found necessary to give results approximately the same as the random overlap assumption. Despite the simplicity of this assumption for dealing with partial cloud cover and cloud overlap effects, the resulting heating rates in a cloudy atmosphere are well represented when compared with the benchmark calculations [see Briegleb, 1992].

A uniform (in space and time) background boundary layer aerosol is included in CCM3. The aerosol is well mixed in the bottom three layers of the model. The aerosol mass mixing ratio in these layers is specified to yield a visible optical depth of 0.14. We view this prescription of aerosol as a "place holder" for future implementations of various aerosol types that have realistic spatial and temporal variability. The optical properties of the aerosol are identical to sulfate aerosols described by Kiehl and Briegleb (1993).

The δ-Eddington scheme is implemented so that the solar radiation is evaluated once every model hour over the sunlit portions of the model earth. The surface albedo is specified in two wavebands (0.2-0.7 μm, and 0.7-5.0 μm) and distinguishes albedos for direct and diffuse incident radiation. Albedos for ocean surfaces, geographically varying land surfaces, and sea ice surfaces are distinguished. Ozone is prescribed, and CO_2 is assumed to be uniformly mixed with constant mass mixing ratio. Diagnostic cloud amount (A_c) is evaluated every model hour just prior to the solar radiation calculation.

For some diagnostic purposes, such as estimating cloud radiative forcing (Kiehl and Ramanathan, 1990) a clear-sky absorbed solar flux is required. A diagnostic calculation is included to give an estimate of clear-sky column absorbed and surface absorbed flux. For computational efficiency, the clear sky top of atmosphere and surface fluxes are evaluated assuming two homogeneous atmospheric layers. The top layer contains only O_3, while the lower layer contains all other absorbers/scatterers except clouds. The actual surface albedos are employed.

Details of the implementation are as follows. The CCM3 model atmosphere is divided into $K+1$ layers in the vertical; an extra top layer (beyond the K layers specified by CCM3) is added. This extra layer prevents excessive heating in the top layer when the top pressure is not very low; also, as the model does not specify absorber properties above its top layer, the optical properties of the top layer must be used for the extra layer. Layers are assumed to be horizontally and vertically homogeneous for each model gridpoint and are bounded vertically by layer interfaces. For each spectral band, upward and downward fluxes are computed on the layer interfaces (which include the surface and top interface). The spectral fluxes are summed and differenced across layers to evaluate the solar heating rate. The following discussion refers to each of the spectral intervals.

In general, several constituents absorb and/or scatter in each homogeneous layer (e.g. cloud, aerosol, gases...). Every constituent is defined in terms of a layer extinction optical depth τ, single scattering albedo ω, asymmetry parameter g, and the forward scattering fraction f. To define bulk layer properties, the combination formulas of Cess [1985] are used:

$$\tau = \sum_i \tau_i, \tag{4.b.11}$$

$$\omega = \frac{\sum_i \omega_i \tau_i}{\tau}, \tag{4.b.12}$$

$$g = \frac{\sum_i g_i \omega_i \tau_i}{\omega\tau}, \tag{4.b.13}$$

$$f = \frac{\sum_i f_i \omega_i \tau_i}{\omega\tau}, \tag{4.b.14}$$

where the sums are over all constituents.

The δ-Eddington solution for each layer requires scaled properties for τ, ω, g, given by the expressions:

$$\tau^* = \tau(1-\omega f), \tag{4.b.15}$$

$$\omega^* = \omega\left(\frac{1-f}{1-\omega f}\right), \tag{4.b.16}$$

$$g^* = \frac{g-f}{1-f}. \tag{4.b.17}$$

The scaling accounts for the scattering effects of the strong forward peak in particle scattering. The δ-Eddington nonconservative ($\omega < 1$) solutions for each layer for direct radiation at cosine zenith angle μ_0 are (following the notation of Coakley, Cess, and Yurevich, 1983):

$$R(\mu_0) = (\alpha-\gamma)\overline{T}e^{-\tau^*/\mu_0} + (\alpha+\gamma)\overline{R} - (\alpha-\gamma), \tag{4.b.18}$$

$$T(\mu_0) = (\alpha+\gamma)\overline{T} + (\alpha-\gamma)\overline{R}e^{-\tau^*/\mu_0} - (\alpha+\gamma-1)e^{-\tau^*/\mu_0}, \tag{4.b.19}$$

$$\overline{R} = (u+1)(u-1)(e^{\lambda\tau^*} - e^{-\lambda\tau^*})N^{-1}, \tag{4.b.10}$$

$$\overline{T} = 4uN^{-1}, \tag{4.b.21}$$

where

$$\alpha = \frac{3}{4}\omega^*\mu_0\left(\frac{1+g^*(1-\omega^*)}{1-\lambda^2\mu_0^2}\right), \tag{4.b.22}$$

$$\gamma = \frac{1}{2}\omega^*\left(\frac{1+3g^*(1-\omega^*)\mu_0^2}{1-\lambda^2\mu_0^2}\right), \tag{4.b.23}$$

$$N = (u+1)^2e^{\lambda\tau^*} - (u-1)^2e^{-\lambda\tau^*}, \tag{4.b.24}$$

$$u = \frac{3}{2}\left(\frac{1-\omega^*g^*}{\lambda}\right), \tag{4.b.25}$$

$$\lambda = \sqrt{3(1-\omega^*)(1-\omega^*g^*)}, \tag{4.b.26}$$

where R(μ_0), T(μ_0) are the layer reflectivity and transmissivity to direct radiation respectively, and $\overline{\mathrm{R}}$, $\overline{\mathrm{T}}$ are the layer reflectivity and transmissivity to diffuse radiation respectively. It should be noted that in some cases of small but nonzero ω, the diffuse reflectivity can be negative. For these cases, $\overline{\mathrm{R}}$ is set to 0, which produces negligible impact on fluxes and the heating rate.

To combine layers, it is assumed that radiation, once scattered, is diffuse and isotropic (including from the surface). For an arbitrary layer 1 (or combination of layers with radiative properties $R_1(\mu_0)$, $T_1(\mu_0)$,$\overline{R}_1$,$\overline{T}_1$) overlying layer 2 (or combination of layers with radiative properties $R_2(\mu_0)$, $T_2(\mu_0)$, and $\overline{R}_2$,$\overline{T}_2$), the combination formulas for direct and diffuse radiation incident from above are:

$$R_{12}(\mu_0) = R_1(\mu_0) + \frac{\overline{T}_1\{(T_1(\mu_0) - e^{-\tau_1^*/\mu_0})\overline{R}_2 + e^{-\tau_1^*/\mu_0}R_2(\mu_0)\}}{1 - \overline{R}_1\overline{R}_2}, \tag{4.b.27}$$

$$T_{12}(\mu_0) = e^{-\tau_1^*/\mu_0}T_2(\mu_0) + \frac{\overline{T}_2\{(T_1(\mu_0) - e^{-\tau_1^*/\mu_0}) + e^{-\tau_1^*/\mu_0}R_2(\mu_0)\overline{R}_1\}}{1 - \overline{R}_1\overline{R}_2}, \tag{4.b.28}$$

$$\overline{R}_{12} = \overline{R}_1 + \frac{\overline{T}_1\overline{R}_2\overline{T}_1}{1 - \overline{R}_1\overline{R}_2}, \tag{4.b.29}$$

$$\overline{T}_{12} = \frac{\overline{T}_1\overline{T}_2}{1 - \overline{R}_1\overline{R}_2}. \tag{4.b.30}$$

Note that the transmissions for each layer ($T_1(\mu_0), T_2(\mu_0)$) and for the combined layers ($T_{12}(\mu_0)$) are total transmissions, containing both direct and diffuse transmission. Note also that the two layers (or combination of layers), once combined, are no longer a homogeneous system.

To combine the layers over the entire column, two passes are made through the layers, one starting from the top and proceeding downward, the other starting from the surface and proceeding upward. (In passing from the top down, the layer δ-Eddington computation of R(μ_0), T(μ_0), $\overline{\mathrm{R}}$, $\overline{\mathrm{T}}$ is terminated if the total transmission to direct radiation for the spectral band (normalized to 1.0 at top) is less than .001; this produces a negligible error and saves computational overhead). The result is that for every interface, the following combined reflectivities and transmissivities are available:

$e^{-\tau^*/\mu_0}$ = direct beam transmission from top of atmosphere to the interface (τ^* is the scaled optical depth from top-of-atmosphere to the interface),

$R_{up}(\mu_0)$ = reflectivity to direct solar radiation of entire atmosphere *below* the interface,

$T_{dn}(\mu_0)$ = total transmission to direct solar radiation incident from above to entire atmosphere *above* the interface,

$\overline{R}_{up}$ = reflectivity of atmosphere *below* the interface to diffuse radiation from above,

$\overline{R}_{dn}$ = reflectivity of atmosphere *above* the interface to diffuse radiation from below.

With these quantities, the upward and downward fluxes at every interface can be computed. For example, the upward flux would be the directly transmitted flux ($e^{-\tau*/\mu_0}$) times the reflection of the entire column below the interface to direct radiation ($R_{up}(\mu_0)$), plus the diffusely transmitted radiation from above that reaches the interface ($T_{dn}(\mu_0) - e^{-\tau*/\mu_0}$) times the reflectivity of the entire atmosphere below the interface to diffuse radiation from above ($\overline{R}_{up}$), all times a factor that accounts for multiple reflections at the interface. A similar derivation of the downward flux is straightforward. The resulting expressions for the upward and downward flux are:

$$F_{up} = \frac{e^{-\tau^*/\mu_0} R_{up}(\mu_0) + (T_{dn}(\mu_0) - e^{-\tau^*/\mu_0})\overline{R}_{up}}{1 - \overline{R}_{dn}\overline{R}_{up}}, \tag{4.b.31}$$

$$\begin{aligned} F_{dn} &= e^{-\tau^*/\mu_0} \\ &+ \frac{(T_{dn}(\mu_0) - e^{-\tau^*/\mu_0}) + e^{-\tau^*/\mu_0} R_{up}(\mu_0)\overline{R}_{dn}}{1 - \overline{R}_{dn}\overline{R}_{up}}. \end{aligned} \tag{4.b.32}$$

The upward and downward spectral fluxes at each interface are summed to evaluate the spectrally integrated fluxes, then differenced to produce the solar heating rate,

$$Q_{\mathrm{sol}} = \frac{g}{c_p} \frac{F_{dn}\,(p_{k+1}) - F_{\mathrm{up}}\,(p_{k+1}) - F_{dn}\,(p_k) + F_{up}\,(p_k)}{p_{k+1} - p_k} \tag{4.b.33}$$

which is added to the nonlinear term (Q) in the thermodynamic equation.

Longwave radiation

The method employed in the CCM to represent longwave radiative transfer is based on an absorptivity/emissivity formulation (Ramanathan and Downey, 1986),

$$F^{\downarrow}(p) = B(0)\varepsilon(0,p) + \int_0^p \alpha(p,p')dB(p') \tag{4.b.34}$$

$$F^{\uparrow}(p) = B(T_s) - \int_p^{p_s} \alpha(p,p')dB(p') \tag{4.b.35}$$

where $B(T) = \sigma T^4$, is the Stefan-Boltzmann relation. α and ϵ are the absorptivity and emissivity,

$$\alpha(p,p') = \frac{\int_0^\infty \{dB_\nu(p')/dT(p')\}\,(1 - \mathcal{T}_\nu(p,p'))\,d\nu}{dB(p')/dT(p')} \tag{4.b.36}$$

$$\varepsilon(0,p) = \frac{\int_0^\infty B_\nu(\mathcal{T}_\infty)\,(1 - \mathcal{T}_\nu(0,p))\,d\nu}{B(0)} \tag{4.b.37}$$

where the integration is over wavenumber, ν. $B_\nu(p)$ is the Planck function, and $\mathcal{T}_\nu$ is the atmospheric transmission. Thus, to solve for fluxes at each model layer we need solutions to the following,

$$\int_0^\infty (1 - \mathcal{T}_\nu) F(B_\nu) d\nu \tag{4.b.38}$$

where $F(B_\nu)$ is the Planck function for the emissivity, or the derivative of the Planck function with respect to temperature for the absorptivity.

The general method employed for the solution of (4.b.38) for a given gas is based on the broad band model approach described by Kiehl and Briegleb (1991) and Kiehl and Ramanathan (1983). This approach is based on the earlier work of Ramanathan (1976). The broad band approach assumes that the spectral range of absorption by a gas is limited to a relatively small range in wavenumber, ν, and hence, can be evaluated at the band center, i.e.

$$\int_{\nu_1}^{\nu_2} (1 - \mathcal{T}_\nu) F\left(B_\nu\right) d\nu \approx F\left(B_{\bar{\nu}}\right) \int_{\nu_1}^{\nu_2} (1 - \mathcal{T}_\nu) d\nu = F(B_{\bar{\nu}}) A \tag{4.b.39}$$

where A is the band absorptance (or equivalent width) in units of cm^{-1}. Note that A, in general, is a function of the absorber amount, the local emitting temperature, and the pressure. Thus, the broad band model is based on finding analytic expressions for the band absorptance. Ramanathan (1976) proposed the following functional form for A,

$$A(u, T, P) = 2A_0 \ln \left\{ 1 + \frac{u}{\sqrt{4 + u(1 + 1/\beta)}} \right\} \tag{4.b.40}$$

where A_0 is an empirical constant, u is the scaled dimensionless path length,

$$u = \int \frac{S(T)}{A_0(T)} \mu \rho_a dz \tag{4.b.41}$$

where $S(T)$ is the band strength, μ is the mass mixing ratio of the absorber, ρ_a is the density of air. β is a line width factor,

$$\beta = \frac{4}{ud} \int \gamma(T) \left(\frac{P}{P_0}\right) du \tag{4.b.42}$$

where $\gamma(T)$ is the mean line halfwidth for the band, P is the atmospheric pressure and P_0 is a reference pressure and d is the mean line spacing for the band. The determination of γ, d, S from spectroscopic line databases, such as the FASCODE database is described in detail in Kiehl and Ramanathan (1983). Kiehl and Briegleb (1991) describe how (4.b.40) can be extended to account for sub-bands within a spectral region. Essentially, the argument in the log function is replaced by a summation over the subbands. This broad band formalism is employed for CO_2, O_3, CH_4, N_2O and minor absorption bands of CO_2, while for the CFCs we employ the exponential transmission approximation discussed by Ramanathan et al. (1985),

$$T = \exp\left[-D\left(S(T)/\Delta\nu\right)W\right] \tag{4.b.43}$$

where $\Delta\nu$ is the band width, and W is the absorber path length,

$$W = \int \mu\rho_a dz, \tag{4.b.44}$$

and D is a diffusivity factor. The final problem that must be incorporated into the broad band method is the overlap of one or more absorbers within the same spectral region. Thus, for the wavenumber range of interest, namely 500 to 1500 cm^{-1}, the radiative flux is determined in part by the integral,

$$\int_{500}^{1500} \left(1 - \mathcal{T}_\nu\right) F\left(B_\nu\right) d\nu \tag{4.b.45}$$

which can be re-formulated for given sub intervals in wavenumber as,

$$\begin{aligned}
\int_{500}^{1500} \left(1 - \mathcal{T}_\nu\right) F\left(B_\nu\right) d\nu &= \int_{500}^{750} \left(1 - \mathcal{T}^1_{CO_2}\mathcal{T}^1_{N_2O}\mathcal{T}_{H_2O}\right) F\left(B_\nu\right) d\nu \\
&+ \int_{750}^{820} \left(1 - \mathcal{T}^1_{CFC11}\mathcal{T}_{H_2O}\right) F\left(B_\nu\right) d\nu + \int_{820}^{880} \left(1 - \mathcal{T}^2_{CFC11}\mathcal{T}_{H_2O}\right) F\left(B_\nu\right) d\nu \\
&+ \int_{880}^{900} \left(1 - \mathcal{T}^1_{CFC12}\mathcal{T}_{H_2O}\right) F\left(B_\nu\right) d\nu + \int_{900}^{1000} \left(1 - \mathcal{T}^2_{CO_2}\mathcal{T}_{H_2O}\mathcal{T}^3_{CFC11}\mathcal{T}^2_{CFC12}\right) F\left(B_\nu\right) d\nu \\
&+ \int_{1000}^{1120} \left(1 - \mathcal{T}^3_{CO_2}\mathcal{T}_{O_3}\mathcal{T}_{H_2O}\mathcal{T}^4_{CFC11}\mathcal{T}^3_{CFC12}\right) F\left(B_\nu\right) d\nu \\
&+ \int_{1120}^{1170} \left(1 - \mathcal{T}^4_{CFC12}\mathcal{T}_{H_2O}\mathcal{T}^2_{N_2O}\right) F\left(B_\nu\right) d\nu + \int_{1170}^{1500} \left(1 - \mathcal{T}_{CH_4}\mathcal{T}^3_{N_2O}\mathcal{T}_{H_2O}\right) F\left(B_\nu\right) d\nu
\end{aligned} \tag{4.b.46}$$

The sub-intervals, in turn, can be reformulated in terms of the absorptance for a given gas and the "overlap" transmission factors that multiply this transmission. Note that in the broad band formulation there is an explicit assumption that these two are uncorrelated (see Kiehl and Ramanathan, 1983). The specific parameterizations for each of these sub-intervals depends on spectroscopic data particular to a given gas and absorption band for that absorber.

Major absorbers

Details of the parameterization for the three major absorbers, H_2O, CO_2 and O_3, are given in Ramanathan and Downey (1986), Kiehl and Briegleb (1991) and Ramanathan and Dickinson (1979), respectively. Therefore, we only provide a brief description of how these gases are treated in the CCM.

For CO_2

$$\alpha_{CO_2}(p,p') = \frac{1}{4\sigma T^3(p')}\frac{dB_{CO_2}}{dT'}(p')A_{CO_2}(p',p). \tag{4.b.47}$$

B_{CO_2} is evaluated for $\tilde{\nu} = 667$ cm^{-1}, where $A_{CO_2}(p', p)$ is the broad–band absorptance from Kiehl and Briegleb (1991). Similarly,

$$\epsilon_{CO_2}(0, p) = \frac{1}{\sigma T^4(0)} B_{CO_2}(0) A_{CO_2}(0, p). \tag{4.b.48}$$

For ozone,

$$\alpha_{O_3}(p, p') = \frac{1}{4\sigma T^3(p')} \frac{dB_{O_3}}{dT'}(p') A_{O_3}(p', p), \tag{4.b.49}$$

and

$$\epsilon_{O_3}(0, p) = \frac{1}{\sigma T^4(0)} B_{O_3}(0) A_{O_3}(0, p), \tag{4.b.50}$$

where A_{O_3} is the ozone broad–band absorptance from Ramanathan and Dickinson (1979). The longwave absorptance formulation includes a Voigt line profile effects for CO_2 and O_3. For the mid-to-upper stratosphere ($p \lesssim 10$mb), spectral absorption lines are no longer Lorentzian in shape. To account for the transition to Voigt lines a method described in Kiehl and Briegleb (1991) is employed. Essentially the pressure appearing in the mean line width parameter, γ,

$$\gamma = \gamma_o \frac{p}{p_0} \tag{4.b.51}$$

is replaced with

$$\gamma = \gamma_0 \left[\frac{p}{p_0} + \delta \sqrt{\frac{T}{250}} \right], \tag{4.b.52}$$

where $\delta = 5.0 \times 10^{-3}$ for CO_2 and $\delta = 2.5 \times 10^{-3}$ for O_3. These values insure agreement with line-by-line cooling rate calculations up to $p \approx 0.3$ mb. Water vapor cannot employ the broad–band absorptance method since H_2O absorption extends throughout the entire longwave region. Thus, we cannot factor out the Planck function dependence as in (4.b.39). The method of Ramanathan and Downey (1986) is used for water–vapor absorptivities and emissivities. The overlap treatment between water vapor and other gases is also described in Ramanathan and Downey (1986).

Trace gas paramaterizations

Methane. The radiative effects of methane are represented by the last term in (4.b.46). We re-write this in terms of the absorptivity due to methane as,

$$\int_{1170}^{1500} (1 - \mathcal{T}_{CH_4} \mathcal{T}^3_{N_2O} \mathcal{T}_{H_2O}) F(B_\nu)\, d\nu =$$
$$\int (1 - \mathcal{T}_{H_2O}) F(B_\nu)\, d\nu + \int \mathcal{A}_{CH_4} \mathcal{T}_{H_2O} F(B_\nu)\, d\nu + \int A^3_{N_2O} \mathcal{T}_{CH_4} \mathcal{T}_{H_2O} F(B_\nu)\, d\nu \tag{4.b.53}$$

Note that this expression also incorporates the absorptance due to the 7.7 micron band of nitrous oxide as well. The first term is due to the rotation band of water vapor and is already accounted for in the CCM radiation model by the parameterization described in Ramanathan and Downey (1986). The second term in (4.b.53) accounts for the absorptance due to the 7.7 micron band of methane. The spectroscopic parameters are from Donner and Ramanathan (1980). In terms of the broad band approximation we have,

$$\int \mathcal{A}_{CH_4} \mathcal{T}_{H_2O} F\left(B_\nu\right) d\nu \approx A_{CH_4} \bar{T}_{H_2O} F\left(B_{\bar{\nu}}\right) \tag{4.b.54}$$

where according to (4.b.40),

$$A_{CH_4} = 6.00444 \sqrt{T_p} \ln \left\{ 1 + \frac{u}{\sqrt{4 + u\left(1 + 1/\beta\right)}} \right\} \tag{4.b.55}$$

where T_p is a path weighted temperature,

$$T_p = \frac{\int T(p) dp}{\int dp} \tag{4.b.56}$$

The dimensionless path length is,

$$u = \frac{D \; 8.60957 \times 10^4}{g} \int \frac{\mu_{CH_4}}{\sqrt{T}} dp \tag{4.b.57}$$

and the mean line width factor is,

$$\beta = 2.94449 \frac{\int \frac{1}{T} \left(\frac{P}{P_0}\right) \mu_{CH_4} dp}{\int \frac{1}{\sqrt{T}} \mu_{CH_4} dp} \tag{4.b.58}$$

where μ_{CH_4} is the mass mixing ratio of methane, T is the local layer temperature in Kelvin and P is the pressure in Pascals, and P_0 is 1×10^5 Pa. D is a diffusivity factor of 1.66. The water vapor overlap factor for this spectral region is,

$$\bar{T}_{H_2O} = \exp(-U_{H_2O}) \tag{4.b.59}$$

where,

$$U_{H_2O} = D \int \mu_{H_2O} \left(\frac{P}{P_0}\right) \frac{dp}{g} \tag{4.b.60}$$

and μ_{H_2O} is the mass mixing ratio of water vapor.

Nitrous Oxide. For nitrous oxide there are three absorption bands of interest: 589, 1168 and 1285 cm^{-1} bands. The radiative effects of the 1285 cm^{-1} band is given by the last term in (4.b.53),

$$\int \mathcal{A}^3_{N_2O} \mathcal{T}_{CH_4} \mathcal{T}_{H_2O} F\left(B_\nu\right) d\nu \approx A^3_{N_2O} \bar{T}_{CH_4} \bar{T}_{H_2O} F\left(B_{\bar{\nu}}\right) \tag{4.b.61}$$

The absorptance for the 1285 cm^{-1} N_2O band is given by,

$$A^3_{N_2O} = 2.35558\sqrt{T_p}\ln\left\{1 + \frac{u^3_0}{\sqrt{4 + u^3_0\left(1 + 1/\beta^3_0\right)}} + \frac{u^3_1}{\sqrt{4 + u^3_1\left(1 + 1/\beta^3_1\right)}}\right\} \tag{4b.62}$$

where u^3_0, β^3_0 account for the fundamental transition, while u^3_1, β^3_1 account for the first "hot" band transition. These parameters are defined as,

$$u^3_0 = D\ 1.02346 \times 10^5 \int \frac{\mu_{N_2O}}{\sqrt{T}}\frac{dp}{g} \tag{4.b.63}$$

and,

$$\beta^3_0 = 19.399\frac{\int \frac{1}{\sqrt{T}}\left(\frac{P}{P_0}\right) du_0}{\int du^3_0} \tag{4.b.64}$$

While the "hot" band parameters are defined as,

$$u^3_1 = D\ 2.06646 \times 10^5 \int \frac{1}{\sqrt{T}} e^{-847.36/T}\mu_{N_2O}\frac{dp}{g} \tag{4.b.65}$$

and,

$$\beta^3_1 = 19.399\frac{\int \frac{1}{\sqrt{T}}\left(\frac{P}{P_0}\right) du^3_1}{\int du^3_1} \tag{4.b.66}$$

The overlap factors in (4.b.61) due to water vapor is the same factor defined by (4.b.59), while the overlap due to methane is obtained by using the definition of the transmission factor in terms of the equivalent width (Ramanathan, 1976),

$$\bar{\mathcal{T}}_{CH_4} = e^{-A_{CH_4}/2A_0} \tag{4.b.67}$$

Substitution of (4.b.55) into (4.b.61) leads to,

$$\bar{\mathcal{T}}_{CH_4} = \frac{1}{1 + 0.02\frac{u}{\sqrt{4 + u(1 + 1/\beta)}}} \tag{4.b.68}$$

where u and β are given by (4.b.57) and (4.b.58), respectively, and the 0.02 factor is an empirical constant to match the overlap effect obtained from narrow band model benchmark calculations. This factor can physically be justified as accounting for the fact that the entire methane band does not overlap the N_2O band.

The 1168 cm^{-1} N_2O band system is represented by the seventh term on the RHS of (4.b.46). This term can be re-written as,

$$\int_{1120}^{1170} (1 - \mathcal{T}^4_{CFC12}\mathcal{T}_{H_2O}\mathcal{T}^2_{N_2O})F(B_\nu)\,d\nu =$$
$$\int (1 - \mathcal{T}_{H_2O})F(B_\nu)\,d\nu + \int \mathcal{A}^4_{CFC12}\mathcal{T}_{H_2O}F(B_\nu)\,d\nu + \int \mathcal{A}^2_{N_2O}\mathcal{T}^4_{CFC12}\mathcal{T}_{H_2O}F(B_\nu)\,d\nu \tag{4.b.69}$$

where the last term accounts for the 1168 cm^{-1} N_2O band. For the broad band formulation this expression becomes,

$$\int \mathcal{A}^2_{N_2O}\mathcal{T}^4_{CFC12}\mathcal{T}_{H_2O}F(B_\nu)d\nu \approx A^2_{N_2O}\bar{T}^4_{CFC12}\bar{T}_{H_2O}F(B_{\bar{\nu}}) \tag{4.b.70}$$

The band absorptance for the 1168 cm^{-1} N_2O band is given by,

$$A^2_{N_2O} = 2.54034\sqrt{T_p}\ln\left\{1+\frac{u_0^2}{\sqrt{4+u_0^2\left(1+1/\beta_0^2\right)}}\right\} \tag{4.b.71}$$

where the fundamental band pathlength and mean line parameters can be simply expressed in terms of the parameters defined for the 1285 cm^{-1} band (eq. 4.b.63-4.b.64).

$$u_0^2 = 0.0333767u_0^3 \tag{4.b.72}$$

and,

$$\beta_0^2 = 0.982143\beta_0^3 \tag{4.b.73}$$

Note that the 1168 cm^{-1} band does not include a "hot" band transition. The overlap by water vapor includes the effects of water vapor rotation lines, the so called "e-type" and "p-type" continnua (e.g. Roberts et al., 1976). The combined effect of these three absorption features is,

$$\bar{T}_{H_2O} = \bar{T}_l\bar{T}_e\bar{T}_p \tag{4.b.74}$$

where the contribution by line absorption is modeled by a Malkmus model formulation,

$$\bar{T}_l = \exp\left\{-\delta_1\bar{\Pi}\left(\sqrt{1+\delta_2\frac{\bar{u}_l}{\bar{\Pi}}}-1\right)\right\} \tag{4.b.75}$$

where δ_1 and δ_2 are coefficients that are obtained by fitting (4.b.75) to the averaged transmission from a 10 cm^{-1} narrow band Malkmus. The path length $\bar{u}_l$ is,

$$\bar{u}_l = D\ \bar{\Phi}\int\rho_w\frac{dP}{g} \tag{4.b.76}$$

and,

$$\bar{\Pi} = \left(\frac{P}{P_0}\right)\left(\frac{\bar{\Psi}}{\bar{\Phi}}\right), \tag{4.b.77}$$

where $\bar{\Phi}$ and $\bar{\Psi}$ account for the temperature dependence of the spectroscopic parameters (Rodgers and Walshaw, 1966),

$$\bar{\Psi} = e^{-\alpha|T_p-250|-\beta|T_p-250|^2} \tag{4.b.78}$$

$$\bar{\Phi} = e^{-\alpha'|T_p-250|-\beta'|T_p-250|^2} \tag{4.b.79}$$

The coefficients for various spectral intervals are given in Table 4.3. The transmission due to the e-type continuum is given by,

$$\bar{T}_e = e^{-\delta_3\bar{u}_e} \tag{4.b.80}$$

where the pathlength is defined as,

$$\bar{u}_e = \frac{D}{P_0 \varepsilon g} \int e^{1800\left(\frac{1}{T} - \frac{1}{296}\right)} w_{H_2O}^2 P dP \qquad (4.b.81)$$

The p-type continuum is represented by

$$T_p = e^{-\delta_4 \bar{u}_p} \qquad (4.b.82)$$

where,

$$\bar{u}_p = \frac{D}{g P_0} \int e^{1800\left(\frac{1}{T} - \frac{1}{296}\right)} w_{H_2O} P dP \qquad (4.b.83)$$

The factors δ_1, δ_2, δ_3 and δ_4 are listed for specific spectral intervals in Table 4.2.

TABLE 4.2: Coefficients for the broad band water vapor overlap transmission factors

Index	$\nu_1 - \nu_2$	δ_1	δ_2	δ_3	δ_4
1	750 - 820	0.0468556	14.4832	26.1891	0.0261782
2	820 - 880	0.0397454	4.30242	18.4476	0.0369516
3	880 - 900	0.0407664	5.23523	15.3633	0.0307266
4	900 - 1000	0.0304380	3.25342	12.1927	0.0243854
5	1000 - 1120	0.0540398	0.698935	9.14992	0.0182932
6	1120 - 1170	0.0321962	16.5599	8.07092	0.0161418

TABLE 4.3: Coefficients for the Temperature Dependence Factors (4.b.78) and (4.b.79)

Index	$\nu_1 - \nu_2$	α	β	α'	β'
1	750 - 820	2.9129e-2	-1.3139e-4	3.0857e-2	-1.3512e-4
2	820 - 880	2.4101e-2	-5.5688e-5	2.3524e-2	-6.8320e-5
3	880 - 900	1.9821e-2	-4.6380e-5	1.7310e-2	-3.2609e-5
4	900 - 1000	2.6904e-2	-8.0362e-5	2.6661e-2	-1.0228e-5
5	1000 - 1120	2.9458e-2	-1.0115e-4	2.8074e-2	-9.5743e-5
6	1120 - 1170	1.9892e-2	-8.8061e-5	2.2915e-2	-1.0304e-4

The final N_2O band centered at 589 cm^{-1} is represented by the first term on the RHS of (4.b.46),

$$\begin{aligned} &\int_{500}^{750} \left(1 - \mathcal{T}_{CO_2}^1 \mathcal{T}_{N_2O}^1 \mathcal{T}_{H_2O}\right) F\left(B_\nu\right) d\nu = \\ &\int \left(1 - \mathcal{T}_{CO_2}^1 \mathcal{T}_{H_2O}\right) F\left(B_\nu\right) d\nu + \int \mathcal{A}_{N_2O}^1 \mathcal{T}_{CO_2}^1 \mathcal{T}_{H_2O} F\left(B_\nu\right) d\nu \end{aligned} \qquad (4.b.84)$$

where the last term in (4.b.84) represents the radiative effects of the 589 cm^{-1} N_2O band,

$$\int \mathcal{A}^1_{N_2O}\mathcal{T}^1_{CO_2}\mathcal{T}_{H_2O}F\left(B_\nu\right)d\nu \approx A^1_{N_2O}\bar{T}^1_{CO_2}\bar{T}_{H_2O}F\left(B_{\bar{\nu}}\right) \tag{4.b.85}$$

The absorptance for this band includes both the fundamental and hot band transitions,

$$A^1_{N_2O} = 2.65581\sqrt{T_p}\ln\left\{1 + \frac{u^1_0}{\sqrt{4 + u^1_0\left(1 + 1/\beta^1_0\right)}} + \frac{u^1_1}{\sqrt{4 + u^1_1\left(1 + 1/\beta^1_1\right)}}\right\} \tag{4.b.86}$$

where the pathlengths for this band can also be defined in terms of the 1285 cm^{-1} band path length and mean lines parameters (4.b.63 - 4.b.66),

$$u^1_0 = 0.100090u^3_0 \tag{4.b.87}$$

and,

$$\beta^1_0 = 0.964282\beta^3_0 \tag{4.b.88}$$

and,

$$u^1_1 = 0.0992746u^3_1 \tag{4.b.89}$$

and,

$$\beta^1_1 = 0.964282\beta^3_1 \tag{4.b.90}$$

The overlap effect of water vapor is given by the transmission factor for the 500 to 800 cm^{-1} spectral region defined by Ramanathan and Downey (1986) in their Table A2. This expression is thus consistent with the transmission factor for this spectral region employed for the water vapor formulation of the first term on the right hand side of (4.b.84). The overlap factor due to the CO_2 bands near 589 cm^{-1} is obtained from the formulation in Kiehl and Briegleb (1991),

$$\bar{T}^1_{CO_2} = \frac{1}{1 + 0.2\frac{u_{CO_2}}{\sqrt{4+u_{CO_2}\left(1+1/\beta_{CO_2}\right)}}} \tag{4.b.91}$$

where the functional form is obtained in the same manner as the transmission factor for CH_4 was determined in (4.b.67). The 0.2 factor is empirically determined by comparing (4.b.91) with results from 5 cm^{-1} Malkmus narrow band calculations. The pathlength parameters are given by,

$$u_{CO_2} = \frac{D\ 4.9411 \times 10^4\left(1 - e^{-960/T}\right)^3}{\sqrt{T_p}}e^{-960/T}\int w_{CO_2}\frac{dP}{g} \tag{4.b.92}$$

and,

$$\beta_{CO_2} = \frac{5.3228}{\sqrt{T_p}}\left\{\frac{P}{P_0} + 5 \times e^{-3}\sqrt{\frac{T}{250}\frac{T}{300}}\right\} \tag{4.b.93}$$

CFCs. The effects of both CFC11 and CFC12 are included by using the approach of Ramanathan et al. (1985). Thus, the band absorptance of the CFCs is given by,

$$A_{CFC} = \Delta\nu \left(1 - e^{-D\frac{S}{\Delta\nu}u_{CFC}}\right) \tag{4.b.94}$$

where $\Delta\nu$ is the width of the CFC absorption band, S is the band strength, u_{CFC} is the abundance of CFC (g cm^{-2}),

$$u_{CFC} = \int \mu_{CFC}\frac{dp}{g} \tag{4.b.95}$$

where μ_{CFC} is the mass mixing ratio of either CFC11 or CFC12. D is the diffusivity factor. In the linear limit $D = 2$, since (4.b.94) deviates slightly from the pure linear limit we let $D = 1.8$. We account for the radiative effects of four bands due to CFC11 and four bands due to CFC12. The band parameters used in (4.b.94) for these eighth bands are given in Table 4.4.

TABLE 4.4: Band Parameters for the CFCs transmission factors

Band Number	Band Center (cm^{-1})	$\Delta\nu$ (cm^{-1})	$S/\Delta\nu$ (cm^2 gm^{-1})
	CFC11		
1[1]	798	50	54.09
2[2]	846	60	5130.03
3[1]	933	60	175.005
4[2]	1085	100	1202.18
	CFC12		
1[1]	889	45	1272.35
2[2]	923	50	5786.73
3[2]	1102	80	2873.51
4[2]	1161	70	2085.59

[1]Data are from Kagann et al. (1983)
[2]Data are from Varanasi and Chudamani (1988)

The contribution by these CFC absorption bands is accounted for by the following terms in (4.b.46).

$$\int_{750}^{820} \left(1 - \mathcal{T}^1_{CFC11}\mathcal{T}_{H_2O}\right) F\left(B_\nu\right) d\nu = \int \left(1 - \mathcal{T}_{H_2O}\right) F\left(B_\nu\right) d\nu + \int \mathcal{A}^1_{CFC11}\mathcal{T}_{H_2O} F\left(B_\nu\right) d\nu \tag{4.b.96}$$

$$\int_{820}^{880} \left(1 - \mathcal{T}^2_{CFC11}\mathcal{T}_{H_2O}\right) F\left(B_\nu\right) d\nu = \int \left(1 - \mathcal{T}_{H_2O}\right) F\left(B_\nu\right) d\nu + \int \mathcal{A}^2_{CFC11}\mathcal{T}_{H_2O} F\left(B_\nu\right) d\nu \tag{4.b.97}$$

$$\int_{880}^{900} \left(1 - \mathcal{T}^1_{CFC12}\mathcal{T}_{H_2O}\right) F\left(B_\nu\right) d\nu = \int \left(1 - \mathcal{T}_{H_2O}\right) F\left(B_\nu\right) d\nu + \int \mathcal{A}^1_{CFC12}\mathcal{T}_{H_2O} F\left(B_\nu\right) d\nu \tag{4.b.98}$$

$$\begin{aligned} &\int_{900}^{1000} \left(1 - \mathcal{T}^2_{CO_2}\mathcal{T}_{H_2O}\mathcal{T}^3_{CFC11}\mathcal{T}^2_{CFC12}\right) F\left(B_\nu\right) d\nu = \int \left(1 - \mathcal{T}_{H_2O}\right) F\left(B_\nu\right) d\nu + \\ &\int \mathcal{A}^2_{CFC12}\mathcal{T}_{H_2O} F\left(B_\nu\right) d\nu + \int \mathcal{A}^3_{CFC11}\mathcal{T}_{H_2O}\mathcal{T}^2_{CFC12} F\left(B_\nu\right) d\nu + \\ &\int \mathcal{A}^2_{CO_2}\mathcal{T}_{H_2O}\mathcal{T}^3_{CFC11}\mathcal{T}^2_{CFC12} F\left(B_\nu\right) d\nu \end{aligned} \tag{4.b.99}$$

$$\begin{aligned} &\int_{1000}^{1120} \left(1 - \mathcal{T}^3_{CO_2}\mathcal{T}_{O_3}\mathcal{T}_{H_2O}\mathcal{T}^4_{CFC11}\mathcal{T}^3_{CFC12}\right) F\left(B_\nu\right) d\nu = \int \left(1 - \mathcal{T}_{H_2O}\right) F\left(B_\nu\right) d\nu + \\ &\int \mathcal{A}_{O_3}\mathcal{T}_{H_2O} F\left(B_\nu\right) d\nu + \\ &\int \mathcal{A}^3_{CO_2}\mathcal{T}_{O_3}\mathcal{T}_{H_2O}\mathcal{T}^4_{CFC11}\mathcal{T}^3_{CFC12} F\left(B_\nu\right) d\nu + \\ &\int \mathcal{A}^4_{CFC11}\mathcal{T}_{O_3}\mathcal{T}_{H_2O} F\left(B_\nu\right) d\nu + \int \mathcal{A}^3_{CFC12}\mathcal{T}_{O_3}\mathcal{T}_{H_2O} F\left(B_\nu\right) d\nu \end{aligned} \tag{4.b.100}$$

For the 798 cm^{-1} CFC11 band, the absorption effect is given by the second term on the right hand side of (4.*b*.96),

$$\int \mathcal{A}^1_{CFC11}\mathcal{T}_{H_2O} F\left(B_\nu\right) d\nu \approx A^1_{CFC11}\bar{T}_{H_2O} F\left(B_{\bar{\nu}}\right) \tag{4.b.101}$$

where the band absorptance for the CFC is given by (4.*b*.94) and the overlap factor due to water vapor is given by (4.*b*.74) using the index 1 factors from Tables 4.2 and 4.3. Similarly, the 846 cm^{-1} CFC11 band is represented by the second term on the RHS of (4.*b*.97),

$$\int \mathcal{A}^2_{CFC11}\mathcal{T}_{H_2O} F\left(B_\nu\right) d\nu \approx A^2_{CFC11}\bar{T}_{H_2O} F\left(B_{\bar{\nu}}\right) \tag{4.b.102}$$

where the H_2O overlap factor is given by index 2 in tables 4.2 and 4.3. The 933 cm^{-1} CFC11 band is given by the third term on the RHS of (4.*b*.99),

$$\int \mathcal{A}^3_{CFC11}\mathcal{T}_{H_2O}\mathcal{T}^3_{CFC12} F\left(B_\nu\right) d\nu \approx A^3_{CFC11}\bar{T}_{H_2O} T^3_{CFC12} F\left(B_{\bar{\nu}}\right) \tag{4.b.103}$$

where the H_2O overlap factor is defined as index 4 in Tables 4.2 and 4.3, and the CFC12 transmission factor is obtained from (4.*b*.94). The final CFC11 band centered at 1085 cm^{-1} is represented by the fourth term on the RHS of (4.*b*.100),

$$\int \mathcal{A}^4_{CFC11} \mathcal{T}_{O_3} \mathcal{T}_{H_2O} F(B_\nu)\, d\nu \approx A^4_{CFC11} \bar{T}_{O_3} \bar{T}_{H_2O} F(B_{\bar{\nu}}) \qquad (4.b.104)$$

where the transmission due to the 9.6 micron ozone band is defined similar to (4.*b*.91) for CO_2 as,

$$\bar{T}_{O_3} = \frac{1}{1 + \sum_{i=1}^{2} \frac{u^i_{O_3}}{\sqrt{4 + u^i_{O_3}\left(1 + 1/\beta^i_{O_3}\right)}}} \qquad (4.b.105)$$

where the pathlengths are defined in Ramanathan and Dickinson (1979). The H_2O overlap factor is defined by index 5 in Tables 4.2 and 4.3.

For the 889 cm^{-1} CFC12 band the absorption is defined by the second term in (4.*b*.98) as,

$$\int \mathcal{A}^1_{CFC12} \mathcal{T}_{H_2O} F(B_\nu)\, d\nu \approx A^1_{CFC12} \bar{T}_{H_2O} F(B_{\bar{\nu}}) \qquad (4.b.106)$$

where the H_2O overlap factor is defined by index 3 of Tables 4.2 and 4.3, and the CFC absorptance is given by (4.*b*.94). The 923 cm^{-1} CFC12 band is described by the second term in (4.*b*.99),

$$\int \mathcal{A}^2_{CFC12} \mathcal{T}_{H_2O} F(B_\nu)\, d\nu \approx A^2_{CFC12} \bar{T}_{H_2O} F(B_{\bar{\nu}}) \qquad (4.b.107)$$

where the H_2O overlap is defined as index 4 in Tables 4.2 and 4.3. The 1102 cm^{-1} CFC12 band is represented by the last term on the RHS of (4.*b*.100),

$$\int \mathcal{A}^3_{CFC12} \mathcal{T}_{O_3} \mathcal{T}_{H_2O} F(B_\nu)\, d\nu \approx A^3_{CFC12} \bar{T}_{O_3} \bar{T}_{H_2O} F(B_{\bar{\nu}}) \qquad (4.b.102)$$

where the transmission by ozone is described by (4.*b*.105) and the H_2O overlap factor is represented by index 5 in tables 1 and 2. The final CFC12 band at 1161 cm^{-1} is represented by the second term on the RHS of (4.*b*.69),

$$\int \mathcal{A}^4_{CFC12} \mathcal{T}_{H_2O} F(B_\nu)\, d\nu \approx A^4_{CFC12} \bar{T}_{H_2O} F(B_{\bar{\nu}}) \qquad (4.b.109)$$

where the H_2O overlap factor is defined as index 6 in Tables 4.2 and 4.3.

Minor CO_2 Bands. There are two minor bands of carbon dioxide that have been added to the CCM longwave model. These bands play a minor role in the present day radiative budget, but are very important for high levels of CO_2, such as during the Archean. The first band we consider is centered at 961 cm^{-1}. The radiative contribution of this band is represented by the last term in (4.*b*.99),

$$\int \mathcal{A}^2_{CO_2} \mathcal{T}_{H_2O} \mathcal{T}^3_{CFC11} \mathcal{T}^2_{CFC12} F(B_\nu)\, d\nu \approx A^2_{CO_2} \bar{T}_{H_2O} \bar{T}^3_{CFC11} \bar{T}^2_{CFC12} F(B_{\bar{\nu}}) \qquad (4.b.110)$$

where the transmission factors for water vapor, CFC11 and CFC12 are defined in the previous section for the 900 to 1000 cm^{-1} spectral interval. The absorptance due to CO_2 is given by,

$$A^2_{CO_2} = 3.8443\sqrt{T_p}\ln\left\{1 + \sum_{i=1}^{3}\frac{u_i}{\sqrt{4 + u_i\left(1 + 1/\beta_i\right)}}\right\} \tag{4.b.111}$$

where the pathlength parameters are defined as,

$$u_1 = 3.88984 \times 10^3\alpha\left(T_p\right) we^{-1997.6/T} \tag{4.b.112}$$

$$u_1 = 3.88984 \times 10^3\alpha\left(T_p\right) we^{-1997.6/T} \tag{4.b.113}$$

$$u_3 = 6.50642 \times 10^3\alpha\left(T_p\right) we^{-2989.7/T} \tag{4.b.114}$$

and the pressure parameter is,

$$\beta_1 = 2.97558\left(\frac{P}{P_0}\right)\frac{1}{\sqrt{T}} \tag{4.b.115}$$

$$\beta_2 = \beta_1 \tag{4.b.116}$$

$$\beta_3 = 2\beta_1 \tag{4.b.117}$$

and,

$$\alpha\left(T_p\right) = \frac{\left(1 - e^{-1360.0/T_p}\right)^3}{\sqrt{T_p}} \tag{4.b.118}$$

The CO_2 band centered at 1064 cm^{-1} is represented by the third term on the RHS of (4.b.100),

$$\int \mathcal{A}^3_{CO_2}\mathcal{T}_{O_3}\mathcal{T}_{H_2O}\mathcal{T}^4_{CFC11}\mathcal{T}^3_{CFC12}F(B_\nu)d\nu \approx A^3_{CO_2}\bar{T}_{O_3}\bar{T}_{H_2O}\bar{T}^4_{CFC11}\bar{T}^3_{CFC12}F(B_{\bar{\nu}}) \tag{4.b.119}$$

where the transmission factors due to ozone, water vapor, CFC11 and CFC12 are defined in the previous section. The absorptance due to the 1064 cm^{-1} CO_2 band is given by,

$$A^3_{CO_2} = 3.8443\sqrt{T_p}\ln\left\{1 + \sum_{i=1}^{3}\frac{u_i}{\sqrt{4 + u_i\left(1 + 1/\beta_i\right)}}\right\} \tag{4.b.120}$$

where the dimensionless pathlength is defined as,

$$u_1 = 3.42217 \times 10^3\alpha\left(T_p\right) we^{-1849.7/T} \tag{4.b.121}$$

$$u_2 = 6.02454 \times 10^3\alpha\left(T_p\right) we^{-2782.1/T} \tag{4.b.122}$$

$$u_3 = 5.53143 \times 10^3\alpha\left(T_p\right) we^{-3723.2/T} \tag{4.b.123}$$

where

$$\alpha\left(T_p\right) = \frac{\left(1 - e^{-1540.0/T_p}\right)^3}{\sqrt{T_p}} \tag{4.b.124}$$

The pressure factor, β_1, for (4.b.120) is the same as defined in (4.b.115), while the other factors are,

$$\beta_2 = 2\beta_1 \tag{4.b.125}$$

$$\beta_3 = \beta_2 \tag{4.b.126}$$

In the above expressions, w is the column mass abundance of CO_2,

$$w = \int \mu_{CO_2} \frac{dP}{g} = \frac{\mu_{CO_2}}{g} \Delta P \tag{4.b.127}$$

where μ_{CO_2} is the mass mixing ratio of CO_2 (assumed constant).

Mixing ratio of trace gases

The mixing ratios of methane, nitrous oxide, CFC11 and CFC12 are specified as zonally averaged quantities. The stratospheric mixing ratios of these various gases do vary with latitude. This is to mimic the effects of stratospheric circulation on these tracers. The exact latitude dependence of the mixing ratio scale height was based on information from a two dimensional chemical model (S. Solomon, personal communication). In the troposphere the gases are assumed to be well mixed,

$$\mu^0_{CH_4} = 0.55241 w_{CH_4} \tag{4.b.128}$$

$$\mu^0_{N_2O} = 1.51913 w_{N_2O} \tag{4.b.129}$$

$$\mu^0_{CFC11} = 4.69548 w_{CFC11} \tag{4.b.130}$$

$$\mu^0_{CFC12} = 4.14307 w_{CFC12} \tag{4.b.131}$$

where w denotes the volume mixing ratio of these gases. The CCM3 employs volume mixing ratios for the year 1992 based on the 1994 IPCC report, $w_{CH_4} = 1.714$ *ppmv*, $w_{N_2O} = 0.311$ *ppmv*, $w_{CFC11} = 0.280$ *ppbv* and $w_{CFC12} = 0.503$ *ppbv*. The pressure level (mb) of the tropopause is defined as,

$$p_{trop} = 250.0 - 150.0 \cos^2 \phi \tag{4.b.126}$$

For $p \leq p_{trop}$, the stratospheric mixing ratios are defined as,

$$\mu_{CH_4} = \mu^0_{CH_4} \left(\frac{p}{p_{trop}} \right)^{X_{CH_4}} \tag{4.b.133}$$

$$\mu_{N_2O} = \mu^0_{N_2O} \left(\frac{p}{p_{trop}} \right)^{X_{N_2O}} \tag{4.b.134}$$

$$\mu_{CFC11} = \mu^0_{CFC11} \left(\frac{p}{p_{trop}} \right)^{X_{CFC11}} \tag{4.b.135}$$

$$\mu_{CFC12} = \mu^0_{CFC12} \left(\frac{p}{p_{trop}} \right)^{X_{CFC12}} \tag{4.b.136}$$

where the mixing ratio scale heights are defined as,

$$\left.\begin{aligned} X_{CH_4} &= 0.2353 \\ X_{N_2O} &= 0.3478 + 0.00116\,|\phi| \\ X_{CFC11} &= 0.7273 + 0.00606\,|\phi| \\ X_{CFC12} &= 0.4000 + 0.00222\,|\phi| \end{aligned}\right\} |\phi| \leq 45 \tag{4.b.137}$$

and,

$$\left.\begin{aligned} X_{CH_4} &= 0.2353 + 0.22549\,|\phi| \\ X_{N_2O} &= 0.4000 + 0.01333\,|\phi| \\ X_{CFC11} &= 1.0000 + 0.01333\,|\phi| \\ X_{CFC12} &= 0.5000 + 0.02444\,|\phi| \end{aligned}\right\} |\phi| \geq 45 \tag{4.b.138}$$

where ϕ is latitude in degrees.

Cloud emissivity

The cloud emissivity is accounted for by defining an effective cloud amount for each model layer,

$$A_c' = \epsilon_{cld} A_c \tag{4.b.139}$$

The cloud emissivity is defined as,

$$\epsilon_{cld} = 1 - e^{-D\kappa_{abs} CWP} \tag{4.b.140}$$

where D is a diffusivity factor set to 1.66, κ_{abs} is the longwave absorption coefficient ($m^2 g^{-1}$), and CWP is the cloud water path (gm^{-2}). The absorption coefficient is defined as,

$$\kappa_{abs} = \kappa_l \left(1 - f_{ice}\right) + \kappa_i f_{ice} \tag{4.b.141}$$

where κ_l is the longwave absorption coefficient for liquid cloud water and has a value of 0.090361, such that $D\kappa_l$ is 0.15. κ_i is the absorption coefficient for ice clouds and is based on a broad band fit to the emissivity given by Ebert and Curry's formulation,

$$\kappa_i = 0.005 + \frac{1}{r_{ei}}. \tag{4.b.142}$$

Numerical algorithms

The downward longwave clear–sky flux at the surface is,

$$F_{clr}^{\downarrow}(p_s) = B(0)\epsilon(0, p_s) + \int_o^{p_s} \alpha(p', p_s) \frac{dB}{dp'}(p')dp', \tag{4.b.143}$$

while the upward flux at the surface is just

$$F^{\uparrow}(p_s) = \sigma_B T_S^4. \tag{4.b.144}$$

The downward cloudy–sky flux at the surface is

$$F^{\downarrow}(p_s) = F^{\downarrow}_{clr}(p_s) f_{clear} + \sigma T^4(p_{clbk}) A'(p_{cl2})$$

$$+ \sum_{k=3}^{K} \left\{ \sigma T^4(p_{clbk}) + \int_{p_{clbk}}^{p_s} \alpha(p_s, p') \frac{dB(p')}{dp'} dp' \right\} f_{cld}(k), \tag{4.b.145}$$

where p_{clbk} is the pressure level of the cloud <u>base</u> at k.

$f_{cld}(k)$ is the probability of a cloud existing in layer k, and clear sky below this layer,

$$f_{cld}(k) = A'_k \prod_{i=2}^{k-1} (1 - A'_i), \tag{4.b.146}$$

or

$$f_{cld}(k) = A'_k \frac{\prod_{i=2}^{K} (1 - A'_i)}{\prod_{i=k}^{K} (1 - A'_i)}. \tag{4.b.147}$$

The clear-sky fraction for the total atmospheric column, f_{clear}, is given by

$$f_{clear} = \prod_{i=1}^{K} (1 - A'_i), \tag{4.b.148}$$

where A'_i is the fractional cloud cover in layer i and N is the total number of atmospheric layers.

Fluxes within the atmosphere are evaluated at each interface (Figure 1) so that longwave heating–rates are on model levels. The upward flux between the surface and the lowest cloud layer is equal to the clear–sky upward flux,

$$F^{\uparrow}_{blw}(p_k) = F^{\uparrow}_{clr}(p_k). \tag{4.b.149}$$

Within the layers that contain clouds, the upward flux is

$$F^{\uparrow}_{cld}(p_k) = F^{\uparrow}_{clr}(p_k) f_{clear}(k) + \sum_{\ell=k_{low}}^{k} \left\{ \sigma T^4(p_{cltl}) \right.$$

$$\left. - \int_{p_{cltl}}^{p_k} \alpha(p', p_{cltl}) \frac{dB}{dp'}(p') dp' \right\} \times f_{cld}(\ell) \quad p_{k_{low}} \leq p_k \leq p_{k+1}, \tag{4.b.150}$$

where $f_{cld}(\ell)$ is the probability that a cloud is in layer ℓ and clear sky exists <u>above</u> layer ℓ:

$$f_{cld}(\ell) = A'_\ell \prod_{i=\ell+1}^{k} (1 - A'_i) = A'_\ell \frac{\prod_{i=\ell+1}^{K} (1 - A'_i)}{\prod_{i=k+1}^{K} (1 - A'_i)}. \tag{4.b.151}$$

k_{low} is the lowest level of cloud, k_{HI} is the highest layer of cloud, and p_{cltl} is the cloud–top level. The upward flux above the clouds is obtained from a similar expression. The downward flux above the cloudy region is equal to the clear–sky flux,

$$F^{\downarrow}_{abv}(p_k) = F^{\downarrow}_{clr}(p_k). \tag{4.b.152}$$

Within the clouds and below the clouds, the downward flux is

$$F^{\downarrow}_{cld,blw}(p_k) = F^{\downarrow}_{clr}(p_k) f_{cld}(k) + \sum_{\ell=k}^{k_{HI}} \left\{ \sigma T^4(p_{clbl}) + \int_{p_{clbl}}^{p_k} \alpha(p', p) \frac{dB}{dp'}(p')dp' \right\} \tag{4.b.153}$$

$$\times f_{cld}(\ell), \qquad p_s \leq p_k \leq p_{HI},$$

where p_{clbl} is the cloud–base level, $f_{cld}(\ell)$ is the probability of a cloud existing in layer ℓ and clear sky below this level,

$$f_{cld(\ell)} = A'_\ell \prod_{i=k}^{\ell=1} (1 - A'_i) = A'_\ell \frac{\prod_{i=k}^{K} (1 - A'_i)}{\prod_{i=\ell}^{K} (1 - A'_i)}. \tag{4.b.154}$$

The longwave atmospheric heating rate is obtained from

$$Q_{\ell w}(p_k) = \frac{g}{c_p} \frac{F^{\uparrow}(p_{k+1}) - F^{\downarrow}(p_{k+1}) - F^{\uparrow}(p_k) + F^{\downarrow}(p_k)}{p_{k+1} - p_k}. \tag{4.b.155}$$

which is added to the nonlinear term (Q) in the thermodynamic equation.

The full calculation of longwave radiation (which includes heating rates as well as boundary fluxes) is computationally expensive. Therefore, modifications to the longwave scheme were developed to improve its efficiency for the diurnal framework. For illustration, consider the clear-sky fluxes defined in (4.b.34) and (4.b.35). Well over 90% of the longwave computational cost involves evaluating the absorptivity α and emissivity ϵ. To reduce this computational burden, α and ϵ are computed at a user defined frequency that is set to every 12 model hours in the standard configuration, while longwave heating rates are computed at the diurnal cycle frequency of once every model hour.

Calculation of α and ϵ with a period longer than the evaluation of the longwave heating rates neglects the dependence of these quantities on variations in temperature, water vapor, and ozone. However, variations in radiative fluxes due to changes in cloud amount are fully accounted for at each radiation calculation, which is regarded to be the dominant effect on diurnal time scales. The dominant effect on the heating rates of changes in temperature occurs through the Planck function and is accounted for with this method.

The continuous equations for the longwave calculations require a sophisticated vertical finite–differencing scheme due to the integral term $\int \alpha dB$ in Equations (4.b.34)–

(4.b.35). The reason for the additional care in evaluating this integral arises from the nonlinear behavior of α across a given model layer. For example, if the flux at interface p_k is required, an integral of the form $\int_{p_s}^{p_k} \alpha(p', p_k) dB(p')$ must be evaluated. For the nearest layer to level p_k, the following terms will arise:

$$\int_{p_{k+1}}^{p_k} \alpha(p', p_k) dB(p') = \frac{[\alpha(p_{k+1}, p_k) + \alpha(p_k, p_k)]}{2} [B(p_k) - B(p_{k+1})], \tag{4.b.156}$$

employing the trapezoidal rule. The problem arises with the second absorptivity $\alpha(p_k, p_k)$, since this term is zero. It is also known that α is nearly exponential in form within a layer. Thus, to accurately account for the variation of $\alpha(p, p')$ across a layer, many more grid points are required than are available in CCM3. The nearest layer must, therefore, be subdivided and α must be evaluated across the subdivided layers. The algorithm that is employed in is to use a trapezoid method for all layers <u>except</u> the nearest layer. For the nearest layer a subdivision, as illustrated in Figure 4, is employed.

For the upward flux, the nearest layer contribution to the integral is evaluated from

$$\int_{p_H^k}^{p_H^{k+1}} \alpha dB(p') = \alpha_{22} \left[B(p_H^{k+1}) - B(p^k)\right] + \alpha_{21} \left[B(p^k) - B(p_H^k)\right], \tag{4.b.157}$$

while for the downward flux, the integral is evaluated according to

$$\int_{p_H^{k+1}}^{p_H^k} \alpha dB(p') = \alpha_{11} \left[B(p^k) - B(p_H^k)\right] + \alpha_{12} \left[B(p_H^{k+1}) - B(p^k)\right]. \tag{4.b.158}$$

The α_{ij}, $i = 1, 2$; $j = 1, 2$, are absorptivities evaluated for the subdivided paths shown in Figure 4. The path–length dependence for the absorptivities arises from the dependence on the absorptance $A(p, p')$ [*e.g.*, Eq. (4.b.155)]. Temperatures are known at model levels. Temperatures at layer interfaces are determined through linear interpolation in $\log p$ between layer midpoint temperatures. Thus, $B(p_k) = \sigma_B T_k^4$ can be evaluated at all required levels. The most involved calculation arises from the evaluation of the fraction of layers shown in Figure 3. In general, the absorptance of a layer can require the evaluation of the following path lengths:

$$\xi(p_k, p_{k+1}) = f(\overline{T}) \overline{p} \Delta p, \tag{4.b.159}$$

and

$$u(p_k, p_{k+1}) = g(\overline{T}) \Delta p, \tag{4.b.160}$$

and

$$\beta(p_k, p_{k+1}) = h(\overline{T}) \overline{p}, \tag{4.b.161}$$

where f, g, and h are functions of temperature due to band parameters (see Kiehl and Ramanathan, 1983), and $\overline{T}$ is an absorber mass–weighted mean temperature.

These pathlengths are used extensively in the evaluation of A_{O_3} (Ramanathan and Dickinson, 1979) and A_{CO_2} (Kiehl and Briegleb, 1991) and the trace gases. But path

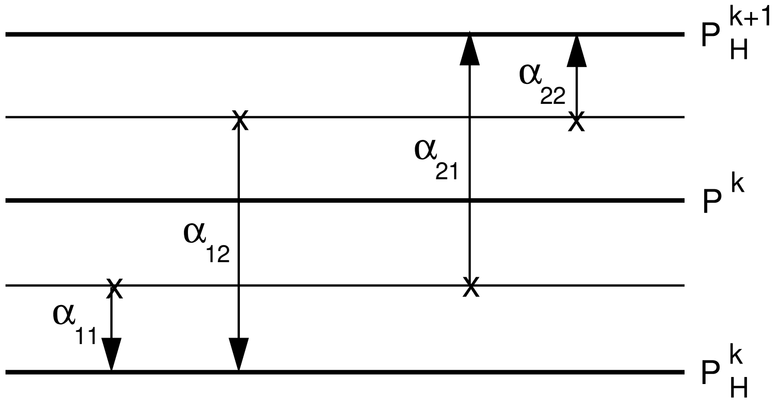

Figure 3. Subdivision of model layers for radiation flux calculation

lengths dependent on both p^2 (*i.e.*, ξ) and p (*i.e.*, u) are also needed in calculating the water–vapor absorptivity, α_{H_2O} (Ramanathan and Downey, 1986). To account for the subdivided layer, a fractional layer amount must be multiplied by ξ and u, *e.g.*,

$$\overline{\xi}_{11} = \xi(p_H^k p_H^{k+1}) \times UINPL(1,k), \tag{4.b.162}$$

$$\overline{u}_{11} = u(p_H^k, p_H^{k+1}) \times WINPL(1,k), \tag{4.b.163}$$

and

$$\overline{\beta}_{11} = \beta(p_H^k, p_H^{k+1}) \times PINPL(1,k), \tag{4.b.164}$$

where $UINPL$, $WINPL$, and $PINPL$ are factors to account for the fractional subdivided layer amount. These quantities are derived for the case where the mixing ratio is assumed to be constant within a given layer (CO_2 and H_2O). For ozone, the mixing ratio is assumed to interpolate linearly in physical thickness; thus, another fractional layer amount $ZINPL$ is required for evaluating $A_{O_3}(p,p')$ across subdivided layers.

Consider the subdivided path for α_{22}; the total path length from p_H^k to p_H^{k+1} for the p^2 path length will be

$$\xi(p_H^k, p_H^{k+1}) \approx \overline{p}_H \left[p_H^k - p_H^{k+1}\right], \tag{4.b.165}$$

where $\overline{p}_H \equiv \frac{p_H^k + p_H^{k+1}}{2}$. The <u>total</u> layer path length is, therefore, proportional to

$$\xi(p_H^k, p_H^{k+1}) \approx \frac{1}{2}\left(\left(p_H^k\right)^2 - \left(p_H^{k+1}\right)^2\right). \tag{4.b.166}$$

The path length ξ for α_{22} requires the mean pressure

$$\overline{p}_{22} \approx \frac{1}{2}\left\{\frac{p^k + p_H^{k+1}}{2} + p_H^{k+1}\right\}, \tag{4.b.167}$$

and the pressure difference

$$\Delta p_{22} \approx \frac{p^k + p_H^{k+1}}{2} - p_H^{k+1}. \tag{4.b.168}$$

Therefore, the path ξ_{22} is

$$\xi_{22} \approx \overline{p}_{22}\ \Delta p_{22} = \frac{1}{2}\left\{\left(\frac{p^k + p_H^{k+1}}{2}\right)^2 - \left(p_H^{k+1}\right)^2\right\}. \tag{4.b.169}$$

The fractional path length is obtained by normalizing this by $\xi(p_H^k, p_H^{k+1})$,

$$UINPL(2,k) = DAF3(k)\left\{\left(\frac{p^k + p_H^{k+1}}{2}\right)^2 - \left(p_H^{k+1}\right)^2\right\}, \tag{4.b.170}$$

where

$$DAF3(k) = \frac{1}{\left(p_H^k\right)^2 - \left(p_H^{k+1}\right)^2}. \tag{4.b.171}$$

Similar reasoning leads to the following expressions for the remaining fractional path lengths, for α_{21},

$$UINPL(3,k) = DAF3(k)\left\{\left(\frac{p^k + p_H^k}{2}\right)^2 - \left(p_H^{k+1}\right)^2\right\}, \tag{4.b.172}$$

for α_{11},

$$UINPL(1,k) = DAF3(k)\left\{\left(p_H^k\right)^2 - \left(\frac{p^k + p_H^k}{2}\right)^2\right\}, \tag{4.b.173}$$

and for α_{12},

$$UINPL(4,k) = DAF3(k)\left\{\left(p_H^k\right)^2 - \left(\frac{p^k + p_H^{k+1}}{2}\right)^2\right\}. \tag{4.b.174}$$

The $UINPL$ are fractional layer amounts for path length that scale as p^2, *i.e.*, $\overline{\xi}_{ij}$.

For variables that scale linearly in p, *e.g.*, $\overline{u}_{ij}$, the following fractional layer amounts are used:

$$WINPL(1,k) = DAF4(k)\left\{\frac{p_H^k - p^k}{2}\right\}, \tag{4.b.175}$$

$$WINPL(2,k) = DAF4(k)\left\{\frac{p^k - p_H^{k+1}}{2}\right\}, \tag{4.b.176}$$

$$WINPL(3,k) = DAF4(k)\left\{\left(\frac{p_H^k + p^k}{2}\right) - p_H^{k+1}\right\}, \tag{4.b.177}$$

$$WINPL(4,k) = DAF4(k)\left\{p_H^k - \left(\frac{p_H^{k+1}+p^k}{2}\right)\right\}, \tag{4.b.178}$$

where

$$DAF4(k) = \frac{1}{p_H^k - p_H^{k+1}}. \tag{4.b.179}$$

These fractional layer amounts are directly analogous to the $UINPL$, but since $\overline{u}$ is linear in p, the squared terms are not present.

The variable $\overline{\beta}_{ij}$ requires a mean pressure for the subdivided layer. These are

$$PINPL(1,k) = \frac{1}{2}\left\{\frac{p^k+p_H^k}{2} + p_H^k\right\}, \tag{4.b.180}$$

$$PINPL(2,k) = \frac{1}{2}\left\{\frac{p^k+p_H^{k+1}}{2} + p_h^{k+1}\right\}, \tag{4.b.181}$$

$$PINPL(3,k) = \frac{1}{2}\left\{\frac{p^k+p_H^k}{2} + p_H^{k+1}\right\}, \tag{4.b.182}$$

$$PINPL(4,k) = \frac{1}{2}\left\{\frac{p^k+p_H^{k+1}}{2} + p_H^k\right\}. \tag{4.b.183}$$

Finally, fractional layer amounts for ozone path lengths are needed, since ozone is interpolated linearly in physical thickness. These are given by

$$ZINPL(1,k) = \frac{1}{2}\frac{\ell n\left(\frac{p_H^k}{p_k}\right)}{\ell n\left(\frac{p_H^k}{p_H^{k+1}}\right)}, \tag{4.b.184}$$

$$ZINPL(2,k) = \frac{1}{2}\frac{\ell n\left(\frac{p^k}{p_H^{k+1}}\right)}{\ell n\left(\frac{p_H^k}{p_H^{k+1}}\right)}, \tag{4.b.185}$$

$$ZINPL(3,k) = ZINPL(1,k) + 2ZINPL(2,k), \tag{4.b.186}$$

$$ZINPL(4,k) = ZINPL(2,k) + 2ZINPL(1,k). \tag{4.b.187}$$

c. Surface Exchange Formulations

The surface exchange of heat, moisture and momentum between the atmosphere and land, ocean or ice surfaces are treated with a bulk exchange formulation. We present a description of each surface exchange separately. Although the functional forms of the exchange relations are identical, we present the descriptions of these components as developed and represented in the various subroutines in CCM3. The differences in the exchange expressions are predominantly in the definition of roughness lengths and exchange coefficients. The description of surface exchange over ocean and sea ice follows from Bryan et al. 1996

Land

Land surface fluxes of momentum, sensible heat, and latent heat are calculated from Monin-Obukhov similarity theory applied to the surface (i.e., constant flux) layer. The zonal τ_x and meridional τ_y momentum fluxes (kg m^{-1} s^{-2}) are

$$\tau_x = -\rho_1 \frac{(u_1 - u_s)}{r_{am}} \tag{4.c.1}$$

$$\tau_y = -\rho_1 \frac{(v_1 - v_s)}{r_{am}} \tag{4.c.2}$$

where ρ_1, u_1, and v_1 are the density (kg m^{-3}), zonal wind (m s^{-1}), and meridional wind (m s^{-1}) at the lowest model level. By definition, the surface winds u_s and v_s equal zero. r_{am} is the aerodynamic resistance (s m^{-1}) for momentum between the lowest model level at height z_1 and the surface at height $z_{0m} + d$, where z_{0m} is the roughness length (m) for momentum and d is the displacement height (m)

$$r_{am} = \frac{1}{k^2 |\mathbf{V}|_1} \left[\ln\left(\frac{z_1 - d}{z_{0m}}\right) - \psi_m(\zeta) \right] \left[\ln\left(\frac{z_1 - d}{z_{0m}}\right) - \psi_m(\zeta) \right] \tag{4.c.3}$$

where $k = 0.4$ is the von Karman constant and $|\mathbf{V}|_1 = \sqrt{u_1^2 + v_1^2}$. Atmospheric stability is defined by $\zeta = \dfrac{z_1 - d}{L}$. The length scale L (m) is

$$L = \frac{-u_*^3}{k\left(\frac{g}{T_{v1}}\right)\left(\frac{H + 0.61 c_p\, T_1\, E}{\rho_1 c_p}\right)} \tag{4.c.4}$$

where u_* is the friction velocity (m s^{-1}), g is gravitational acceleration (m s^{-2}), T_{v1} is the virtual temperature of the lowest model level (K), H is the sensible heat flux (W m^{-2}), c_p is the heat capacity of air (J kg^{-1} K^{-1}), T_1 is the temperature of the lowest model level (K), and E is the water vapor flux (kg m^{-2} s^{-1}). The term $0.61 c_p\, T_1\, E$ accounts for the buoyancy effects of water vapor. ψ_m is a function that increases this resistance for stable conditions ($\zeta > 0$) and decreases this resistance for unstable conditions ($\zeta < 0$)

$$\psi_m(\zeta) = -5\zeta \quad \text{for } \zeta > 0 \tag{4.c.5}$$

$$\psi_m(\zeta) = 2\ln\left(\frac{1+x}{2}\right) + \ln\left(\frac{1+x^2}{2}\right) - 2\tan^{-1}x + \frac{\pi}{2} \quad \text{for } \zeta < 0 \tag{4.c.6}$$

where $x = (1 - 16\zeta)^{1/4}$.

The sensible and latent heat fluxes are calculated in a manner analogous to the momentum fluxes, but are complicated by the need to partition these fluxes into ground and vegetation components. Land surface fluxes of sensible heat and latent heat are calculated by finding the vegetation T_v and ground T_g temperatures (K) that balance the vegetation and ground energy budgets

$$-\overrightarrow{S}_v + \overrightarrow{L}_v + H_v + \lambda E_v = 0 \tag{4.c.7}$$

$$-\overrightarrow{S}_g + \overrightarrow{L}_g + H_g + \lambda E_g + G = 0 \tag{4.c.8}$$

where $\overrightarrow{S}$ is the absorbed solar radiation (W m^{-2}), $\overrightarrow{L}$ is the absorbed longwave radiation (W m^{-2}), H is the sensible heat flux (W m^{-2}), λE is the latent heat flux (W m^{-2}), G is the soil heat flux (W m^{-2}), and the subscripts "v" and "g" indicated vegetation and ground, respectively. The solar radiation absorbed by the vegetation and the ground depends on the amount of leaf and stem material present (i.e., the leaf and stem areas), their optical properties, and the optical properties of snow and soil. The other terms in these two equations depend on the vegetation and ground temperatures, which are found through Newton-Raphson iteration. The soil heat flux is then used to melt snow, if the conditions are right, and to update soil temperatures for a six-layer soil column using a heat diffusion equation that accounts for phase change. The latent heat fluxes are used to update vegetation, snow, and soil water pools. Soilwater is calculated for the six-layer column using a one-dimensional conservation equation that accounts for infiltration input, gravitational drainage at the bottom of the column, evapotranspirational losses, and vertical water flow based on lead gradients.

The vegetation and ground sensible heat fluxes are

$$H_v = -\rho_1 c_p (T_s - T_v) c_{hv} \tag{4.c.9}$$

$$H_g = -\rho_1 c_p (T_s - T_g) c_{hg} \tag{4.c.10}$$

where T_s is the "surface" temperature (K). c_{hv} is a vegetation conductance (m s^{-1}) that depends on leaf and stem area and the wind within the canopy. c_{hg} is a ground conductance that depends on turbulent transfer processes within the vegetation canopy. The surface temperature T_s is eliminated from these equations by assuming the canopy air has negligible capacity to store heat so that the total sensible heat flux between the surface and the atmosphere is

$$H = -\rho_1 c_p \frac{(\theta_1 - T_s)}{r_{ah}} = H_v + H_g \tag{4.c.11}$$

where θ_1 is the potential temperature (K) at the lowest model level and r_{ah} is an aerodynamic resistance (s m^{-1}) for sensible heat.

Similarly, the vegetation and ground latent heat fluxes are

$$\lambda E_v = -\frac{\rho_1 c_p}{\gamma}[e_s - e_*(T_v)](c_{we} + c_{wt}) \tag{4.c.12}$$

$$\lambda E_g = -\frac{\rho_1 c_p}{\gamma}[e_s - e_*(T_g)] c_{wg} \tag{4.c.13}$$

where γ is the psychrometric constant (Pa K^{-1}), e_s is the vapor pressure (Pa) at the surface, and $e_*(T_v)$ and $e_*(T_g)$ are the saturation vapor pressures (Pa) evaluated at the vegetation and ground temperatures. c_{we} is a vegetation conductance for evaporation of intercepted water. It depends on leaf and stem area, the fraction of the canopy that is wet, and the wind within the canopy. Water is lost from the soil as transpiration from the non-wetted fraction of the canopy with a conductance c_{wt} that depends on leaf area, the wind within the canopy, and stomatal responses to light, temperature, soil water, vapor pressure, and CO_2 concentration. c_{wg} is a ground conductance for evaporation of soil water, which decreases as the soil becomes drier. The surface vapor pressure e_s is eliminated from these equations by assuming negligible capacity to store water vapor so that the total latent heat flux between the surface and the atmosphere is

$$\lambda E = -\frac{\rho_1 c_p}{\gamma} \frac{(e_1 - e_s)}{r_{aw}} = \lambda E_v + \lambda E_g \tag{4.c.14}$$

where e_1 is the vapor pressure (Pa) at the lowest model level and r_{aw} is an aerodynamic resistance (s m^{-1}) for water vapor.

The resistances r_{ah} and r_{aw} are analogous to the aerodynamic resistance for momentum

$$r_{ah} = \frac{1}{k^2 |\mathbf{V}|_1} \left[\ln\left(\frac{z_1 - d}{z_{0m}}\right) - \psi_m(\zeta) \right] \left[\ln\left(\frac{z_1 - d}{z_{0h}}\right) - \psi_h(\zeta) \right] \tag{4.c.15}$$

$$r_{aw} = \frac{1}{k^2 |\mathbf{V}|_1} \left[\ln\left(\frac{z_1 - d}{z_{0m}}\right) - \psi_m(\zeta) \right] \left[\ln\left(\frac{z_1 - d}{z_{0w}}\right) - \psi_w(\zeta) \right] \tag{4.c.16}$$

where z_{0h} and z_{0w} are the roughness lengths (m) for sensible and latent heat. ψ_h, and ψ_w are functions, similar to ψ_m, that increase these resistances for stable conditions ($\zeta > 0$) and decrease thse resistances for unstable conditions ($\zeta < 0$)

$$\psi_h(\zeta) = \psi_w(\zeta) = -5\zeta \quad \text{for } \zeta > 0 \tag{4.c.17}$$

$$\psi_h(\zeta) = \psi_w(\zeta) = 2 \ln\left(\frac{1 + x^2}{2}\right) \quad \text{for } \zeta < 0 \tag{4.c.18}$$

where $x = (1 - 16\zeta)^{1/4}$.

In addition to the momentum, sensible heat, and latent heat fluxes, land surface albedos and upward longwave radiation are needed for the atmospheric radiation calculations. Surface albedos depend on the solar zenith angle, the amount of leaf and stem material present, their optical properties, and the optical properties of snow and soil. The upward longwave radiation is the difference between the incident and absorbed fluxes.

These and other aspects of the land surface fluxes have been described by Bonan (1996a).

Ocean and sea ice

The bulk formulae used for the ocean-atmosphere or sea ice-atmosphere exchange are:

$$\begin{aligned} \tau &= \rho_A CD \|\Delta\vec{U}\| \Delta\vec{U} \\ E &= \rho_A CD \|\Delta\vec{U}\| \Delta q \\ H &= \rho_A C_p CH \|\Delta\vec{U}\| \Delta\vartheta \end{aligned} \tag{4.c.19}$$

where ρ_A is atmospheric surface density, and C_p is the specific heat.

The transfer coefficients between ocean and atmosphere ($i = ocn$) or sea-ice and atmosphere ($i = si$), shifted to a height, Z_A,and to the stability, ζ_i, appropriate to the particular interface, are :

$$\begin{aligned} CD_i &= \kappa^2 \left[\ln\left(\frac{Z_i}{Z_i^o}\right) - \psi_m\right]^{-2} \\ CE_i &= \kappa^2 \left[\ln\left(\frac{Z_i}{Z_i^o}\right) - \psi_m\right]^{-1} \left[\ln\left(\frac{Z_i}{Z_i^e}\right) - \psi_s\right]^{-1} \\ CH_i &= \kappa^2 \left[\ln\left(\frac{Z_i}{Z_i^o}\right) - \psi_m\right]^{-1} \left[\ln\left(\frac{Z_i}{Z_i^h}\right) - \psi_s\right]^{-1}, \end{aligned}$$

where $\kappa = 0.4$ is von Karman's constant and the integrated flux profiles, ψ_m for momentum and ψ_s for scalars, are functions of the stability parameter, ζ_i. These functions as used in the model are:

$$\begin{aligned} \psi_m(\zeta) &= \psi_s(\zeta) = -5\zeta & \zeta &> 0 \\ \psi_m(\zeta) &= 2\ln[0.5(1+X)] + \ln[0.5(1+X^2)] - 2\tan^{-1}X + 0.5\pi & \zeta &< 0 \\ \psi_s(\zeta) &= 2\ln[0.5(1+X^2)] & \zeta &< 0 \\ X &= (1-16\zeta)^{1/4} \end{aligned}$$

The stability parameter is,

$$\zeta_i = \frac{\kappa\ g\ Z_A}{u_i^{*2}} \left(\frac{\theta_i^*}{\theta_v} + \frac{Q_i^*}{(Z_v^{-1} + q_A)}\right) ,$$

where virtual potential temperature is computed as $\theta_v = \theta_A(1 + Z_v q_A)$, q_0 and θ_A are the lowest level atmospheric humidity, and potential temperature, respectively, and $Z_v = (\varrho(water)/\varrho(air)) - 1 = 0.606$. Since ζ_i is itself a function of the turbulent scales and hence the fluxes, an iterative procedure is generally required to solve (4.*c*.19). And where the turbulent velocity scales are given by

$$\begin{aligned} u_i^* &= CD_i^{1/2} \quad |\Delta\vec{U}_i| \\ Q_i^* &= CE_i \ |\Delta\vec{U}_i| \ (\Delta q_i) \ u_i^{*-1} \\ \theta_i^* &= CH_i \ |\Delta\vec{U}_i| \ (\Delta\theta_i) \ u_i^{*-1}, \end{aligned} \tag{4.c.20}$$

For the ocean interface ($i = ocn$),

$$\begin{aligned} &\Delta\vec{U} = \vec{U}_0 \\ &\Delta q = q_0 - 0.98\rho_a^{-1} C_5 \exp(C_6/T_s) \\ &\Delta\theta = \theta_0 - T_s \end{aligned}$$

where the factor 0.98 accounts for the salinity of the ocean,C_5 = 640380 kg m^{-3} and C_6 = -5107.4 K.

The roughness length for momentum, Z^o_{ocn} in meters, is a function of the atmospheric wind at 10 meters height, U_{10}:

$$Z^o_{ocn} = 10 \ \exp - \left[\kappa \left(\frac{C_1}{U_{10}} + C_2 + C_3 U_{10} \right)^{-1} \right],$$

where C_1 = 0.0027 m/s, C_2 = 0.000142, and C_3 = 0.0000764 m^{-1}s. The corresponding drag coefficient at 10m height and neutral stability is

$$C_{10}^N \ = \ C_1 \ U_{10}^{-1} \ + \ C_2 \ + \ C_3 \ U_{10} \ .$$

The roughness length for heat, Z^h_{ocn}, is a function of stability, and for evaporation, Z^o_{ocn}, is a different constant:

$$\begin{aligned} Z^h_{ocn} &= 2.2 \times 10^{-9} m \qquad \zeta_3 > 0 \\ &= 4.9 \times 10^{-5} m \qquad \zeta_3 \le 0 \\ Z^e_{ocn} &= 9.5 \times 10^{-5} m \ . \end{aligned}$$

Since the roughness lengths are neither constant nor equal, the iterative solution for the fluxes (4.c.19)is as follows: first, ζ_{ocn} is set incrementally greater than zero when the air–sea temperature difference suggests stable stratification, otherwise it is set to zero. In either case, $\psi_m = \psi_s = 0$, and the initial transfer coefficients are then found from the roughness lengths at this ζ_{ocn} and $U_{10} = U_A$. As with sea–ice, these coefficients are used to approximate the initial flux scales (4.c.20) and the first iteration begins with an updated ζ_{ocn} and calculations of ψ_m and ψ_s. The wind speed, U_A, is then shifted to its equivalent neutral value at 10m height :

$$U_{10} = U_A \ \left(1 + \frac{\sqrt{C_{10}^N}}{\kappa} \ln(\frac{Z_A}{10} - \psi_m(\zeta_{ocn})) \right)^{-1} \ .$$

This wind speed is used to update the transfer coefficients and hence the flux scales. The second and final iteration begins with another update of ζ_{ocn}. The final flux scales then give the fluxes calculated by (4.c.19).

The state variables required to calculate the fluxes over sea ice $(i - si)$ (4.c.19) are the atmospheric wind velocity, potential temperature, density and specific humidity in (kg/kg) at a height Z_A, and the ice surface temperature T_{si}.

$$\begin{aligned}\Delta\vec{U} &= \vec{U}_0 \\ \Delta q &= q_0 \rho_A^{-1} C_5 \exp(C_6/T_{si}) \\ \Delta\vartheta &= \vartheta_0 - T_{si}\end{aligned}$$

Presently the coupler assumes constant and equal roughness lengths for ice :

$$Z_{si}^o = Z_{si}^h = Z_{si}^e = 0.04m.$$

To start the iterative solver for the fluxes (4.c.19), ζ_{si} is set to zero : $\psi_m = \psi_s = 0$, and the neutral coefficients are used to approximate the flux scales (4.c.20). The iteration begins by computing ζ_{si}, finding the non-neutral transfer coefficients and updating the flux scales. After two such iterations there is sufficient convergence to compute the fluxes (4.c.19).

d. Vertical Diffusion and Atmospheric Boundary Layer Processes

Local diffusion scheme

An explicit, non-local Atmospheric Boundary Layer (ABL) parameterization is incorporated into the vertical diffusion parameterization in CCM3. The ABL parameterization includes a determination of the boundary layer depth. Above the top of the ABL, CCM3 employs a standard local diffusion parameterization for the free atmosphere. In practice, the free atmosphere diffusivities are calculated first at all levels. The ABL scheme then determines the ABL depth and diffusivities and replaces the free atmosphere values for all levels within the ABL. The implementation of the ABL parameterization in CCM is discussed in Holtslag and Boville (1993), while the formalism only is discussed here.

The local form of the vertical diffusion terms of momentum, sensible heat, and moisture follows those described by Smagorinsky *et al.* (1965) and Manabe *et al.* (1965) where the tendencies are given by

$$\frac{\partial u}{\partial t} = -\frac{1}{\rho}\frac{\partial \tau_\lambda}{\partial z} = g\,\frac{\partial \tau_\lambda}{\partial p}, \tag{4.d.1}$$

$$\frac{\partial v}{\partial t} = -\frac{1}{\rho}\frac{\partial \tau_\mu}{\partial z} = g\,\frac{\partial \tau_\mu}{\partial p}, \tag{4.d.2}$$

$$\frac{\partial \theta}{\partial t} = -\frac{1}{\rho c_p}\frac{\partial H}{\partial z} = \frac{g}{c_p}\frac{\partial H}{\partial p}, \tag{4.d.3}$$

$$\frac{\partial q}{\partial t} = -\frac{1}{\rho}\frac{\partial R}{\partial z} = g\,\frac{\partial R}{\partial p}. \qquad (4.d.4)$$

Above the surface layer, the upward fluxes of momentum, sensible heat, and moisture due to turbulent motions are given by

$$\tau_\lambda = \rho\overline{w'u'} = -\rho K_m\frac{\partial u}{\partial z} = g\rho^2 K_c\frac{\partial u}{\partial p}, \qquad (4.d.5)$$

$$\tau_\mu = \rho\overline{w'v'} = -\rho K_m\frac{\partial v}{\partial z} = g\rho^2 K_c\frac{\partial v}{\partial p}, \qquad (4.d.6)$$

$$H = \rho\overline{w'\theta'} = -c_p\rho K_\theta\frac{\partial \theta}{\partial z} = c_p g\rho^2 K_c\frac{\partial \theta}{\partial p}, \qquad (4.d.7)$$

$$R = \rho\overline{w'q'} = -\rho K_q\frac{\partial q}{\partial z} = g\rho^2 K_c\frac{\partial q}{\partial p}, \qquad (4.d.8)$$

where $\theta = T\left(\frac{p^*}{p}\right)^\kappa$ and p^* is a reference pressure which in practice is taken to be p_s. The variables K_c, where $c \in (q, \theta, u, v)$ are "eddy-diffusivities" that are typically taken as functions of length scales ℓ_c and local vertical gradients of wind and virtual potential temperature, *e.g.*,

$$K_c = {\ell_c}^2 S F_c(Ri). \qquad (4.d.9)$$

Here S is the local shear, defined by

$$S = \left|\frac{\partial \mathbf{V}}{\partial z}\right|, \qquad (4.d.10)$$

and the mixing length ℓ_c is generally given by

$$\frac{1}{\ell_c} = \frac{1}{kz} + \frac{1}{\lambda_c}, \qquad (4.d.11)$$

where k is the Von Karman constant, and λ_c is the so-called asymptotic length scale, taken to be 30 m above the ABL. Since the lowest model level is always greater than 30 m in depth, ℓ_c is simply set to 30 m in CCM3. Furthermore, $F_c(Ri)$ denotes a functional dependence of K_c on the gradient Richardson number:

$$Ri = \frac{g}{\theta_v}\frac{\partial\theta_v/\partial z}{S^2}, \qquad (4.d.12)$$

where θ_v is the virtual potential temperature,

$$\theta_v = \theta\left[1 + \left(\frac{R_v}{R} - 1\right)q\right]. \qquad (4.d.13)$$

For simplicity, in our present implementation of the local K approach, we specify the same stability functions F_c for all c. For unstable conditions ($Ri < 0$) we choose

$$F_c(Ri) = (1 - 18Ri)^{1/2}, \qquad (4.d.14)$$

and we use (4.c.12) for stable conditions ($Ri > 0$). This means that no distinction is made between vertical diffusion of heat, scalars and momentum.

"Non-local" atmospheric boundary layer scheme

In a local diffusion approach, the turbulent flux of a quantity is proportional to the local gradient of that quantity (*e.g.*, (4.d.5)–(4.d.8)). In such an approach the eddy diffusivity depends on local gradients of mean wind and mean virtual temperature (see (4.d.9)). These are reasonable assumptions when the length scale of the largest turbulent eddies is smaller than the size of the domain over which the turbulence extends. In the Atmospheric Boundary Layer (ABL) this is typically true for neutral and stable conditions only. For unstable and convective conditions, however, the largest transporting eddies may have a similar size as the boundary layer height itself, and the flux can be counter to the local gradient (Deardorff, 1972; Holtslag and Moeng, 1991). In such conditions a local diffusion approach is no longer appropriate, and the eddy diffusivity is better represented with turbulent properties characteristic of the ABL. We will refer to such an approach as non-local diffusion.

To account for "non-local" transport by convective turbulence in the ABL, the local diffusion term for constituent c is modified as

$$\overline{w'C'} = -K_c \left(\frac{\partial C}{\partial z} - \gamma_c \right) , \tag{4.d.15}$$

where K_c is the non-local eddy diffusivity for the quantity of interest. The term γ_c is a "non-local" transport term and reflects non-local transport due to dry convection. Eq. (4.d.15) applies to potential temperature, water vapor, and passive scalars. No countergradient term is applied to the wind components, so (4.d.1) and (4.d.2) remain unchanged. For stable and neutral conditions the non-local term is not relevant for any of the quantities. The eddy diffusivity formalism is, however, modified for unstable conditions.

In the non-local diffusion scheme the eddy diffusivity is given by

$$K_c = k \ w_t \ z \left(1 - \frac{z}{h} \right)^2 , \tag{4.d.16}$$

where w_t is a turbulent velocity scale and h is the boundary layer height. Equation (4.d.16) applies for heat, water vapor and passive scalars. The eddy diffusivity of momentum K_m, is also defined as (4.d.16) but with w_t replaced by another velocity scale w_m. With proper formulation of w_t (or w_m) and h, it can be shown that equation (4.d.16) behaves well from very stable to very unstable conditions in horizontally homogeneous and quasi-stationary conditions. For unstable conditions w_t and w_m are proportional to the so-called convective velocity scale w_*, while for neutral and stable conditions w_t and w_m are proportional to the friction velocity u_*.

The major advantage of the present approach over the local eddy diffusivity approach is that large eddy transport in the ABL is accounted for and entrainment effects are treated implicitly. Above the ABL, $\gamma_c = 0$ so ($4.d.15$) reduces to a local form with K_c given by ($4.d.9$). Near the top of the ABL we use the maximum of the values by ($4.d.9$) and ($4.d.16$), although ($4.d.16$) almost always gives the larger value in practice.

The non-local transport term in ($4.d.15$), γ_c, represents non-local influences on the mixing by turbulence (Deardorff, 1972). As such, this term is small in stable conditions, and is therefore neglected under these conditions. For unstable conditions, however, most heat and moisture transport is achieved by turbulent eddies with sizes on the order of the depth h of the ABL. In such cases, a formulation for γ_c consistent with the eddy formulation of ($4.d.15$) is given by

$$\gamma_c = a \frac{w_* (\overline{w'C'})_s}{{w_m}^2 h} \ , \qquad (4.d.17)$$

where a is a constant and $(\overline{w'C'})_s$ is the surface flux (in kinematic units) of the transported scalar. The form of ($4.d.17$) is similar to the one proposed in Holtslag and Moeng (1991). The non-local correction vanishes under neutral conditions, for which $w_* = 0$.

The formulations of the eddy-diffusivity and the non-local terms are dependent on the boundary layer height h. The CCM2 configuration of this non-local scheme made use of a traditional approach to estimating the boundary layer depth by assuming a constant value for the bulk Richardson number across the boundary layer depth so that h was iteratively determined using

$$h = \frac{Ri_{cr} \left\{ u(h)^2 + v(h)^2 \right\}}{(g/\theta_s)\,(\theta_v(h) - \theta_s)} \ , \qquad (4.d.18)$$

where Ri_{cr} is a critical bulk Richardson number for the ABL; $u(h)$ and $v(h)$ are the horizontal velocity components at h; g/θ_s is the buoyancy parameter and $\theta_v(h)$ is the virtual temperature at h. The quantity θ_s is a measure of the surface air temperature, which under unstable conditions was given by

$$\theta_s = \theta_v\,(z_s) + b\,\frac{(\overline{w'\theta_v'})_s}{w_m} \ , \qquad (4.d.19)$$

where b is a constant, $(\overline{w'\theta_v'})_s$ is the virtual heat flux at the surface, $\theta_v\,(z_s)$ is a virtual temperature in the atmospheric surface layer (nominally 10 m), $b\,(\overline{w'\theta_v'})_s/w_m$ represents a temperature excess (a measure of the strength of convective thermals in the lower part of the ABL) and unstable conditions are determined by $(\overline{w'\theta_v'})_s > 0$. The quantity $\theta_v\,(z_s)$ was calculated from the temperature and moisture of the first model level and of the surface by applying the procedure in Geleyn (1988). The value of the critical bulk Richardson number Ri_{cr} in ($4.d.18$), which generally depends on the vertical resolution of the model, was chosen as $Ri_{cr} = 0.5$ for the CCM2.

Vogelezang and Holtslag (1996) have recently studied the suitability of this formulation in the context of field observations, large-eddy simulations (Moeng and Sullivan, 1994), and an $E - \epsilon$ turbulence closure model (Duynkerke, 1988). They propose a revised formulation which combines shear production in the outer region of the boundary layer with surface friction, where the Richardson number estimate is based on the differences in wind and virtual temperature between the top of the ABL and a lower height that is well outside the surface layer (i.e., 20 m - 80 m). In addition to providing more realistic estimates of boundary layer depth, the revised formulation provides a smoother transition between stable and neutral boundary layers. Consequently, CCM3 employs the Vogelezang and Holtslag (1996) formulation for estimating the atmospheric boundary layer height, which can be written as

$$h = z_s + \frac{Ri_{cr}\left\{(u(h) - u_{SL})^2 + (v(h) - v_{SL})^2 + \mathcal{B}u_*^2\right\}}{(g/\theta_{SL})\,(\theta_v(h) - \theta_{SL})} \; . \qquad (4.d.19.1)$$

The quantities u_{SL}, v_{SL}, and θ_{SL} represent the horizontal wind components and virtual potential temperature just above the surface layer (nominally $0.1h$). In practice, the lowest model level values for these quantities are used to iteratively determine h for all stability conditions, where the critical Richardson number, Ri_{cr}, is assumed to be 0.3. The disposable parameter $\mathcal{B}$ has been experimentally determined to be equal to 100 (see Vogelezang and Holtslag, 1996). The computation starts by calculating the bulk Richardson number Ri between the level of θ_{SL} and subsequent higher levels of the model. Once Ri exceeds the critical value, the value of h is derived by linear interpolation between the level with $Ri > Ri_{cr}$ and the level below.

Using the calculated value for h and the surface fluxes, we calculate the velocity scales, the eddy diffusivities with ($4.d.16$), and the countergradient terms with ($4.d.17$), for each of the transported constituents. Subsequently, the new profiles for θ, q, u, and v are calculated using an implicit diffusion formulation.

The turbulent velocity scale of ($4.d.16$) depends primarily on the relative height z/h (h is boundary layer height), and the stability within the ABL. Here stability is defined with respect to the surface virtual heat flux $(\overline{w'\theta_v'})_s$. Secondly, the velocity scales are also generally dependent on the specific quantity of interest. We will assume that the velocity scales for mixing of passive scalars and specific humidity are equal to the one for heat, denoted by w_t. For the wind components, the velocity scale is different and denoted by w_m. The specification of w_t and w_m is given in detail by Troen and Mahrt (1986). Holtslag *et al.,* (1990) have rewritten the velocity scale, in terms of the more widely accepted profile functions of Dyer (1974), and have given a new formulation for very stable conditions. Below we follow the latter approach.

For stable ($(\overline{w'\theta_v'})_s < 0$) and neutral surface conditions ($(\overline{w'\theta_v'})_s = 0$), the velocity scale for scalar transport is

$$w_t = \frac{u_*}{\phi_h} \; , \tag{4.d.21}$$

where u_* is the friction velocity defined by

$$u_* = \left[(\overline{u'w'})_s^2 + (\overline{v'w'})_s^2 \right]^{1/4} . \tag{4.d.22}$$

Furthermore, ϕ_h is the dimensionless vertical temperature gradient given by (Dyer, 1974),

$$\phi_h = 1 + 5\frac{z}{L} \; , \tag{4.d.23}$$

for $0 \leq z/L \leq 1$. Here L is the Obukhov length, defined by

$$L = \frac{-u_*^3}{k(g/\theta_{v0})(\overline{w'\theta_v'})_0} . \tag{4.d.24}$$

For $z/L > 1$,

$$\phi_h = 5 + \frac{z}{L} \; , \tag{4.d.25}$$

which matches (4.d.23) for $z/L = 1$. Equation (4.d.25) is a simple means to prevent ϕ_h from becoming too large (and K_c too small) in very stable conditions. In stable conditions, the exchange coefficients for heat and momentum are often found to be similar. Therefore we may use w_m=w_t.

For unstable conditions $(\overline{w'\theta_v'})_s > 0$, we have that w_t and w_m differ in the surface layer ($z/h \leq 0.1$) and in the outer layer of the ABL ($z/h > 0.1$). For the surface layer, w_t is given by (4.d.21) with

$$\phi_h = \left(1 - 15\frac{z}{L}\right)^{-1/2} . \tag{4.d.26}$$

Similarly, w_m is written as

$$w_m = \frac{u_*}{\phi_m} \; , \tag{4.d.27}$$

where ϕ_m is the dimensionless wind gradient given by

$$\phi_m = \left(1 - 15\frac{z}{L}\right)^{-1/3} . \tag{4.d.28}$$

In the surface layer, the scalar flux is normally given by

$$(\overline{w'c'})_0 = -\frac{k u_* z}{\phi_h} \left(\frac{\partial C}{\partial z}\right) . \tag{4.d.29}$$

Comparison with (4.d.15) and (4.d.16) shows that, in the surface layer, we should have $a = 0$ in (4.d.17) for consistency.

For the outer layer, w_t and w_m are given by

$$w_t = w_m / Pr \; , \tag{4.d.30}$$

where

$$w_m = \left(u_*^3 + c_1 w_*^3\right)^{1/3} \ , \tag{4.d.31}$$

and

$$w_* = \left((g/\theta_{v0})\ (\overline{w'\theta_v'})_0 h\right)^{1/3} \tag{4.d.32}$$

is the convective velocity scale. Furthermore, Pr is the turbulent Prandtl number and c_1 is a constant. The latter is obtained by evaluating the dimensionless vertical wind gradient ϕ_m by (4.d.28) at the top of the surface layer, as discussed by Troen and Mahrt (1986). This results in $c_1 = 0.6$. For very unstable conditions ($h \gg -L$ or $w_*/u_* \gg 0$), it can be shown with (4.d.30) that w_m is proportional to 0.85 w_*, while for the neutral case $w_m = u_*$. The turbulent Prandtl number Pr ($= K_m/K_h = w_m/w_t$) of (4.d.30) is evaluated from

$$Pr = \frac{\phi_h}{\phi_m}\ \left(\frac{z}{L}\right) + ak\frac{z}{h}\frac{w_*}{w_m} \tag{4.d.33}$$

for $z = 0.1h$. Equation (4.d.33) arises from matching (4.d.15), (4.d.16), (4.d.17), and (4.d.29) at the top of the surface layer. As in Troen and Mahrt we assume that Pr is independent of height in the unstable outer layer. Its value decreases from $Pr = 1$ for the neutral case ($z/L = 0$ and $w_* = 0$), to $Pr = 0.6$ for $w_*/u_* \simeq 10$ in very unstable conditions.

In very unstable conditions, the countergradient term of (4.d.17) approaches

$$\gamma_c = d\frac{\overline{wC_0}}{w_* h} \ , \tag{4.d.34}$$

where $d \simeq a/0.85^2$, because for very unstable conditions we obtain $w_m \simeq 0.85 w_*$. Since typically $d \simeq 10$ (Troen and Mahrt 1986), we have $a = 7.2$. Similarly, the temperature excess of (4.d.19) reads in this limit as $d(\overline{w'\theta_v'})_0/w_*$. This leads to b ($= 0.85\ d$) $= 8.5$ in (4.d.19).

Finally, using the velocity scales described above, the flux equation (4.d.15) is continuous in relative height (z/h) and in the boundary layer stability parameter (h/L or w_*/u_*).

In summary, the vertical diffusion tendency is given by the vertical derivative of the turbulent flux defined in (4.d.15):

$$\begin{aligned} \frac{\partial C}{\partial t} &= -\frac{1}{\rho}\frac{\partial}{\partial z}\left[\rho\overline{w'C'}\right] \\ &= \frac{1}{\rho}\frac{\partial}{\partial z}\left[\rho K_c\left(\frac{\partial C}{\partial z} - \gamma_c\right)\right] . \end{aligned} \tag{4.d.35}$$

The vertical diffusion is implemented using a time-split implicit method. The countergradient term in the non-local ABL scheme depends on the surface flux, the boundary layer depth and the velocity scale, but not explicitly on the diffused quantity. Therefore the countergradient term cannot be treated implicitly. Forward time differencing is used for the diffusion, whereas a leap frog (centered) method is used for the dynamics. Thus, the diffusive forward step is over two time steps. The time discretization then results in:

$$\frac{C^{n+1}-C^{n-1}}{2\Delta t} = \frac{1}{\rho^{n-1}}\frac{\partial}{\partial z}\left[\rho^{n-1}K_c^{n-1}\left(\frac{\partial C^{n+1}}{\partial z}-\gamma_c^{n-1}\right)\right], \tag{4.d.36}$$

where subscripts $n-1$ and $n+1$ refer to time levels, with K_c^{n-1} and γ_c^{n-1} evaluated using model variables at time $n-1$. The whole diffusion process is time split from all other processes so that time $n-1$ variables may already have contributions from the dynamics and other physical process. Equation $(4.d.36)$ can be rewritten as

$$C^{n+1} = (1-2\Delta t G^{n-1})^{-1}C^*, \tag{4.d.37}$$

$$C^* = C^{n-1} - 2\Delta t H^{n-1}(\gamma_c^{n-1}), \tag{4.d.38}$$

where G and H are differential operators. There can be a problem in applying $(4.d.38)$ for trace constituents, including water vapor, because these quantities are positive definite. The application of the countergradient term, $H^{n-1}(\gamma^{n-1})$ may result in negative values for C^*, which are not removed by the subsequent implicit diffusion step. This problem is not strictly numerical; it arises under highly non-stationary conditions for which the ABL formulation is not strictly applicable. In practice, we evaluate C^* and check for negative values in the constituent profiles. If a negative value is found, we set $C^* = C^{n-1}$ for that constituent profile (but not for other constituents at the same point). Note that $(4.d.37)$ is just the normal diffusion equation, which is solved using the numerical techniques discussed in the next sub-section.

Numerical solution of nonlinear, time–split vertical diffusion

As described in section 2, the vertical diffusion is calculated prior to the main dynamical calculation. This time–split diffusion is

$$u_k^{n+1} = u_k^{n-1} + 2\Delta t\frac{\tau_{\lambda k+1/2}^{n+1}-\tau_{\lambda k-1/2}^{n+1}}{\rho_k\Delta z_k^{n-1}}, \tag{4.d.39}$$

$$v_k^{n+1} = v_k^{n-1} + 2\Delta t\frac{\tau_{\mu k+1/2}^{n+1}-\tau_{\mu k-1/2}^{n+1}}{\rho_k\Delta z_k^{n-1}}, \tag{4.d.40}$$

$$\theta_k^{n+1} = \theta_k^{n-1} + 2\Delta t\,\frac{g}{c_{p_k}}\,\frac{H_{k+1/2}^{n+1}-H_{k-1/2}^{n+1}}{\rho_k\Delta z_k^{n-1}}, \tag{4.d.41}$$

$$q_k^{n+1} = q_k^{n-1} + 2\Delta t\frac{R_{k+1/2}^{n+1}-R_{k-1/2}^{n+1}}{\rho_k\Delta z_k^{n-1}}.$$

The surface fluxes are given by the explicit forms (4.d.5)–(4.d.8):

$$R^{n+1}_{K+1/2} = R^{n-1}_{K+1/2} = L\rho\left(\overline{w'q'}\right)_s , \tag{4.d.44}$$

$$H^{n+1}_{K+1/2} = H^{n-1}_{K+1/2} = c_p\rho_1\left(\overline{w'\theta'}\right)_s , \tag{4.d.45}$$

$$\tau^{n+1}_{\lambda K+1/2} = \tau^{n-1}_{\lambda K+1/2} = \rho_1\left(\overline{w'u'}\right)_s , \tag{4.d.46}$$

$$\tau^{n+1}_{\mu K+1/2} = \tau^{n-1}_{\mu K+1/2} = \rho_1\left(\overline{w'v'}\right)_s . \tag{4.d.47}$$

Note that these surface fluxes are explicit and ensure conservation of energy and moisture in the surface exchange. The surface stresses τ_λ and τ_μ could be made implicit without affecting this conservation. In the free atmosphere, for $k = 1$ to $K-1$,

$$\tau^{n+1}_{\lambda k+1/2} = \left(\rho^{n-1}_{k+1/2}\right) K^{n-1}_{k+1/2} \frac{u^{n+1}_{k+1} - u^{n+1}_k}{z^{n-1}_{k+1} - z^{n-1}_k}, \tag{4.d.48}$$

$$\tau^{n+1}_{\mu k+1/2} = \left(\rho^{n-1}_{k+1/2}\right) K^{n-1}_{k+1/2} \frac{v^{n+1}_{k+1} - v^{n+1}_k}{z^{n-1}_{k+1} - z^{n-1}_k}, \tag{4.d.49}$$

$$R^{n+1}_{k+1/2} = \left(\rho^{n-1}_{k+1/2}\right) K^{n-1}_{k+1/2} \frac{q^{n+1}_{k+1} - q^{n+1}_k}{z^{n-1}_{k+1} - z^{n-1}_k}, \tag{4.d.50}$$

$$H^{n+1}_{k+1/2} = c_{p_{k+1/2}}\left(\rho^{n-1}_{k+1/2}\right) K^{n-1}_{k+1/2} \frac{\theta^{n+1}_{k+1} - \theta^{n+1}_k}{z^{n-1}_{k+1} - z^{n-1}_k}, \tag{4.d.51}$$

where

$$\rho^{n-1}_{k+1/2} = \frac{2p^{n-1}_{k+1/2}}{R\left(T^{n-1}_{k+1} + T^{n-1}_k\right)\left[1 + \left(\frac{R_v}{R} - 1\right)\frac{1}{2}\left(q^{n-1}_{k+1} + q^{n-1}_k\right)\right]}. \tag{4.d.52}$$

$K^{n-1}_{k+1/2}$ is then determined from the neutral K modulated by a function of Richardson number

$$K^{n-1}_{k+1/2} = \left(K^{n-1}_N\right)_{k+1/2} \cdot f\left(R_{I_{k+1/2}}\right), \tag{4.d.54}$$

with a minimum value for $K^{n-1}_{k+1/2}$ of $K_{min} = 0.01$.

$$f(R_I) = \begin{cases} \max\left(0, 1 - R_I/R_{IC}\right) & \text{for } R_I \geq 0 \text{ (stable)} , \\ \sqrt{1 - 18R_I} & \text{for } R_I < 0 \text{ (unstable)} , \end{cases} \tag{4.d.55}$$

with a critical Richardson number at which f goes to zero of

$$R_{IC} = 0.2 \ . \tag{4.d.56}$$

The neutral K_N is calculated by

$$\left(K_N^{n-1}\right)_{k+1/2} = \ell_{k+1/2}^2 \frac{\left[\left(u_{k+1}^{n-1} - u_k^{n-1}\right)^2 + \left(v_{k+1}^{n-1} - v_k^{n-1}\right)^2\right]^{1/2}}{\Delta z_{k+1/2}^{n-1}}, \tag{4.d.57}$$

with

$$\Delta z_{k+1/2}^{n-1} = z_{k+1}^{n-1} - z_k^{n-1}, \tag{4.d.59}$$

and $\ell_{k+1/2}$ is determined from (4.d.11) and (4.d.13). The Richardson number in the free atmosphere is calculated from

$$\begin{aligned} R_{I_{k+1/2}} = \quad & \frac{2g\left(z_k^{n-1} - z_{k+1}^{n-1}\right)}{\left(\theta_{v_k}^{n-1} + \theta_{v_{k+1}}^{n-1}\right)} \\ & \times \left[\frac{\theta_{v_k}^{n-1} - \theta_{v_{k+1}}^{n-1}}{\left(u_{k+1}^{n-1} - u_k^{n-1}\right)^2 + \left(v_{k+1}^{n-1} - v_k^{n-1}\right)^2}\right] \end{aligned} \tag{4.d.60}$$

where

$$\theta_{v_k}^{n-1} = \theta_k^{n-1}\left(1.0 + \left(\frac{R_v}{R} - 1\right) q_k^{n-1}\right). \tag{4.d.60.1}$$

Within the diagnosed atmospheric boundary layer, the diffusivities are modified by the non-local atmospheric boundary layer scheme described earlier. At the top of the model, the fluxes are set to 0,

$$\tau_{\lambda 1/2}^{n+1} = \tau_{\mu 1/2}^{n+1} = R_{1/2}^{n+1} = H_{1/2}^{n+1} = 0. \tag{4.d.61}$$

The diffusion equations can be summarized as

$$u_k^{n+1} - \left\{u^{n-1}\right\}_k = a_k\left(u_{k+1}^{n+1} - u_k^{n+1}\right) - c_k\left(u_k^{n+1} - u_{k-1}^{n+1}\right), \tag{4.d.62}$$

$$v_k^{n+1} - \left\{v^{n-1}\right\}_k = a_k\left(v_{k+1}^{n+1} - v_k^{n+1}\right) - c_k\left(v_k^{n+1} - v_{k-1}^{n+1}\right), \tag{4.d.63}$$

$$q_k^{n+1} - \left\{q^{n-1}\right\}_k = a_k\left(q_{k+1}^{n+1} - q_k^{n+1}\right) - c_k\left(q_k^{n+1} - q_{k-1}^{n+1}\right), \tag{4.d.64}$$

$$\theta_k^{n+1} - \left\{\theta^{n-1}\right\}_k = a_k\left[\theta_{k+1}^{n+1} - \theta_k^{n+1}\right] - c_k\left[\theta_k^{n+1} - \theta_{k-1}^{n+1}\right], \tag{4.d.65}$$

for $1 \le k \le K-1$,

$$\left\{u^{n-1}\right\}_k = u_k^{n-1}, \tag{4.d.66}$$

$$\left\{v^{n-1}\right\}_k = v_k^{n-1}, \tag{4.d.67}$$

$$\left\{q^{n-1}\right\}_k = q_k^{n-1}, \tag{4.d.68}$$

$$\left\{\theta^{n-1}\right\}_k = \theta_k^{n-1}, \tag{4.d.69}$$

and for $k = K$,

$$\left\{u^{n-1}\right\}_K = u_K^{n-1} + \frac{2\Delta t}{\rho_{K+\frac{1}{2}} \Delta z_K^{n-1}} \tau_{\lambda K+1/2}^{n+1} , \tag{4.d.70}$$

$$\left\{v^{n-1}\right\}_K = v_K^{n-1} + \frac{2\Delta t}{\rho_{K+\frac{1}{2}} \Delta z_k^{n-1}} \tau_{\mu K+1/2}^{n+1} , \tag{4.d.71}$$

$$\left\{q^{n-1}\right\}_K = q_K^{n-1} + \frac{2\Delta t}{\rho_{K+\frac{1}{2}} \Delta z_K^{n-1}} R_{K+1/2}^{n+1} , \tag{4.d.72}$$

$$\left\{\theta^{n-1}\right\}_K = \theta_K^{n-1} + \frac{2\Delta t}{c_{p_K}^* \rho_{K+\frac{1}{2}} \Delta z_K^{n-1}} H_{K+1/2}^{n+1} , \tag{4.d.73}$$

where

$$a_k = \frac{2\Delta t}{\Delta p_k \left(p_{k+1} - p_k\right)} \left(\frac{g\rho_{k+1/2}^{n-1}}{p_s^{n-1}}\right)^2 K_{k+1/2}^{n-1} \qquad 1 \le k \le K-1, \tag{4.d.74}$$

$$a_K = 0, \tag{4.d.75}$$

$$c_1 = 0, \tag{4.d.76}$$

$$c_k = \frac{2\Delta t}{\Delta p_k^{n-1} \left(p_k^{n-1} - p_{k-1}^{n-1}\right)} \left(g\overline{\rho}_{k-1/2}^{n-1}\right) K_{k-1/2}^{n-1} \qquad 2 \le k \le K. \tag{4.d.77}$$

The left-hand side of (4.d.65) can be written in terms of T because it is represented as a difference.

Following Richtmeyer and Morton (1967, pp. 198–201), the solutions for u, v, θ, and q have the form,

$$u_k^{n+1} = Fu_k + E_k u_{k+1}^{n+1}, \tag{4.d.78}$$

where for $k = 1$,

$$Fu_1 = \frac{\left\{u^{n-1}\right\}_1}{b_1}, \tag{4.d.79}$$

$$E_1 = \frac{a_1}{b_1}, \tag{4.d.80}$$

and for $2 \le k \le K-1$,

$$Fu_k = \frac{\left\{u^{n-1}\right\}_k + c_k Fu_{k-1}}{b_k - c_k E_{k-1}}, \tag{4.d.81}$$

$$E_k = \frac{a_k}{b_k - c_k E_{k-1}}, \tag{4.d.82}$$

and for $k = K$,

$$E_K = 0, \tag{4.d.83}$$

$$Fu_K = \frac{\left\{u^{n-1}\right\}_K + c_K Fu_{K-1}}{b_K - c_K E_{K-1}}. \tag{4.d.84}$$

In the above, the diagonal coefficient is given by

$$b_k = 1 + a_k + c_k. \tag{4.d.85}$$

Note that, since the model actually forecasts vorticity and divergence, the new diffused velocity fields u_k^{n+1} and v_k^{n+1} are not explicitly carried by the model, and the corresponding diffused vorticity and divergence are not calculated. Rather, the net effects of the diffusion $F_{u_V}\left(u^{n+1}\right)$ and $F_{v_V}\left(v^{n+1}\right)$ are saved for addition to the nonlinear terms n_U and n_V in the vorticity and divergence equations (after multiplication by $\cos\phi$),

$$F_{u_V} = \frac{u^{n+1} - u^{n-1}}{2\Delta t}, \tag{4.d.86}$$

$$F_{v_V} = \frac{v^{n+1} - v^{n-1}}{2\Delta t}. \tag{4.d.87}$$

The heating rate due to the diffusion is also calculated,

$$F_{T_V} = \frac{T^{n+1} - T^{n-1}}{2\Delta t}, \tag{4.d.88}$$

and added to the nonlinear term in the temperature tendency equation. The frictional heating associated with (4.d.86) and (4.d.87) is also added to the nonlinear term in the thermodynamic equation. The individual heating rates $F_{T_V}\left(T^{n+1}\right), -u^{n-1}F_{u_V}\left(u^{n+1}\right)/c_p^*$, and $-v^{n-1}F_{v_V}\left(v^{n+1}\right)/c_p^*$ are saved for diagnostic purposes. The new moisture q^{n+1} is retained as the basis for the next time–split step in the moisture equation. The moisture tendency due to vertical diffusion is also saved for diagnostic purposes,

$$F_{q_V}\left(q^{n+1}\right) = \frac{q^{n+1} - q^{n-1}}{2\Delta t}. \tag{4.d.89}$$

e. Gravity Wave Drag

Vertically propagating gravity waves can be excited in the atmosphere where stably stratified air flows over an irregular lower boundary and by internal heating and shear. These waves are capable of transporting significant quantities of horizontal momentum between their source regions and regions where they are absorbed or dissipated. Previous GCM results have shown that the large-scale momentum sinks resulting from breaking gravity waves play an important role in determining the structure of the large-scale flow, particularly for higher resolution truncations. The CCM3 incorporates a parameterization for a spectrum of vertically propagating internal gravity waves based on the work of Lindzen (1981), Holton (1982), Garcia and Solomon (1985) and MacFarlane (1987). Although the parameterization can treat a fairly general spectrum of monochromatic waves, in the standard tropospheric version of CCM3, the spectrum is reduced to a single stationary wave generated by flow over orography, following McFarlane (1987) and similar to the parameterization in CCM3. A more complete spectrum is used for middle atmosphere studies. As with all CCM3 physical parameterizations, non-resolvable-scale effects of vertically propagating gravity waves are determined in physical space on the transform grid.

Adiabiatic inviscid formulation

Following Lindzen (1981), the continous equations for the gravity wave parameterization are obtained from the two-dimensional hydrostatic momentum, continuity and thermodynamic equations in a vertical plane:

$$\left(\frac{\partial}{\partial t} + u\frac{\partial}{\partial x}\right) u = -\frac{\partial \Phi}{\partial x}\,, \tag{4.e.1}$$

$$\frac{\partial u}{\partial x} + \frac{\partial w}{\partial z} = 0\,, \tag{4.e.2}$$

$$\left(\frac{\partial}{\partial t} + u\frac{\partial}{\partial x}\right) \frac{\partial \Phi}{\partial z} + N^2 w = 0\,. \tag{4.e.3}$$

Where N is the local Brunt-Väisällä frequency, and w is the vertical velocity in (log pressure) height coordinates. Eqs. (4.e.1)–(4.e.3) are linearized about a large scale background wind $\overline{u}$, with perturbations u', and combined to obtain:

$$\left(\frac{\partial}{\partial t} + \overline{u}\frac{\partial}{\partial x}\right)^2 \frac{\partial^2 w'}{\partial z^2} + N^2 \frac{\partial^2 w'}{\partial x^2} = 0\,. \tag{4.e.4}$$

Solutions to (4.e.4) are assumed to be of the form:

$$w' = \hat{w} e^{ik(x-ct)} e^{z/2H} + \text{conjugate}\,, \tag{4.e.5}$$

where H is the scale height, k is the horizontal wavenumber and c is the phase speed of the wave. Subsituting (4.e.5) into (4.e.4), one obtains:

$$-k^2(\overline{u} - c)^2 \left(\frac{\partial}{\partial z} + \frac{1}{2H}\right)^2 \hat{w} - k^2 N^2 \hat{w} = 0\,. \tag{4.e.6}$$

Neglecting $\frac{1}{2H}$ compared to $\frac{\partial}{\partial z}$ in (4.e.6), one obtains the final form of the two dimensional wave equation:

$$\frac{d^2\hat{w}}{dz^2} + \lambda^2\hat{w} = 0\,, \qquad (4.e.7)$$

with the coefficient defined as:

$$\lambda = \frac{N}{(\overline{u} - c)}\,. \qquad (4.e.8)$$

The WKB solution of (4.e.8) is:

$$\hat{w} = A\lambda^{-1/2}\exp\left(i\int_0^z \lambda dz'\right)\,, \qquad (4.e.9)$$

where A is determined from the wave amplitude at the source ($z = 0$), The Reynolds stress associated with the (4.e.9) is:

$$\tau(z) = \tau(z=0) = \rho\overline{u'w'} = -\frac{2}{k}|A|^2\rho_0\mathrm{sgn}(\lambda)\,, \qquad (4.e.10)$$

and is conserved while the momentum flux $\overline{u'w'}$ grows exponentially with height as the inverse of the density.

Saturation condition

The wave amplitude in (4.e.1) grows as $e^{z/2H}$ until the wave becomes unstable to convective overturning, Kelvin-Helmholtz instability, or other nonlinear processes. At that point, the wave amplitude is assumed to be controlled at the amplitude which would lead to the onset of the instability and the wave is "saturated". The saturation condition used in CCM3 is from McFarlane (1987), based on a maximum Froude number (F_c), or streamline slope.

$$|\rho\overline{u'w'}| \leq \tau^* = F_c^2 E\frac{k}{2}\rho\frac{|\overline{u} - c|^3}{N}\,, \qquad (4.e.11)$$

where τ^* is the saturation stress, E is an "efficiency factor", and $F_c^2 E \sim 0.1$. Following Lindzen (1981), within a saturated region the momentum tendency can be determined analytically from the divergence of the saturation stress (4.e.11):

$$\begin{aligned}\frac{\partial u}{\partial t} &= -\frac{1}{\rho}\frac{\partial}{\partial z}\rho\overline{u'w'}\,,\\ &\simeq E\frac{k}{2}\frac{(\overline{u} - c)^3}{N}\frac{1}{\rho}\frac{\partial\rho}{\partial z}\,,\\ &\simeq E\frac{k}{2}\frac{(\overline{u} - c)^3}{N}\frac{g}{RT}\,,\end{aligned} \qquad (4.e.12)$$

The analytic solution (4.e.12) is used below as an upper bound on the tendency computed by differentiating the stress profile. This condition is usually invoked when the wave saturates close to a critical level ($\overline{u} - c = 0$).

Radiative damping and dissipation

The effect of radative damping of the vertically propagating gravity waves can be included in the solutions (4.e.9) and (4.e.10) relatively easily through the Newtonian cooling approximation. The effect of mechanical mixing can also be included through an eddy viscosity, giving a damped vertical stress profile:

$$\tau(z) = \tau(0)\exp\left(-\frac{2}{H}\int_0^z \lambda_i dz'\right) , \tag{4.e.13}$$

where the imaginary part of the local vertical wavenumber, λ_i depends on the Newtonian cooling coefficient α and eddy viscosity D as:

$$\lambda_i = \frac{N}{2k(\overline{u}-c)^2}\left(\alpha + \frac{N^2}{(\overline{u}-c)^2}D\right) . \tag{4.e.14}$$

In CCM3, $\alpha = 10^{-6}$ s^{-1} and is not important in the solution. D is determined from the saturation condition, but is only of modest importance, particularly in the standard tropospheric model with only a single wave. Again following Lindzen (1981), one can assume that within a region of wave staturation, the wave damping balances the exponential growth with height. The required diffusivity is then:

$$D^* = \frac{(\overline{u}-c)^2}{N^2}\left[\frac{Ek}{HN}(\overline{u}-c)^2 - \alpha\right] . \tag{4.e.15}$$

We define D^* as the saturation diffusivity, analogous to the saturation stress τ^*, for use below.

Orographic source function

For orographically generated waves, the source is taken from McFarlane (1987):

$$\tau_g = |\rho\overline{u'w'}|_0 = E\frac{k}{2}h_0^2\rho_0 N_0 \overline{u}_0 , \tag{4.e.16}$$

where h_0 is the streamline displacement at the source level, and ρ_0, N_0, and $\overline{u}_0$ are also defined at the source level. For orographic waves, the subgrid-scale standard deviation of the orography σ is used to estimate the average mountain height, determining the typical streamline displacement. An upper bound is used on the displacement which corresponds to requiring that the wave not be supersaturated at the source level.

$$h_0 = \min(2\sigma, F_c\frac{\overline{u}_0}{N_0}) . \tag{4.e.17}$$

The source level quantities ρ_0, N_0, and $\overline{u}_0$ are defined by vertical averages over the source region, taken to be 2σ, the depth to which the average mountain penetrates into the domain:

$$\psi_0 = \int_0^{2\sigma} \psi\rho dz, \qquad \psi \in \{\rho, N, u, v\} . \tag{4.e.18}$$

The source level wind vector (u_0, v_0) determines the orientation of the coordinate system in (4.e.1)–(4.e.3) and the magnitude of the source wind $\overline{u}_0$.

Gravity wave spectrum

A small background gravity wave stress τ_b is assumed to be present at all points and the actual source stress is determined from the maximum of the orographic source (4.e.16) and the background value. When the background stress is used, the source level is assumed to be the bottom model level and the gravity wave stress at the source level is aligned with source wind, as usual. At all other levels, the local wind vector is projected onto the source wind vector, reducing the problem to two dimensions.

A gravity wave spectrum can be included by setting the number of waves to be greater than zero. In that case,

$$\begin{aligned} \tau_s(c_\ell) &= \tau_b \exp\left[-\left(\frac{c_\ell}{30}\right)^2\right] \\ c_\ell &\in [0, \pm 10, \pm 20, ...] \,. \end{aligned} \tag{4.e.19}$$

Above the source region, the saturation condition is enforced separately for each wave:

$$\tau(c_\ell) \le \tau_\ell^* = F_c^2 E \frac{k}{2} \rho \frac{|\overline{u} - c_\ell|^3}{N} \,, \tag{4.e.20}$$

$$\frac{\partial \overline{u}_\ell}{\partial t} = -\frac{1}{\rho}\frac{\partial \tau_\ell}{\partial z} \le -\frac{1}{\rho}\frac{\partial \tau_\ell^*}{\partial z} = E\frac{k}{2}\frac{|\overline{u} - c_\ell|^3}{N}\frac{g}{RT} \,, \tag{4.e.21}$$

$$\frac{\partial \mathbf{V}}{\partial t} = \frac{\mathbf{V}_s}{|\mathbf{V}_s|}\sum_l \frac{\partial \overline{u}_\ell}{\partial t} \,. \tag{4.e.22}$$

Finally, the diffusivity used to determine the stress profile (4.e.13) outside of saturated regions is

$$D = \max\left(D_\ell^* \frac{\tau_\ell}{\tau_\ell^*}, \forall \ell\right) \,. \tag{4.e.23}$$

Although the standard CCM3 only uses a single gravity wave with $c = 0$, the code allows for the more general spectrum described above.

Numerical approximations

The gravity wave drag parameterization is applied immediately after the nonlinear vertical diffusion. The interface temperatures are first determined from:

$$T_{k+1/2}^{n-1} = \frac{T_k^{n-1} + T_{k+1}^{n-1}}{2} \,, . \tag{4.e.24}$$

The interface Brunt-Väisällä frequency is

$$N_{k+1/2}^2 = \frac{g^2}{T_{k+1/2}^{n-1}} \left(\frac{1}{c_p} - \rho \frac{\partial T}{\partial p} \right)_{k+1/2} , \tag{4.e.25}$$

Where the interface density and temperature gradient are:

$$\rho_{k+1/2}^{n-1} = \frac{RT_{k+1/2}^{n-1}}{p_{k+1/2}} , \tag{4.e.26}$$

$$\left(\frac{\partial T^{n-1}}{\partial p} \right)_{k+1/2} = \frac{T_k^{n-1} - T_{k+1}^{n-1}}{p_k - p_{k+1}} . \tag{4.e.26}$$

The midpoint Brunt-Väisällä frequencies are determined as $N_k = (N_{k+1/2} + N_{k-1/2})/2$.

The level for the orographic source is an interface determined from an estimate of the vertical penetration of the subgrid mountains within the grid box. The subgrid scale standard deviation of the orography, σ_h, gives the variation of the mountains about the mean elevation, which defines the Earth's surface in the model. Therefore the source level is defined as the interface, $k_s - 1/2$, for which $z_{k_s+1/2} < 2\sigma_h < z_{k_s-1/2}$, where the interface heights are defined from the midpoint heights by $z_{k+1/2} = \sqrt{(z_k z_{k+1})}$.

The source level wind vector, density and Brunt-Väisällä frequency are determined by vertical integration over the region from the surface to interface $k_s + 1/2$:

$$\psi_0 = \sum_{k=k_s}^{K} \psi_k (p_{k+1/2} - p_{-1/2}) , \qquad \psi \in \{\rho, N, u, v\} . \tag{4.e.27}$$

The source level background wind is $\overline{u}_0 = \sqrt{(u_0^2 + v_0^2)}$ and the unit vector for the source wind is

$$(x_0, y_0) = (u_0, v_0)/\overline{u}_0 , \tag{4.e.28}$$

the projection of the midpoint winds onto the source wind is

$$\overline{u}_k = u_k^{n-1} x_0 + v_k^{n-1} y_0 , \tag{4.e.29}$$

and the projected interface winds are

$$\overline{u}_{k+1/2} = (\overline{u}_k + \overline{u}_{k+1})/2 . \tag{4.e.30}$$

Assuming that $\overline{u}_0 > 2$ m s^{-1} and $2\sigma^h > 10$ m, then the orographic source term, τ_g is given by (4.e.16) and (4.e.17), with F_c =0.5, E = .125, and $k = 2\pi/10^5$ m^{-1}. The gravity wave source term is then

$$\tau_0 = \max(\tau_g, \tau_b) , \tag{4.e.31}$$

$$\tau_b = \tau_e + \tau_{(N,S)} , \tag{4.e.32}$$

where $\tau_N = 0.75 \sin |2\phi|$ and $\tau_S = 1.2 \sin |2\phi|$ are applied in the Northern and Southern Hemispheres, respectively, and $\tau_e = \exp\left[-(\phi/10)^2\right]$ Pa. The background values are not significant in tropospheric version of CCM3, but become important for middle atmosphere studies.

Although the code contains a provision for a linear stress profile within a "low level deposition region", this part of the code is not used in the standard model, since $\tau_{\text{ldv}} = 0$.

The stress profiles are determined by scanning up from the bottom of the model to the top. The stress at the source level is determined by (4.e.31). The saturation stress, τ^* at each interface is determined by (4.e.11), where we note that $\tau^* = 0$ if a critical level is passed. A critical level is contained within a layer if $(\overline{u}_{k+1/2} - c)/(\overline{u}_{k-1/2} - c) < 0$. The diffusivity at each interface is determined by

$$D_{k-1/2} = D^*_{k-1/2} \frac{\tau_{k+1/2}}{\tau^*_{k-1/2}}, \tag{4.e.33}$$

where D^* is given by (4.e.15). The interface stress is then determined from the stress on the interface below by:

$$\tau_{k-1/2} = \min(\tau^*_{k-1/2}, \tau_{k+1/2} \exp\left[-2m_i \frac{R}{g} T_k (\ln p_{k+1/2} - \ln p_{k-1/2})\right], \tag{4.e.34}$$

Limits on the range of stresses within the spectrum are present in the code, but are only applied when the spectrum contains more than a single wave, so are not relevant to the standard model.

Once the complete stress profile has been obtained, the forcing of the background wind is determined by differentiating the profile during a downward scan:

$$\frac{\partial \overline{u}_k}{\partial t} = g \frac{\tau_{k+1/2} - \tau_{k-1/2}}{p_{k+1/2} - p_{k-1/2}} < \left(\frac{\partial \overline{u}_k}{\partial t}\right)^{\max}. \tag{4.e.35}$$

$$\left(\frac{\partial \overline{u}_k}{\partial t}\right)^{\max} = \min\left[\left(\frac{\partial \overline{u}_k}{\partial t}\right)^*, \frac{.5|c - \overline{u}_k|}{2\Delta t}, 500\text{m/s}^{-1}/\text{day}^{-1}\right]. \tag{4.e.36}$$

The first bound on the forcing, $(\partial \overline{u}_k / \partial t)^*$ is given by the analytic solution (4.e.12). This bound typically comes into play when a critical level is near and the background wind is rapidly varying in the vertical. The second bound comes from requiring that the forcing not be large enough to push the wind mode than half way towards a critical level within a time step and takes the place of an implicit solution. This bound is present for numerical stability, it comes into play when the time step is too large for the forcing. It is not feasible to change the time step, or to write an implicit solver, so an *a priori* bound is used instead. The third bound is used to constrain the forcing to lie within a physically plausible range (although the value used is extremely large) and is rarely invoked.

When any of the bounds in (4.e.35) are invoked, conservation of stress is violated. In this case, stress conservation is ensured by decreasing the stress on the lower interface to match the actual stress divergence in the layer:

$$\tau_{k+1/2} = \tau_{k-1/2} + \frac{\partial \overline{u}_k}{\partial t} \frac{p_{k+1/2} - p_{k-1/2}}{g}. \tag{4.e.37}$$

This has the effect of pushing some of the stress divergence into the layer below, a reasonable choice since the waves are propagating up from below.

Finally, the vector momentum forcing by the gravity waves is determined by projecting the background wind forcing with the unit vectors of the source wind:

$$\frac{\partial \mathbf{V}_k}{\partial t} = \frac{\partial \overline{u}_k}{\partial t}(x_0, y_0). \tag{4.e.38}$$

The gravity wave source is also projected in the direction of the source wind for recording on the history files. The momentum tendencies from (4.e.38) are added to the nonlinear terms in the vorticity and divergence equations. In addition, the frictional heating implied by the momentum tendencies, $\frac{1}{c_p^*}\mathbf{V}_k^{n-1}\partial \mathbf{V}_k/\partial t$, is added to the thermodynamic equation.

f. Rayleigh Friction

The Rayleigh friction term in CCM3 is a carryover from CCM2. It was only used for the stratosphere and, for those applications, it has been superseded by the gravity wave spectrum parameterization described in the previous section. Since the parameterization is still in the CCM3 code, it is described here. However, the parameterization will probably be removed in revised versions of CCM3.

A Rayleigh friction term has been included in the zonal momentum equation to provide a crude parameterization of the effect of breaking gravity waves in the mesosphere and to prevent reflection of waves from the top boundary. This term is implemented in the form

$$\frac{\partial \mathbf{V}}{\partial t} = -K_R \mathbf{V} \tag{4.f.1}$$

The friction coefficient is determined from

$$K_R = \frac{1}{3}\left[1 + \tanh\left(\frac{z - 63 \times 10^3}{7.5 \times 10^3}\right)\right] \text{ days}^{-1}, \tag{4.f.2}$$

where

$$z = -h \ln(A + B), \tag{4.f.3}$$

and $h = 7 \times 10^3$ m. This term, which is not intended to be a faithful representation of mesospheric dynamics is inactive in the standard model configuration.

4.2 Adjustment Physics

After the new temperatures and mixing ratios are computed from (3.*a*.5) and (3.*a*.6), a series of convective adjustment schemes is applied to create mutually adjusted

T and q fields. If the predicted atmosphere is not saturated and the lapse rate exceeds the dry adiabatic lapse rate, the temperatures are reset to give a dry adiabatic lapse rate, but only in the "stratospheric" region of the model (i.e., top three levels in the standard configuration). The moisture field is assumed to be mixed by this process as well and is reset to the average value. The stability–dependent vertical diffusion provides for dry turbulent vertical mixing in the troposphere. Thus, in practice, momentum is mixed as well as heat and moisture. If the atmosphere is moist adiabatically unstable, the moisture and temperature fields are simultaneously modified in accordance with a parametric representation of "deep" cumulus convection, followed by a simple model of shallow and mid-tropospheric moist convection. If the atmosphere is stable but supersaturated, the moisture field is adjusted to be saturated and the temperature field is simultaneously adjusted to reflect the heating due to the release of latent heat. When the moisture field is changed to eliminate supersaturation, the change is assumed to go into precipitation. The details of these processes are presented in the following sections, where we use the notation (T, q) to denote values before the adjustment, and $(\hat{T}, \hat{q})$ after the adjustment.

g. Deep Convection

The process of deep convection is treated with a parameterization scheme developed by Zhang and McFarlane (1995). The scheme is based on a plume ensemble approach where it is assumed that an ensemble of convective scale updrafts (and the associated saturated downdrafts) may exist whenever the atmosphere is conditionally unstable in the lower troposphere. The updraft ensemble is comprised of plumes sufficiently buoyant so as to penetrate the unstable layer, where all plumes have the same upward mass flux at the bottom of the convective layer. Moist convection occurs only when there is convective available potential energy (CAPE) for which parcel ascent from the subcloud layer acts to destroy the CAPE at an exponential rate using a specified adjustment time scale. For the convenience of the reader we will review some aspects of the formulation, but refer the interested reader to Zhang and McFarlane (1995) for additional detail, including behavioral characteristics of the parameterization scheme.

The large-scale budget equations distinguish between a cloud and sub-cloud layer where temperature and moisture response to convection in the cloud layer is written in terms of bulk convective fluxes as

$$c_p \left(\frac{\partial T}{\partial t} \right)_{cu} = -\frac{1}{\rho} \frac{\partial}{\partial z} (M_u S_u + M_d S_d - M_c S) + L(C - E) \tag{4.g.1}$$

$$\left(\frac{\partial q}{\partial t} \right)_{cu} = -\frac{1}{\rho} \frac{\partial}{\partial z} (M_u q_u + M_d q_d - M_c q) + E - C, \tag{4.g.2}$$

and the subcloud layer response is written as

$$c_p\left(\rho\frac{\partial T}{\partial t}\right)_m = -\frac{1}{\Delta z_m}(M_b[S(z_m) - S_u(z_m)] + M_d[S(z_m) - S_d(z_m)]) \qquad (4.g.3)$$

$$\left(\rho\frac{\partial q}{\partial t}\right)_m = -\frac{1}{\Delta z_m}(M_b[q(z_m) - q_u(z_m)] + M_d[q(z_m) - q_d(z_m)])\,, \qquad (4.g.4)$$

where the net vertical mass flux in the convective region, M_c, is comprised of upward, M_u, and downward, M_d, components, C and E are the large-scale condensation and evaporation rates, S, S_u, S_d, q, q_u, q_d, are the corresponding values of the dry static energy and specific humidity, Δz_m is the depth of the mean subcloud layer, the subscript m denotes subcloud layer properties, z_m is the height of the subcloud layer, and M_b is the cloud base mass flux.

The cloud model is composed of two components, the updraft ensemble and the downdraft ensemble. The updraft ensemble is represented as a collection of entraining plumes, each with a characteristic fractional entrainment rate. Mass carried upward by the plumes is detrained into the environment in a thin layer at the top of the plume where the detrained air is assumed to have the same thermal properties as in the environment. The top of the shallowest of the convective plumes is assumed to be no lower than the mid-tropospheric minimum in saturated moist static energy, h^*, ensuring that the cloud top detrainment is confined to the conditionally stable portion of the atmospheric column. Each plume is assumed to have the same value for the cloud base mass flux where the vertical distribution of the cloud updraft mass flux is given by

$$M_u = M_b \int_0^{\lambda_D} \frac{1}{\lambda_0} e^{\lambda(z-z_m)} d\lambda \qquad (4.g.5)$$

λ_0 is the maximum detrainment rate, and λ_D is the entrainment rate for the updraft that detrains at height z which is iteratively determined by requiring that

$$h_b - h^* = \lambda_D \int_{z_m}^{z} [h_b - h(z')] e^{[\lambda_D(z'-z)]} dz' \qquad (4.g.6)$$

Thus, the budget equations for dry static energy, water vapor mixing ratio, and cloud liquid water, ℓ, are written as

$$\frac{\partial}{\partial z}\left(M_u S_u\right) = \left(E_u - D_u\right) S + LC_u \qquad (4.g.7)$$

$$\frac{\partial}{\partial z}\left(M_u q_u\right) = E_u q - D_u q^* + C_u \qquad (4.g.8)$$

$$\frac{\partial}{\partial z}(M_u \ell) = -D_u \ell_d + C_u - R_r \tag{4.g.9}$$

where the conversion from cloud water to rain water is given by

$$R_r = c_0 M_u \ell, \tag{4.g.10}$$

and $c_0 = 2x10^{-3}\mathrm{m}^{-1}$.

Downdrafts are assumed to exist whenever there is precipitation production in the updraft ensemble where the downdrafts start at or below the bottom of the updraft detrainment layer. Detrainment from the downdrafts is confined to the subcloud layer, where all downdrafts have the same mass flux at the top of the downdraft region. Accordingly, the ensemble downdraft mass flux takes a similar form to (4.g.5) but includes a "proportionality factor" to ensure that the downdraft strength is physically consistent with precipitation availability. This coefficient takes the form

$$\alpha = \mu \left[\frac{P}{P + E_d} \right], \tag{4.g.11}$$

where P is the total precipitation in the convective layer and E_d is the rain water evaporation required to maintain the downdraft in a saturated state. This formalism ensures that the downdraft mass flux vanishes in the absence of precipitation, and that evaporation cannot exceed some fraction, μ, of the precipitation, where $\mu = 0.2$.

The parameterization is closed, i.e., the cloud base mass fluxes are determined, as a function of the rate at which the cumulus consume convective available potential energy (CAPE). Since the large-scale temperature and moisture changes in both the cloud and subcloud layer are linearly proportional to the cloud base updraft mass flux (e.g., see eq. 4.g.1 – 4.g.4), the CAPE change due to convective activity can be written as

$$\left(\frac{\partial A}{\partial t} \right)_{cu} = -M_b F \tag{4.g.12}$$

where F is the CAPE consumption rate per unit cloud base mass flux. The closure condition is that the CAPE is consumed at an exponential rate by cumulus convection with characteristic adjustment time scale τ;

$$M_b = \frac{A}{\tau F} \tag{4.g.13}$$

Convective transport of trace species are assumed to follow (4.g.8) where q is a moist mixing ratio of the tracer and $C_u \equiv 0$. The interested reader can find a more complete discussion of the formalism in Zhang and McFarlane (1995).

h. Shallow/Middle Tropospheric Moist Convection

To characterize the convective forcing associated with shallow and middle-level convection (i.e., convective activity not treated by the primary convective parameterization scheme) we write the large-scale budget equations for dry static energy and total water as

$$\begin{aligned}\frac{\partial \overline{s}}{\partial t} &= -\nabla \cdot \overline{\mathbf{V}}\,\overline{s} - \frac{\partial \overline{\omega}\,\overline{s}}{\partial p} - \frac{\partial}{\partial p}\left(\overline{\omega' s'_\ell}\right) + L\mathcal{R} + c_p Q_R \\ &= \left.\frac{\partial \overline{s}}{\partial t}\right|_{R.S.} - \frac{\partial}{\partial p}\left(\overline{\omega' s'_\ell}\right) + L\mathcal{R}\end{aligned} \tag{4.h.1}$$

and

$$\begin{aligned}\frac{\partial \overline{q}}{\partial t} &= -\nabla \cdot \overline{\mathbf{V}}\,\overline{q} - \frac{\partial \overline{\omega}\,\overline{q}}{\partial p} - \frac{\partial}{\partial p}\left(\overline{\omega' (q' + \ell')}\right) - \mathcal{R} \\ &= \left.\frac{\partial \overline{q}}{\partial t}\right|_{R.S.} - \frac{\partial}{\partial p}\left(\overline{\omega' (q' + \ell')}\right) - \mathcal{R},\end{aligned} \tag{4.h.2}$$

where $s \equiv c_p T + gz$ is the dry static energy; ℓ represents liquid water; $s_\ell \equiv s - L\ell$ is the static energy analogue of the liquid water potential temperature introduced by Betts (1975); $\mathcal{R}$ is the "convective-scale" liquid water sink (sometimes denoted by $C - E$); and Q_R is the net radiative heating rate. The subscript $R.S.$ denotes the resolvable-scale contributions to the large-scale budget. Note that variations of the mean liquid water on the large scale have been neglected. The barred quantities represent horizontal averages over an area large enough to contain a collection of cloud elements, but small enough so as to cover only a fraction of a large-scale disturbance. By writing the mean thermodynamic variables in terms of their average cloud and environment properties, and assuming that the convection occupies only a small fraction of the averaging area, the vertical eddy transports $\overline{\omega' s'_\ell}$ and $\overline{\omega' (q' + \ell')}$ can be approximated by the difference between the upward flux inside a typical convective element and the downward flux (*i.e.*, induced subsidence) in the environment (cf. Yanai *et al.*, 1973). Mathematically, this approximation takes the form

$$F_{s_\ell}(p) = -\frac{1}{g}\left(\overline{\omega' s'_\ell}\right) \approx -M_c(p)\left(\overline{s}(p) - s_c(p) + L\ell(p)\right) \tag{4.h.3}$$

and

$$F_{q+\ell}(p) = -\frac{1}{g}\left(\overline{\omega' (q' + \ell')}\right) \approx -M_c(p)\left(\overline{q}(p) - q_c(p) - \ell(p)\right), \tag{4.h.4}$$

where M_c is a convective mass flux, and s_c, q_c, and ℓ represent cloud-scale properties. Thus, (4.h.1) and (4.h.2) can be written as

$$\frac{\partial \overline{s}}{\partial t} = \left.\frac{\partial \overline{s}}{\partial t}\right|_{R.S.} + g\frac{\partial}{\partial p}F_{s_\ell} + L\mathcal{R}\,, \tag{4.h.5}$$

and

$$\frac{\partial \overline{q}}{\partial t} = \left.\frac{\partial \overline{q}}{\partial t}\right|_{R.S.} + g\frac{\partial}{\partial p}F_{q+\ell} - \mathcal{R} \; . \tag{4.h.6}$$

Let us now turn our attention to a vertically discrete model atmosphere and consider the case where layers k and $k+1$ are moist adiabatically unstable, *i.e.,* a non-entraining parcel of air at level $k+1$ (with moist static energy h_c) would be unstable if raised to level k. We assume the existence of a non-entraining convective element with roots in level $k+1$, condensation and rainout processes in level k, and limited detrainment in level $k-1$ (see Figure 5). In accordance with (4.h.5) and (4.h.6), the discrete dry static energy and specific humidity budget equations for these three layers can be written as

$$\hat{\overline{s}}_{k-1} = \overline{s}_{k-1} + \frac{2\Delta t g}{\Delta p_{k-1}}\left\{\beta m_c\left(s_c - \overline{s}_{k-\frac{1}{2}} - L\ell_k\right)\right\} \; , \tag{4.h.7}$$

$$\hat{\overline{s}}_{k} = \overline{s}_{k} + \frac{2\Delta t g}{\Delta p_{k}}\left\{m_c\left(s_c - \overline{s}_{k+\frac{1}{2}}\right) - \beta m_c\left(s_c - L\ell_k - \overline{s}_{k-\frac{1}{2}}\right) + LR_k\right\} \; , \tag{4.h.8}$$

$$\hat{\overline{s}}_{k+1} = \overline{s}_{k+1} + \frac{2\Delta t g}{\Delta p_{k+1}}\left\{m_c\left(\overline{s}_{k+\frac{1}{2}} - s_c\right)\right\} \; , \tag{4.h.9}$$

$$\hat{\overline{q}}_{k-1} = \overline{q}_{k-1} + \frac{2\Delta t g}{\Delta p_{k-1}}\left\{\beta m_c\left(q_c - \overline{q}_{k-\frac{1}{2}}\right)\right\} \; , \tag{4.h.10}$$

$$\hat{\overline{q}}_{k} = \overline{q}_{k} + \frac{2\Delta t g}{\Delta p_{k}}\left\{m_c\left(q_c - \overline{q}_{k+\frac{1}{2}}\right) - \beta m_c\left(q_c - \overline{q}_{k-\frac{1}{2}}\right) - R_k\right\} \; , \tag{4.h.11}$$

$$\hat{\overline{q}}_{k+1} = \overline{q}_{k+1} + \frac{2\Delta t g}{\Delta p_{k+1}}\left\{m_c\left(\overline{q}_{k+\frac{1}{2}} - q_c\right)\right\} \; , \tag{4.h.12}$$

where the subscript c denotes cloud properties in the ascent region, m_c is a convective mass flux at the bottom of the condensation layer (level $k+\frac{1}{2}$, "cloud base"), and β is a yet to be determined "detrainment parameter" at level $k-\frac{1}{2}$ that will take a value between zero and one. Note that the convective-scale liquid water sink $\mathcal{R}$ has been redefined in terms of mass per unit area per unit time (denoted by R), and the resolvable-scale components have been dropped for the convenience of the following discussion. In the general case, the thermodynamic properties of the updraft region can be assumed to be equal to their large-scale values in the sub-cloud layer, level $k+1$, plus some arbitrary thermodynamic perturbation; i.e.,

$$s_c = \overline{s}_{k+1} + s', \tag{4.h.13}$$

$$q_c = \overline{q}_{k+1} + q', \tag{4.h.14}$$

and

$$h_c = s_c + Lq_c. \tag{4.h.15}$$

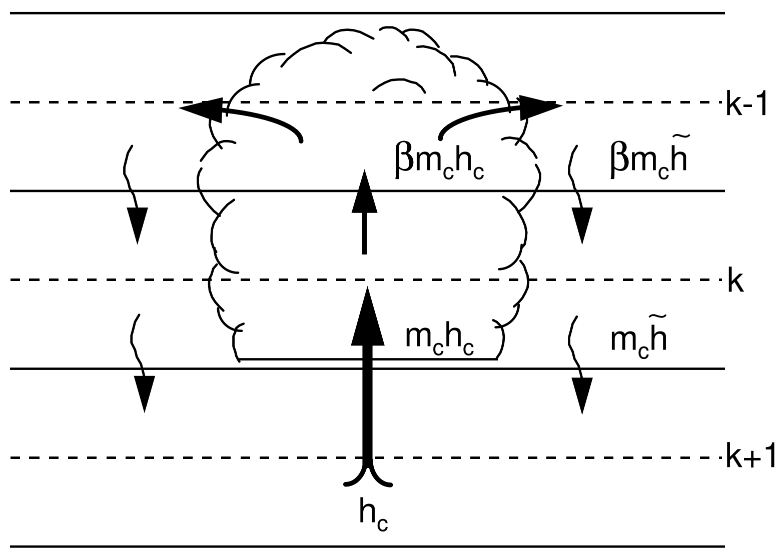

Figure 4. Conceptual three-level non-entraining cloud model

In the CCM3 implementation of this scheme, when a sub-cloud layer lies within the diagnosed atmospheric boundary layer, the perturbation quantities q' and s' are assumed to be equal to $b\,\frac{(\overline{w'q'})_s}{w_m}$ (e.g., see 4.d.19 and the atmospheric boundary layer discussion) and zero.

The liquid water generation rate at level k is given by

$$m_c \ell_k = m_c \left[q_c - (q_c)_k \right] . \tag{4.h.16}$$

Using the saturation relation

$$(q_c)_k = \overline{q}_k^* + \frac{\gamma_k}{1+\gamma_k}\,\frac{1}{L}\left(h_c - \overline{h}_k^* \right) , \tag{4.h.17}$$

where $\overline{q}^*$ denotes the saturated specific humidity

$$\overline{q}^* = \epsilon\,\frac{e_s}{p-(1-\epsilon)e_s} , \tag{4.h.18}$$

h^* denotes the saturated moist state energy, e_s is the saturation vapor pressure (determined from a precomputed table), and $\gamma \equiv (L/c_p)\left(\partial \overline{q}^*/\partial \overline{T}\right)_p$, and assuming that the large-scale liquid water divergence in layer k is zero, (4.h.16) can be manipulated to give the rainout term in layer k as

$$LR_k \equiv L(1-\beta)m_c \ell_k = (1-\beta)m_c \left\{ \overline{s}_k - s_c + \frac{1}{1+\gamma_k}\left(h_c - \overline{h}_k^* \right) \right\} , \tag{4.h.19}$$

and the liquid water flux into layer $k-1$ as

$$\beta m_c L \ell_k = \beta m_c \left\{ \overline{s}_k - s_c + \frac{1}{1+\gamma_k}\left(h_c - \overline{h}_k^* \right) \right\} . \tag{4.h.20}$$

Equations (4.h.9) and (4.h.12) can be combined to give an equation for moist static energy in layer $k+1$

$$\frac{\partial \overline{h}_{k+1}}{\partial t} = \frac{g}{\Delta p_{k+1}} m_c \left(\overline{h}_{k+\frac{1}{2}} - h_c \right) \approx \frac{\partial h_c}{\partial t} \,, \tag{4.h.21}$$

where the approximation follows from the assumption that $\partial h'/\partial t$ can be neglected. Using the relation $(1+\gamma_k)\frac{\partial \overline{s}_k}{\partial t} = \frac{\partial \overline{h}_k^*}{\partial t}$, (4.$h$.8) can be manipulated to give an expression for the time rate of change of saturated moist static energy in layer k

$$\frac{\partial \overline{h}_k^*}{\partial t} = \frac{g m_c}{\Delta p_k} \left(1+\gamma_k\right) \left\{ \left(s_c - \overline{s}_{k+\frac{1}{2}} + L\ell_k \right) - \beta \left(s_c - \overline{s}_{k-\frac{1}{2}} \right) \right\} . \tag{4.h.22}$$

Subtracting (4.h.22) from (4.h.21) results in

$$\begin{aligned} \frac{\partial \left(h_c - \overline{h}_k^* \right)}{\partial t} = m_c \Big\{ & \frac{g}{\Delta p_{k+1}} \left(\overline{h}_{k+\frac{1}{2}} - h_c \right) \\ & - \frac{g}{\Delta p_k} \left(1+\gamma_k\right) \left[\left(\overline{s}_k - \overline{s}_{k+\frac{1}{2}} \right) - \beta \left(s_c - \overline{s}_{k-\frac{1}{2}} \right) \right] \Big\} , \end{aligned} \tag{4.h.23}$$

from which the convective mass flux m_c can be written as

$$m_c = \frac{h_c - \overline{h}_k^*}{g\tau \left\{ \frac{(1+\gamma_k)}{\Delta p_k} \left[\left(s_c - \overline{s}_{k+\frac{1}{2}} + L\ell_k \right) - \beta \left(s_c - \overline{s}_{k-\frac{1}{2}} \right) \right] - \frac{1}{\Delta p_{k+1}} \left[\overline{h}_{k+\frac{1}{2}} - h_c \right] \right\}} \tag{4.h.24}$$

where τ is a characteristic convective adjustment time scale.

Physically realistic solutions require that the convective mass flux m_c be positive, implying the following constraint on the detrainment parameter β

$$\beta \left(1+\gamma_k\right) \left(s_c - \overline{s}_{k-\frac{1}{2}} \right) < \left(1+\gamma_k\right) \left(s_c - \overline{s}_{k+\frac{1}{2}} + L\ell_k \right) - \frac{\Delta p_k}{\Delta p_{k+1}} \left(\overline{h}_{k+\frac{1}{2}} - h_c \right) . \tag{4.h.25}$$

A second physical constraint is imposed to ensure that the adjustment process does not supersaturate the "detrainment layer", $k-1$, which leads to the following constraint on the detrainment parameter, β:

$$\begin{aligned} & \frac{1}{\Delta p_k} \left[\left(1+\gamma_k\right) \left(s_c - \overline{s}_{k+\frac{1}{2}} + L\ell_k \right) \right] - \frac{1}{\Delta p_{k+1}} \left[\overline{h}_{k+\frac{1}{2}} - h_c \right] > \\ & \beta \Bigg\{ \left(\frac{2\Delta t}{\tau} \right) \frac{h_c - \overline{h}_k^*}{\left(\overline{h}_{k-1}^* - \overline{h}_{k-1} \right) \Delta p_{k-1}} \Bigg[\gamma_{k-1} \left\{ \overline{s}_{k-\frac{1}{2}} - s_c + L\ell_k \right\} \\ & + h_c - \overline{h}_{k-\frac{1}{2}} - s_c + \overline{s}_{k-\frac{1}{2}} \Bigg] + \frac{1}{\Delta p_k} \left(1+\gamma_k\right) \left(s_c - \overline{s}_{k-\frac{1}{2}} \right) \Bigg\} . \end{aligned} \tag{4.h.31}$$

A final constraint on the adjustment process attempts to minimize the introduction of $2\Delta\eta$ computational structures in the thermodynamic field by not allowing the procedure to increase the vertical gradient of h when $\frac{\partial h}{\partial p} < 0$ in the upper pair of layers. Mathematically this constraint is formulated by discretizing in time the moist static energy equations in layers k and $k-1$, leading to the following constraint on β

$$\frac{\overline{h}_k - \overline{h}_{k-1} - G}{(h_c - \overline{h}_k^*)} \left(\frac{\tau}{2\Delta t}\right) \left(\frac{1}{\Delta p_h} \left[(1+\gamma_k)(s_c - \overline{s}_{k+\frac{1}{2}} + L\ell_k) \right] - \frac{1}{\Delta p_{k+\frac{1}{2}}} \left[\overline{h}_{k+\frac{1}{2}} - h_c \right] \right)$$

$$+ \frac{1}{\Delta p_k} \left[h_c - \overline{h}_{k+\frac{1}{2}} \right]$$

$$\geq \beta \left\{ \frac{\overline{h}_k - \overline{h}_{k-1} - G}{h_c - \overline{h}_k^*} \left(\frac{\tau}{2\Delta t}\right) \left(\frac{1+\gamma_k}{\Delta p_k}\right) \left(s_c - \overline{s}_{k-\frac{1}{2}}\right) \right.$$

$$\left. + \left(h_c - \overline{h}_{k-\frac{1}{2}} - L\ell_k\right) \left(\frac{1}{\Delta p_k} + \frac{1}{\Delta p_{k+1}}\right) \right\} . \tag{4.h.33}$$

where G is an arbitrary vertical difference in the adjusted moist static energy profile (cf. Hack *et al.*, 1993).

The first guess for the detrainment parameter, β, comes from a crude buoyancy argument where

$$\beta = \max \begin{cases} \beta_{\min} \\ \\ \min \begin{cases} \beta_{\max} \\ 1 + \frac{(h_c - \overline{h}_{k-1}^*)\Delta p_{k-1}}{(h_c - \overline{h}_k^*)\Delta p_k} , \end{cases} \end{cases} \tag{4.h.34}$$

and $\beta_{\min}$ is assumed to be 0.10 (i.e., 10% detrainment). Since β effectively determines the actual autoconversion from cloud water to rainwater, $\beta_{\max}$ is determined from a minimum autoconversion requirement which is mathematically written as

$$\beta_{\max} = \max \begin{cases} \beta_{\min} \\ \\ 1 - c_0 \left(\delta z - \delta z_{\min}\right), \end{cases} \tag{4.h.35}$$

where c_0 is a constant autoconversion coefficient assumed to be equal to 1.0×10^{-4} m^{-1}, δz is the depth of contiguous convective activity (i.e., layers in which condensation and rainout takes place) including and below layer k, and $\delta z_{\min}$ is a minimum depth for precipitating convection. The physical constraints on the adjustment process are then applied to determine the actual value of β appropriate to the stabilization of levels k and $k+1$.

In summary, the adjustment procedure is applied as follows. A first guess at β is determined from (4.h.34) and (4.h.35), and further refined using (4.h.25), (4.h.31), and (4.h.33). The convective mass flux, m_c, is then determined from (4.h.24), followed by application of budget equations (4.h.7) – (4.h.12) to complete the thermodynamic adjustment in layers $k-1$ through $k+1$. By repeated application of this procedure from the bottom of the model to the top, the thermodynamic structure is locally stabilized, and a vertical profile of the total cloud mass flux associated with shallow and mid-level convection, M_c (where $M_{c_{k+\frac{1}{2}}} = m_{c_{k+\frac{1}{2}}} + \beta\, m_{c_{k+\frac{3}{2}}}$) can be constructed. This mass flux profile can also be used to estimate the convective-scale transport of arbitrary passive scalars. The total convective precipitation rate is obtained by vertically integrating the convective-scale liquid water sink

$$P = \frac{1}{\rho_{\mathrm{H_2O}}} \sum_{k=1}^{K} R_k . \qquad (4.h.36)$$

The free parameters for the scheme consist of a minimum convective detrainment, $\beta_{\min}$, a characteristic adjustment time scale for the convection, τ, a cloud-water to rain-water autoconversion coefficient c_0, and a minimum depth for precipitating convection $\delta z_{\min}$.

i. Stable Condensation

If the lapse rate is stable, but the moisture is supersaturated at a point, *i.e.,* if

$$\frac{q_k}{q_k^*} > 1.0 \quad , \qquad (4.i.1)$$

the temperature and moisture are adjusted simultaneously so that the point is just saturated. The new specific humidity is given by

$$\hat{q}_k = \left[q_k^* + \frac{dq_k^*}{dT} \left(\hat{T}_k - T_k \right) \right] , \qquad (4.i.2)$$

where q_k^* is given by (4.g.18). The temperature change due to the release of latent heat during condensation is

$$\left(\hat{T}_k - T_k \right) = \frac{L}{c_p} \left(q_k - \hat{q}_k \right) . \qquad (4.i.3)$$

Substitution of (4.i.3) into (4.i.2) gives the adjusted specific humidity,

$$\hat{q}_k = q_k - \left(q_k - q_k^* \right) / \left(1 + \frac{L}{c_p} \frac{dq_k^*}{dT} \right) . \qquad (4.i.4)$$

Equations (4.i.4) and (4.i.3) are iterated twice. The corresponding stable precipitation rate at level k is given by

$$R_{s_k} = \left(\hat{q}_k - q_k \right) \Delta p_k / \left(2 \Delta t g \right) , \qquad (4.i.5)$$

in units of kg m^{-2} s^{-1}. In previous versions of the model, this stable condensate was assumed to immediately reach the ground allowing for the stable precipitation rate at the surface to be written as

$$P_s = \sum_{k=1}^{K} R_{s_k} / \rho_{H_20}. \tag{4.i.6}$$

The CCM3 employs a Sundqvist (1988) style evaporation of this stratiform (i.e., stable) precipitation as it makes its way to the surface. This scheme relates the rate at which raindrops evaporate to the local large-scale subsaturation, and the rate at which rainwater is made available to the subsaturated model layer

$$E_{s_k} = K_E\ (1 - RH_k)\ (\hat{R}_{s_k})^{1/2}. \tag{4.i.7}$$

where $\hat{R}_{s_k}$ denotes the total rainwater generation rate at level k (which can be larger than the locally diagnosed rainwater generation rate arising from 4.i.5, as will be shown below), the "rate" coefficient K_E takes the value 10^{-5}, and the variable E_{s_k} has units of s^{-1}. The evaporation rate E_{s_k} is used to determine a local change in q_k and T_k, associated with an evaporative reduction of $\hat{R}_{s_k}$. Conceptually, the evaporation process is invoked after a vertical profile of R_{s_k} has been evaluated using (4.i.5). An evaporation rate is then computed for the uppermost level of the model for which $R_{s_k} \neq 0$ using (4.i.7), where in this case $R_{s_k} \equiv \hat{R}_{s_k}$. This rate is used to evaluate an evaporative reduction in R_{s_k} which is then accumulated with the rainwater rate in the layer below,

$$\hat{R}_{s_{k+1}} = \hat{R}_{s_k} - \left(\frac{\Delta p_k}{g}\right)\ E_{s_k} + R_{s_{k+1}}. \tag{4.i.8}$$

A local increase in the specific humidity q_k and a local reduction of T_k are also calculated in accordance with the net evaporation

$$q_k = q_k + E_{s_k}\ 2\Delta t\ , \tag{4.i.9}$$

and

$$T_k = T_k - \left(\frac{L}{c_p}\right) E_{s_k}\ 2\Delta t\ . \tag{4.i.10}$$

The procedure, (4.i.7) $-$ (4.i.10), is then successively repeated for each model level in a downward direction where the stable precipitation rate is that portion of the condensed rainwater in the column to survive the evaporation process

$$P_s = \left(\hat{R}_{s_K} - \left(\frac{\Delta p_K}{g}\right)\ E_{s_K}\right) / \rho_{H_20}. \tag{4.i.11}$$

In global annually averaged terms, this evaporation procedure produces approximately a 20% reduction in the stratiform precipitation rate where the evaporated condensate acts to slightly moisten the middle and lower troposphere.

j. Dry Adiabatic Adjustment

If a layer is unstable with respect to the dry adiabatic lapse rate, dry adiabatic adjustment is performed. The layer is stable if

$$\frac{\partial T}{\partial p} < \frac{\kappa T}{p}. \tag{4.j.1}$$

In finite–difference form, this becomes

$$T_{k+1} - T_k < C1_{k+1}(T_{k+1} + T_k) + \delta, \tag{4.j.2}$$

where

$$C1_{k+1} = \frac{\kappa(p_{k+1} - p_k)}{2p_{k+1/2}}. \tag{4.j.3}$$

If there are any unstable layers in the top three model layers, the temperature is adjusted so that $(4.j.2)$ is satisfied everywhere in the column. The variable δ represents a convergence criterion. The adjustment is done so that sensible heat is conserved,

$$c_p(\hat{T}_k \Delta p_k + \hat{T}_{k+1}\Delta p_{k+1}) = c_p(T_k \Delta p_k + T_{k+1}\Delta p_{k+1}), \tag{4.j.4}$$

and so that the layer has neutral stability:

$$\hat{T}_{k+1} - \hat{T}_k = C1_{k+1}(\hat{T}_{k+1} + \hat{T}_k)\,. \tag{4.j.5}$$

As mentioned above, the hats denote the variables after adjustment. Thus, the adjusted temperatures are given by

$$\hat{T}_{k+1} = \frac{\Delta p_k}{\Delta p_{k+1} + \Delta p_k C2_{k+1}} T_k + \frac{\Delta p_{k+1}}{\Delta p_{k+1} + \Delta p_k C2_{k+1}} T_{k+1}, \tag{4.j.6}$$

and

$$\hat{T}_k = C2_{k+1}\hat{T}_{k+1}, \tag{4.j.7}$$

where

$$C2_{k+1} = \frac{1 - C1_{k+1}}{1 + C1_{k+1}}. \tag{4.j.8}$$

Whenever the two layers undergo dry adjustment, the moisture is assumed to be completely mixed by the process as well. Thus, the specific humidity is changed in the two layers in a conserving manner to be the average value of the original values,

$$\hat{q}_{k+1} = \hat{q}_k = (q_{k+1}\Delta p_{k+1} + q_k \Delta p_k)/(\Delta p_{k+1} + \Delta p_k). \tag{4.j.9}$$

The layers are adjusted iteratively. Initially, $\delta = 0.01$ in the stability check $(4.j.2)$. The column is passed through from $k = 1$ to a user-specifiable lower level (set to 3 in the standard model configuration) up to 15 times; each time unstable layers are adjusted until the entire column is stable. If convergence is not reached by the 15th pass, the convergence criterion is doubled, a message is printed, and the entire process is repeated. If δ exceeds 0.1 and the column is still not stable, the model stops.

As indicated above, the dry convective adjustment is only applied to the top three levels of the standard model. The vertical diffusion provides the stabilizing vertical mixing at other levels. Thus, in practice, momentum is mixed as well as moisture and potential temperature in the unstable case.

5. LAND SURFACE MODEL

The land surface model (LSM version 1) has been described in detail by Bonan (1996a). This model is a one-dimensional model of energy, momentum, water, and CO_2 exchange between the atmosphere and land, accounting for ecological differences among vegetation types, hydraulic and thermal differences among soil types, and allowing for multiple surface types including lakes and wetlands within a grid cell. Vegetation effects are included by allowing for twelve plant types that differ in leaf and stem areas, root profile, height, leaf dimension, optical properties, stomatal physiology, roughness length, displacement height, and biomass. The model allows for 28 different vegetated surfaces, each comprised of multiple plant types and bare ground so that, for example, a mixed broadleaf deciduous and needleleaf evergreen forest consists of patches of broadleaf deciduous, needleleaf evergreen trees, and bare ground. Lakes and wetland, if present, form additional patches. Soil effects are included by allowing thermal properties (heat capacity, thermal conductivity) and hydraulic properties (porosity, saturated hydraulic conductivity, saturated matric potential, slope of retention curve) to vary continuously depending of percent sand and percent clay. Soils also differ in color, which affects soil albedos. Consequently, each grid cell in the domain of interest is assigned a surface type, a fraction covered by lakes, a fraction covered by wetlands, a soil texture (percent sand, percent silt, percent clay), and a soil color.

Major features of the model are: prescribed time-varying leaf and stem areas; absorption, reflection, and transmittance of solar radiation, accounting for the different optical properties of vegetation, soil, water, snow, and ice; absorption and emission of longwave radiation allowing for emissivities less than one; sensible and latent heat fluxes, partitioning latent heat into canopy evaporation, soil evaporation, and transpiration; turbulent transfer above and within plant canopies; vegetation and ground temperatures that balance the surface energy budget (net radiation, sensible heat, latent heat, soil heat); stomatal physiology and CO_2 fluxes; interception, throughfall, and stemflow; snow hydrology; infiltration and runoff; temperatures for a six-layer soil column using a heat diffusion equation that accounts for phase change; soil water for the same six-layer soil column using a one-dimensional conservation equation that accounts for infiltration input, gravitational drainage at the bottom of the column, evapotranspiration losses, and vertical water flow based on head gradients; and temperatures for six-layer deep and shallow lakes accounting for eddy diffusion and convective mixing.

In coupling to the atmospheric model, the land surface model provides to the atmospheric model, at every time step, surface albedos, upward longwave radiation, sensible heat flux, latent heat flux, water vapor flux, and surface stresses. The atmospheric model provides to the land model, at every time step, incident solar and longwave radiation, convective and large-scale precipitation, and lowest model level temperature, wind, specific humidity, pressure, and height.

Bonan (1996a) provides a thorough description of the model. The model has been applied to study land-atmosphere CO_2 exchange (Bonan, 1995a), the effects of lakes and wetlands on climate (Bonan, 1995b), and climate sensitivity to subgrid infiltration and runoff (Bonan, 1996b).

6. SLAB OCEAN MODEL

The Slab Ocean Model (SOM) provides a simple ocean model for coupling with the CCM3. Using sea surface temperature and net surface heat flux available from a control run, the ocean heat flux (also called Q flux) can be defined and the CCM3 run with SOM, allowing for simple ocean/atmosphere interactions.

a. Open Ocean Component

The open ocean slab model is taken from Hansen et.al. (1983). The prognostic equation for ocean mixed layer temperature is:

$$\rho_o C_o h_o \frac{\partial T_o}{\partial t} = F + Q \tag{6.a.1}$$

where T_o is the ocean mixed layer temperature, ρ_o the density of ocean water, C_o the heat capacity of ocean water, h_o the ocean mixed layer depth (m), F = net atmosphere to ocean heat flux (Wm^{-2}), and Q = ocean mixed layer heat flux (Wm^{-2}) simulating deep water heat exchange and ocean transport. ρ_o and C_o are constants (see Appendix for values of constants).

The ocean mixed layer depth h_o is specified from Levitus (1982). Monthly mean mixed layer depths at levels where $\sigma_t(h) - \sigma_t(\text{surface}) = .125$ on a $1^\circ \times 1^\circ$ grid were averaged to the standard CCM (T42) grid (all data falling within a CCM grid box were equally weighted). The data were then horizontally smoothed 10 times using a 1-2-1 smoother and capped at 200m (to prevent excessively long adjustment times in coupled atmosphere ocean experiments). The resulting mixed layer depths in the tropics are generally shallow (10-30m) while at high latitudes in both hemispheres there are large seasonal variations (10m up to 200m maximum).

F is the net atmosphere-to-ocean heat flux in the absence of sea ice, defined as:

$$F = FS - FL - SH - LH \tag{6.a.2}$$

where FS = solar flux absorbed by ocean, FL = longwave cooling flux, SH = sensible heat flux from ocean to atmosphere, and LH = latent heat flux from ocean to atmosphere. The surface temperature used in evaluating these fluxes is T_o.

At CCM iteration n one has: T_o^n, h_o^n, F^n, Q^n, where h_o^n and Q^n are linearly interpolated in time between prescribed mid-monthly values, Q^n has in addition been globally adjusted as required and F^n is the net surface flux (6.a.2). The forecast value to T_o is then:

$$T_o^{n+1} = T_o^n + \frac{F^n + Q^n}{\rho_o C_o h_o^n} \Delta t \tag{6.a.3}$$

where Δt is the model time step.

b. Sea Ice Component

The sea ice component employs a simple formulation that parallels the ocean component. The mixed layer Q flux under sea ice is specified so that the sea ice component is constrained to approximately yield the control sea ice distribution in a coupled run.

A modified version of the thermodynamic ice model of CCM2 is employed. Sea ice is assumed to completely cover each CCM grid square, and is specified by six variables: four sea ice layer temperatures, $T_\ell(\ell = 1...4)(K)$, physical depth of snow overlying sea ice $h_s(m)$ and physical thickness of sea ice $h_i(m)$. Compaction of snow over time, as well as loss of snow through sublimation (latent heat loss) to the atmosphere, are ignored. Thermal conductivity of snow κ_s, the snow mass density ρ_s, and the snow mass heat capacity c_s, are assumed constant. The density ratio of snow to ice is about 1/3, which represents some compaction of original snowfall. Since snowfall in CCM3 is given in liquid water equivalent, a factor of 3 increase in depth is assumed. Snow melts at $T_{sm} = 0°C$. Liquid water melted from snow is assumed to percolate down to the underlying ocean with no effect on snow or ice.

Sea ice physical thickness h_i has an assumed minimum value of $h_i^{min} = 0.25m$. The thermal conductivity of sea ice κ_i, the heat of fusion of sea ice into liquid water L_i, the sea ice mass density ρ_i, and the sea ice mass heat capacity c_i, are all assumed constant. The effects of salt (i.e. brine pockets and variable salinity) are ignored. Sea ice is assumed to form at $T_{of} = -1.9°C$ (appropriate for an ocean salinity of $35°/_{oo}$) and to melt at $0°C$. Sea ice can melt at the surface, but water from such melting is assumed to percolate down with no effect on sea ice or snow albedo. The mixed layer temperature T_o below sea ice is assumed to remain at freezing (T_{of}).

Solar albedo for sea ice in the visible (0.2-0.7μm, solar top-of-atmosphere irradiance fraction 0.465), and near-ir (0.7-4.0μm, solar top-of-atmosphere irradiance fraction 0.535), are given by:

$$\alpha_{vis}(sea\ \ ice) = .50 + (.70 - .50)(h_i - .25)/.25$$

$$\alpha_{nir}(sea\ \ ice) = .26 + (.50 - .26)(h_i - .25)/.25 \tag{6.b.1a}$$

for $h_i \leq .50m$ (a relation based on the observations of Allison et al. (1993)), and:

$$\alpha_{vis}(sea\ \ ice) = .70$$

$$\alpha_{nir}(sea\ \ ice) = .50$$

for $h_i > .50m$ (as in CCM2). These spectral albedos imply broad band albedos of $\approx .37$ and $\approx .59$ respectively. Snow albedos are taken as those of aged snow:

$$\alpha_{vis}(snow) = .84$$

$$\alpha_{nir}(snow) = .60$$

These spectral snow albedos imply broad band snow albedo of $\approx .71$. When snow is present on sea ice, the total albedos are:

$$\alpha_{vis}(total) = f_s\alpha_{vis}(snow) + (1 - f_s)\alpha_{vis}(sea\ \ ice)$$

$$\alpha_{nir}(total) = f_s\alpha_{nir}(snow) + (1 - f_s)\alpha_{nir}(sea\ \ ice) \qquad (6.b.1b)$$

where the fractional horizontal coverage by snow f_s is given by:

$$f_s = \frac{h_s}{h_s + .10} \qquad (6.b.2)$$

similar to the expression used in Briegleb (1992). Thus, for a snow depth of 10cm, snow coverage is 50%.

The penetration of solar flux for snow free ice is $F_{solar}(z) = FS^nTr(z)$ where $Tr(z)$ is the flux transmission of solar radiation to level z (increasing downwards). Based on an expression used in Maykut (1982) we have: $Tr(z) = .805e^{(-k_{solar}z-0.1)}$ for $z > 0$ where k_{solar} is the bulk absorption coefficient of solar radiation through sea ice. If snow cover is present, then $Tr(z) = 0$ for $z > 0$. The total solar flux penetrating the ice is $FS^nTr(z)(1 - f_s)$ where f_s is the horizontal fraction of snow cover given above.

Sea ice is divided into four layers of uniform thickness ($\frac{h_i}{4}$ each). Each layer of sea ice is characterized by mass density, mass heat capacity, and thermal conductivity (ρ_i, C_i, κ_i) respectively. Snow is characterized by similar parameters (ρ_s, C_s, κ_s), and is mixed with the top layer of sea ice for numerical stability:

$$\begin{aligned}
z_1 &= h_s + \tfrac{h_i}{4} \\
\rho_1 &= \frac{\rho_s h_s + \rho_i \frac{h_i}{4}}{z_1} \\
C_1 &= \frac{\rho_s c_s h_s + \rho_i c_i \frac{h_i}{4}}{\rho_1 z_1} \\
\kappa_1 &= \frac{\kappa_s (h_s + \frac{h_i}{4})}{(h_s + \frac{h_i}{4}\frac{\kappa_s}{\kappa_i})}
\end{aligned} \qquad (6.b.3)$$

where $z_0 = 0$ is the top surface interface with the atmosphere, z_1 is the lower interface of the top layer, and $z_{l+1} = z_l + \frac{h_i}{4}$ gives the interface depths for layers 2,3,4. Ice thermal properties are used for layers 2,3,4. The conductivity of the combined snow/ice top layer assumes that snow overlies ice.

The thermodynamic equation for the sea ice temperature tendency is:

$$\rho C\frac{\partial T}{\partial t} = -\frac{\partial F}{\partial z} \qquad (6.b.4)$$

where the total heat flux F is positive downward. The total heat flux is given by:

$$F = F_{solar} + F_{thrml} + F_{top} + F_{bot} \qquad (6.b.5)$$

where F_{thrml} is the thermal conduction flux, given by $F_{thrml} = -\kappa \frac{\partial T}{\partial z}$, F_{top} is the top layer flux between the ice surface and atmosphere, and F_{bot} is the bottom layer flux between the lowest layer and the underlying ocean.

At CCM iteration n one has: $T_\ell^n(\ell = 1 ... 4), h_s^n, h_i^n$. The required input surface fluxes are FS^n, FL^n, SH^n, LH^n, S^n, which are the absorbed solar flux, the net upwards longwave flux, the sensible heat flux from surface to atmosphere, the latent heat flux from surface to atmosphere, and the snow precipitation rate respectively.

The top ice surface net flux is:

$$F_{top}^n = F_{solar}^n(0) - F_{solar}^n(z_1) - FL^n - SH^n - LH^n \tag{6.b.6}$$

where z_1 is the top layer thickness, and where the surface temperature T_s^n used in computing the sensible and latent heat fluxes is the top snow/ice layer temperature T_1^n.

A backward implicit top boundary condition is used:

$$F_{\rm top}^n + \frac{\partial F_{\rm top}^n}{\partial T_s}|_{T_s^n} \left(T_s^{n+1} - T_s^n\right) \tag{6.b.7}$$

where the top flux partial derivative $(\frac{\partial F_{\rm top}}{\partial T_s}|_{T_s^n})$ is evaluated by allowing only the sensible and latent heat flux surface temperature dependencies.

There are three general equations for heat transfer within sea ice: one for the *top* layer, one for the two intermediate layers, and one for the bottom layer. The general fully implicit finite difference equation for times $n+1$ and n is

$$\rho_\ell C_\ell \left(\frac{T_\ell^{n+1} - T_\ell^n}{\Delta t}\right) = -\left(\frac{\partial F}{\partial z}\right)_\ell^{n+1}, \tag{6.b.8}$$

where $\ell =$ layer index (1...4 from top to bottom), and where Δt is the model time step.

We approximate the flux and temperature derivatives as follows (and suppress the time index n for conciseness):

$$F_{thrml}(z_l) = -\left(\kappa \frac{\partial T}{\partial z}\right)_\ell = -\overline{\kappa}_{\ell+1,\ell} \frac{T_{\ell+1} - T_\ell}{\overline{z}_{\ell+1} - \overline{z}_\ell}, \tag{6.b.9}$$

where $\overline{z}_\ell$ is the mid-point depth of layer $\ell = \frac{1}{2}(z_\ell + z_{\ell-1})$, z_ℓ is the geometrical depth of layer interfaces where $\ell = 0$ is the surface/atmosphere top interface and z_4 is the bottom interface with the underlying ocean, and $\overline{\kappa}_{\ell+1,\ell} = \frac{1}{2}(\kappa_\ell + \kappa_{\ell+1})$.

The thermal flux derivative for the $\ell^{\rm th}$ layer is:

$$\left(-\frac{\partial F_{thrml}}{\partial z}\right)_\ell = \frac{\overline{\kappa}_{\ell+1,\ell}\left(\frac{T_{\ell+1} - T_\ell}{\overline{z}_{\ell+1} - \overline{z}_\ell}\right) - \overline{\kappa}_{\ell,\ell-1}\left(\frac{T_\ell - T_{\ell-1}}{\overline{z}_\ell - \overline{z}_{\ell-1}}\right)}{z_\ell - z_{\ell-1}}. \tag{6.b.10}$$

Defining $\Delta z_\ell = z_\ell - z_{\ell-1}$ (ℓ^{th} layer physical thickness)
$\Delta z_\ell^{+} = \overline{z}_{\ell+1} - \overline{z}_\ell$ (ℓ^{th} layer mid-point physical thickness with layer below)
$\Delta z_\ell^{-} = \overline{z}_\ell - \overline{z}_{\ell-1}$ (ℓ^{th} layer mid-point physical thickness with layer above)

gives:

$$\begin{aligned}\left(-\frac{\partial F_{thrml}}{\partial z}\right)_\ell &= \frac{1}{\Delta z_\ell}\left\{\frac{\overline{\kappa}_{\ell+1,\ell}}{\Delta z_\ell^{+}}\left(T_{\ell+1}-T_\ell\right) - \frac{\overline{\kappa}_{\ell,\ell-1}}{\Delta z_\ell^{-}}\left(T_\ell - T_{\ell-1}\right)\right\} \\ &= \frac{1}{\Delta z_\ell}\left\{\frac{\overline{\kappa}_{\ell+1,\ell}}{\Delta z_\ell^{+}}T_{\ell+1} - \left(\frac{\overline{\kappa}_{\ell,\ell-1}}{\Delta z_\ell^{-}} + \frac{\overline{\kappa}_{\ell+1,\ell}}{\Delta z_\ell^{+}}\right)T_\ell + \frac{\overline{\kappa}_{\ell,\ell-1}}{\Delta z_\ell^{-}}T_{\ell-1}\right\}\end{aligned}. \tag{6.b.11}$$

Defining

$$f_\ell^{+} = \frac{1}{\Delta z_\ell \Delta z_\ell^{+}} \qquad f_\ell^{-} = \frac{1}{\Delta z_\ell \Delta z_\ell^{-}} \tag{6.b.12}$$

gives:

$$\left(-\frac{\partial F_{thrml}}{\partial z}\right)_\ell = \left(\overline{\kappa}_{\ell+1,\ell}\; f_\ell^{+}\right)T_{\ell+1} - \left(\overline{\kappa}_{\ell,\ell-1}\; f_\ell^{-} + \overline{\kappa}_{\ell+1,\ell}\; f_\ell^{+}\right)T_\ell + \left(\overline{\kappa}_{\ell,\ell-1}\; f_\ell^{-}\right)T_{\ell-1}. \tag{6.b.13}$$

Consider the *top layer* equation first:

$$\begin{aligned}\rho_1 C_1\left(\frac{T_1^{n+1}-T_1^{n}}{\Delta t}\right) &= -\left(\frac{\partial F}{\partial z}\right)_1^{n+1} \\ &= \left(\frac{\left(\frac{\overline{\kappa}_{21}(T_2^{n+1}-T_1^{n+1})}{\overline{z}_2-\overline{z}_1}\right) + F_{\text{top}}^{n} + \left.\frac{\partial F_{\text{top}}^{n}}{\partial T_s}\right|_{T_s^n}\left(T_1^{n+1}-T_1^{n}\right)}{z_1 - z_0}\right)\end{aligned}. \tag{6.b.14}$$

Collecting the $n+1$ temperatures on the left-hand side and all known terms n on the right-hand side gives

$$\begin{aligned}&\left\{\frac{\rho_1 C_1}{\Delta t} + \overline{\kappa}_{21}\; f_1^{+} - \left(\frac{\left.\frac{\partial F_{\text{top}}^{n}}{\partial T_s}\right|_{T_s^n}}{z_1 - z_0}\right)\right\}T_1^{n+1} + \\ &\left\{-\overline{\kappa}_{21}\; f_1^{+}\right\}T_2^{n+1} = \frac{F_{\text{top}}^{n}}{z_1 - z_0} + \left\{\frac{\rho_1 C_1}{\Delta t} - \frac{\left.\frac{\partial F_{\text{top}}^{n}}{\partial T_s}\right|_{T_s^n}}{z_1 - z_0}\right\}T_1^{n}\end{aligned}. \tag{6.b.15}$$

Next, consider an *intermediate layer* ℓ ($\ell = 2$ and $\ell = 3$):

$$
\begin{aligned}
&\left(-\overline{\kappa}_{\ell,\ell-1}\, f_\ell^-\right) T_{\ell-1}^{n+1} + \left\{ \frac{\rho_\ell C_\ell}{\Delta t} + \left(\overline{\kappa}_{\ell,\ell-1}\, f_\ell^- + \overline{\kappa}_{\ell+1\ell}\, f_\ell^+\right) \right\} T_\ell^{n+1} \\
&- \left(\overline{\kappa}_{\ell+1\ell}\, f_\ell^+\right) T_{\ell+1}^{n+1} = \frac{\rho_\ell C_\ell}{\Delta t} T_\ell^n + \frac{F_{solar}^n(z_{l-1}) - F_{solar}^n(z_l)}{\Delta z_\ell}
\end{aligned} \quad . \tag{6.b.16}
$$

Finally, for *the bottom layer* we consider the bottom boundary condition to be *fixed* temperature equal to $T_{of} = -1.9°$C for the underlying ocean mixed layer. Thus, for the lower boundary temperature we specify $T_5^{n+1} = T_{of}$, and use:

$$
\overline{\kappa}_{5,4} = \kappa_4 \qquad \Delta z_4^+ = z_4 - \overline{z}_4 \qquad f_4^+ = \frac{1}{\Delta z_4 \Delta z_4^+}, \tag{6.b.17}
$$

which results in an equation of the form:

$$
\begin{aligned}
&\left(-\overline{\kappa}_{4,3}\, f_4^-\right) T_3^{n+1} + \left\{ \frac{\rho_4 C_4}{\Delta t} + \left(\overline{\kappa}_{4,3}\, f_4^-\right) \right\} T_4^{n+1} \\
&= \frac{\rho_4 C_4}{\Delta t} T_4^n - \frac{F_{bot}^n}{\Delta z_4} + \frac{F_{solar}^n(z_3) - F_{solar}^n(z_4)}{\Delta z_4}
\end{aligned} \quad . \tag{6.b.18}
$$

where

$$
F_{bot}^n = -\frac{\kappa_4}{\Delta z_4^+}(T_{of} - T_4^n)
$$

The equations for T_ℓ^{n+1} $\ell = 1...4$ form a coupled set of linear equations:

$$
\begin{pmatrix} A_{11} & A_{12} & 0 & 0 \\ A_{21} & A_{22} & A_{23} & 0 \\ 0 & A_{32} & A_{33} & A_{34} \\ 0 & 0 & A_{34} & A_{44} \end{pmatrix} \begin{pmatrix} T_1^{n+1} \\ T_2^{n+1} \\ T_3^{n+1} \\ T_4^{n+1} \end{pmatrix} = \begin{pmatrix} b_1 \\ b_2 \\ b_3 \\ b_4 \end{pmatrix}, \tag{6.b.19}
$$

where the definitions of the $A(4 \times 4)$ matrix and $b(4)$ vector, respectively, can be seen from the finite difference equations above.

The linear equations are solved for T_ℓ^{n+1} ($\ell = 1 \ldots 4$) using a tri-diagonal solver. Then, the layers are checked to see if any melting occurs. For the top layer, if $T_1^{n+1} > T_{sm}$, where $T_{sm} = 0°C$ is the melting temperature of snow and sea ice, then snow depth is modified by:

$$
h_s^{n+1} = h_s^n - \frac{\rho_1 C_1}{L_s}(T_1^{n+1} - T_{sm})(z_1 - z_0) \tag{6.b.20}
$$

where L_s is the volumetric heat of fusion of snow. If $T_1^{n+1} < -0.1°C$, then snow accumulation on the surface is computed as

$$
h_s^{n+1} = h_s^n + 3S^n \Delta t \tag{6.b.21}
$$

After adjustments by (6.b.20) and (6.b.21), if $h_s^{n+1} < 0$ there is sufficient heat to melt sea ice after complete melting of snow:

$$E_{melt} = \rho_1 C_1 (T_1^{n+1} - T_{sm})(z_1 - z_0) - L_s h_s^n \qquad (6.b.22)$$

and

$$h_{i1}^{n+1} = h_{i1}^n - \frac{E_{melt}}{L_i} \qquad (6.b.23)$$

where h_{i1}^{n+1} is the top layer adjusted sea ice thickness, h_{i1}^n is the original top layer sea ice thickness $(= \frac{h_i^n}{4})$, and L_i is the volumetric heat of fusion of sea ice. If $T_\ell^{n+1} > T_{sm}$ for l=2,3,4, then the lower sea ice layers are adjusted in thickness by:

$$h_{i\ell}^{n+1} = h_{i\ell}^n - \frac{\rho_\ell C_\ell}{L_i}(T_\ell^{n+1} - T_{sm})(z_l - z_{l-1}) \qquad (6.b.24)$$

The lowest layer of sea ice can also accrete or ablate ice through heat exchange with the underlying ocean mixed layer as follows:

$$h_{i4}^{n+1} = h_{i4}^n - \frac{F_{solar}^n(z_4) + F_{bot}^n + Q^n}{L_i}\Delta t \qquad (6.b.25)$$

where Q^n is the prescribed heat flux supplied to the ocean mixed layer below the sea ice. Note that the sign convention for Q^n is the same as is used in the open ocean case. For example, positive Q^n tends to warm the ocean mixed layer, and therefore to melt sea ice.

If there is sufficient snow on sea ice to suppress the ice/snow interface below sea-level, a fraction of snow is converted to sea ice to return the ice/snow interface to sea level. The conversion uses mass conservation and force balance. In detail, if $h_s^{n+1} > (\frac{\rho_o - \rho_i}{\rho_s})h_i^{n+1}$, (where h_i^{n+1} is the sum of $h_{il}^{n+1}, l = 1...4$), then $h_{i-adj}^{n+1} = (\rho_s h_s^{n+1} + \rho_i h_i^{n+1})/\rho_o$ is the new total ice thickness. Any increase in ice is added to the top ($l = 1$) layer, the total ice thickness is adjusted accordingly, and the snow depth is adjusted to $h_s^{n+1} = (\frac{\rho_o - \rho_i}{\rho_s})h_{i-adj}^{n+1}$.

There results from these adjustments to sea ice thickness the unevenly spaced thicknesses $h_{i\ell}^{n+1}$ at temperatures T_ℓ^{n+1}, where the temperatures of any melting layers have been set to T_{sm}. These layers and temperatures are restored to a uniform spacing in a manner that conserves total heat. For each uniformly spaced layer ℓ, the final temperature is:

$$T_\ell^{n+1'} = \frac{\int_l T_\ell^{n+1} dz}{(\frac{h_i'}{4})} \qquad (6.b.26)$$

where the new total thickness of sea ice is $h_i' = \sum_{\ell=1}^4 h_{i\ell}^{n+1}$, $T_\ell^{n+1'}$ is the final adjusted temperature, and the integral is over each final layer. The unevenly spaced layers are assumed isothermal. If any $T_\ell^{n+1'} > T_{sm}$, they are not reset to T_{sm}.

If the new sea ice thickness $h_i' < h_i^{min}$, then complete melting is assumed, with the heat of melting coming from the ocean mixed layer itself, so that the ocean temperature is adjusted by:

$$T_o^{n+1} = T_{of} - \frac{L_s h_s^{n+1} + L_i h_i'}{\rho_o C_o h_o^n} \qquad (6.b.27)$$

and where then afterwards $h_s^{n+1} = 0$ and $h_i^{n+1} = 0$.

It should be noted that it is not necessary to do an ocean mixed layer temperature calculation, since the assumption is being made that the ocean mixed layer temperature under sea ice is always at $T_{of} = -1.9°C$. The ocean mixed layer temperature forecast equation is:

$$T_o^{n+1} = T_{of} + \frac{F_{solar}^n(z_4) + F_{bot}^n + Q^n}{\rho_o C_o h_o}\Delta t \qquad (6.b.28)$$

Heat of fusion of sea ice is used to restore the changed ocean temperature to freezing:

$$\rho_o C_o h_o (T_o^{n+1} - T_{of}) = -L_i (h_{i4}^{n+1} - h_{i4}^n) \qquad (6.b.29)$$

Substituting this into the ocean mixed layer temperature equation (6.b.28) results in the heat balance equation for sea ice given above (6.b.25).

This completes the forecast of $T_\ell^n(\ell = 1...4), h_s^n, h_i^n$.

c. Specifications of Ocean Q Flux

For each month m (m=1...12) over open ocean points:

$$Q^m = \rho_o C_o h_o^m \left(\frac{T_{ccm}^{m+1} - T_{ccm}^{m-1}}{d^{m+1} - d^{m-1}}\right) - F^m \qquad (6.c.1)$$

where T_{ccm}^m is the CCM sea-surface temperature for month m used as the lower boundary condition for the control run, F^m is the control run ensemble mean net flux into the ocean for month m, h_o^m is the ocean mixed layer depth for month m, and the d^m are the mid-month calendar days for the m^{th} month. The use of mid-month days is consistent with CCM3, which linearly interpolates in time between mid-monthly values. (6.c.1) is simply (6.b.1) solved for Q and applied to monthly mean data.

According to (6.c.1), if the sea-surface temperature tendency is small, then $Q^m \approx -F^m$. During spring and fall seasons when the tendency is large, Q^m can differ quite a bit from -F^m, but typical values of Q^m can be quite large in any case, and are generally negative in local summer and positive in local winter. Thus Q^m corresponds to heat storage in local summer (negative values) and heat release in local winter (positive values). Typical values of Q^m are from 0 to 150Wm^{-2} in the winter hemisphere, and 0 to -150Wm^{-2} in the summer hemisphere, but winter gulf stream values can reach 300-400Wm^{-2}, and a few regions in the Denmark strait of rapid fall mixed layer deepening combined with rapid cooling have values of near -1000Wm^{-2}.

For the ocean Q flux in the presence of sea ice, one cannot so simply invert the heat balance equations to specify Q. If the details of the sea ice thermal diffusion are ignored however, the vertically integrated thermodynamic equation can be used:

$$-L_i \frac{\partial h_i}{\partial t} + \rho_o C_o h_o \frac{\partial T_o}{\partial t} = F + Q \tag{6.c.2}$$

In the presence of sea ice, the mixed layer temperature tendency term vanishes, since it is assumed that the mixed layer temperature is always at freezing (the term needs to be kept in evaluating Q when ice vanishes seasonally). Note that the term reflecting snow melt is ignored, as this term is much smaller than the ice term.

Most likely, in the CCM control run, h_i and h_s are prescribed. Thus, there is not information available to specify the rate of heat storage term $L_i \frac{\partial h_i}{\partial t}$. The approach taken here was to estimate $L_i \frac{\partial h_i}{\partial t}$ by constructing a synthetic sea ice thickness dataset (see below).

Observations of sea ice thickness on the required geographical scale are limited. Regional measurements of high quality have been made in the Arctic (Moritz, 1992), and the Antarctic (Budd, 1986; Wadhams et al. 1987; Jacka et al. 1987). Sea ice models, both dynamic/thermodynamic and pure thermodynamic, have computed sea ice thickness, but the usefulness of such data for GCM studies is not clear (in the Arctic, one has Hibler 1979; Walsh et al. 1985; Semtner 1987; in the Antarctic, Budd et al. 1991).

In light of this situation, a purely synthetic sea ice thickness dataset has been constructed. It makes use of various regional and point measurements, sea ice concentration, modeling studies on the seasonal variation of sea ice thickness, and approximate information about dynamic influence on Arctic sea ice thickness.

The general idea is that the geographical distribution of sea ice concentration gives the geographical distribution of sea ice thickness. Further, one can assume (crudely speaking) that the greater the sea ice concentration the greater the sea ice thickness. The actual physical relation between concentration and thickness is quite complicated, especially once near-complete coverage occurs, and is determined by both dynamic and thermodynamic processes (see for example, Hibler, 1979). Since a simple relation between c and h cannot reproduce the thickness distribution in many cases, a more realistic relation is derived below.

Arctic sea ice thickness

For the Arctic, the sea ice thickness is specified as a three step process: (1) relation between concentration c and thickness h is assumed, (2) the thickness h from (1) is modified for seasonal variation, and (3) finally, a regional dynamically forced variation is imposed on h from (2).

The assumed relation between c and h for the Arctic is:

$$c < c_{min} \qquad h = h_{min}$$

$$c_{min} < c < c_{max} \qquad h = h_{min} + \frac{(h_{max} - h_{min})(c - c_{min})}{(c_{max} - c_{min})}$$

$$c > c_{max} \qquad h = h_{max},$$

where $c_{min} = 0.1$, $c_{max} = 0.9$, $h_{min} = .25m$, $h_{max} = 3.0m$ for latitudes greater than 70°N and linearly decreasing with decreasing latitude to zero at 50°N.

The reason for the minimum sea ice thickness is taken both from observations, but especially from modeling constraints; very thin sea ice thickness might cause numerical difficulties in computing thermal fluxes and sea ice temperatures. The maximum sea ice thicknesses are taken from observations that multi-year sea ice in the Arctic ranges around 3m (Washington and Parkinson, 1986).

Arctic sea ice not only undergoes geographical expansion and contraction with varying seasonal forcing, but multi-year sea ice undergoes seasonal growth and ablation. A seasonal adjustment is applied to the h values determined from the above c(h) relation. From a calculation (Semtner, 1976) applicable to multi-year central Arctic pack ice, the following coefficients were applied for the appropriate month (January to December): .942, 1.000, 1.058, 1.124, 1.161, 1.175, 1.058, .931, .883, .880, .876, and .912. Thus, if the coefficients are labeled s(m) for the mth month (1...12), then the sea ice thickness is now s(m)h. Note that the annual average of the s(m) coefficients is 1.

The final step for the Arctic sea ice thickness involves accounting for regional variations due to ice flow. In general, high pressure exists in the Beaufort sea, giving rise to a clockwise circulation called the Beaufort gyre (see Battisti et al. 1992). This results in ice production in the Beaufort sea and its transport around the Beaufort gyre, across the pole, and either into the Lincoln sea region north of Greenland and the Canadian archipelago, or out through the Fram Strait between Greenland and Spitsbergen. The sea ice tends to be thicker north of Greenland, and thinner across the Arctic basin (see Bourke and Garrett, 1987). A simple planar modification is made across the Arctic basin and north of 75 degrees, to increase the thickness north of Greenland and decrease it across the basin. In general, this modification produces sea ice thickness in the region adjacent to Ellsmere Island around 4 to 4 1/2 m (depending on season), with thickness around 2 to 2 1/2 m over the pole on the other side of the Arctic basin.

Antarctic sea ice thickness

The situation in the Antarctic is rather different from the Arctic. The relatively open waters adjacent to the continent allow for much more extensive sea ice formation during winter. Ice shelves extend out from near-shore for many regions, with fast ice formations close to shore. However, the bulk of the Antarctic sea ice is first year ice (see Zwally et al. 1983) formed near shore and transported away from the coast. Except for near shore fast ice, pressure ridging is minimal. Most of the sea ice encountered in the Polarstern cruise (Wadhams et al 1987) was undeformed consolidated pancake sea ice, with a relatively narrow range of thicknesses between 40 and 60cm. These thicknesses are confirmed by the data of Jacka et al. (1987). Collected observations of Budd (1986) also suggest relatively thin (0.5 - 1.0m) Antarctic sea ice thickness.

With these observations in mind, the following expressions were used to specify Antarctic sea ice thickness:

$$c < c_{min} \qquad h = h_{min} + c$$

$$c_{min} < c \leq 1.0 \qquad h = h_{mid}$$

where $c_{min} = 0.25$, $h_{min} = .25m$, $h_{mid} = .50m$.

Thus the minimum sea ice thickness is .25m, and maximum is .50m.

d. Ocean Q Flux in Presence of Ice

Given the quantities h^m_{i-syn} (the final synthetic sea ice thickness as discussed above) and F^m (the net heat flux into the ocean from the CCM3 control run), Q^m for month m can be estimated by solving $(6.c.2)$ for Q:

$$Q^m = -F^m + \rho_o C_o h^m_o \left(\frac{T^{m+1}_{ccm} - T^{m-1}_{ccm}}{d^{m+1} - d^{m-1}}\right) - L_i\left(\frac{h^{m+1}_{i-syn} - h^{m-1}_{i-syn}}{d^{m+1} - d^{m-1}}\right) \qquad (6.d.1).$$

Q^m from $(6.d.1)$ is in general positive, indicating upwards heat flux from the deep ocean. Negative values occur (indicating heat flux into the deep ocean) around ice edges during accretion or ablation of ice in the central Arctic, or in regions of ice convergence due to strong ice transport.

In coupled runs, points can exist where there is ice for which the control CCM had open ocean, and conversely. The SOM model is not able to physically handle situations far from equilibrium. It was found that using an unmodified Q flux led to secular growth of sea ice. Any delays of ice melt led to the situation where Q flux under ice was prescribed as large and negative (during local summer), which resulted in excessive ice growth. In the control, such points were open ocean during the summer. To prevent such ice growth in a way which has some physical justification, Q flux under ice was constrained in a globally conserving manner to be larger than a hemispheric minimum value. In particular, at each time step a global mean (over ocean) of Q was calculated. Then, Q under all sea ice points was constrained by the appropriate minimum, found by empirical testing. A global mean (over ocean) was taken again, and the flux change required to conserve global balance was added to all ocean points. This results in very small (order $\pm 1 W m^{-2}$) Q variations to all ocean points. This is necessary to insure that the ocean in the global and annual mean is not a source or sink of heat beyond that inferred in the original calculation $(6.c.1 - 6.d.1)$ of Q flux.

7. INITIAL AND BOUNDARY DATA

a. Initial Data

In this section, we describe how the time integration is started from data consistent with the spectral truncation. The land surface model requires its own initial data, as described by Bonan in (1996a). The basic initial data for the model consist of values of u, v, T, q, Π, and Φ_s on the Gaussian grid at time $t = 0$. From these, U, V, T', and Π are computed on the grid using (3.a.11), and (3.a.49). The Fourier coefficients of these variables U^m, V^m, T'^m, Π^m, and Φ_s^m are determined via an FFT subroutine (3.b.23), and the spherical harmonic coefficients $T_n'^m, \Pi_n^m$, and $(\Phi_s)_n^m$ are determined by Gaussian quadrature (3.b.24). The relative vorticity ζ and divergence δ spherical harmonic coefficients are determined directly from the Fourier coefficients U^m and V^m using the relations,

$$\zeta = \frac{1}{a(1-\mu^2)} \frac{\partial V}{\partial \lambda} - \frac{1}{a} \frac{\partial U}{\partial \mu}, \tag{7.a.1}$$

$$\delta = \frac{1}{a(1-\mu^2)} \frac{\partial U}{\partial \lambda} + \frac{1}{a} \frac{\partial V}{\partial \mu}. \tag{7.a.2}$$

The relative vorticity and divergence coefficients are obtained by Gaussian quadrature directly, using (3.b.27) for the λ–derivative terms and (3.b.30) for the μ–derivatives.

Once the spectral coefficients of the prognostic variables are available, the grid–point values of ζ, δ, T', Π, and Φ_s may be calculated from (3.b.49), the gradient $\nabla\Pi$ from (3.b.52) and (3.b.53), and U and V from (3.b.58) and (3.b.59). The absolute vorticity η is determined from the relative vorticity ζ by adding the appropriate associated Legendre function for f (3.b.4). This process gives grid–point fields for all variables, including the surface geopotential, that are consistent with the spectral truncation even if the original grid–point data were not. These grid–point values are then convectively adjusted (including the mass and negative moisture corrections).

The first time step of the model is forward semi–implicit rather than centered semi–implicit, so only variables at $t = 0$ are needed. The model performs this forward step by setting the variables at time $t = -\Delta t$ equal to those at $t = 0$ and by temporarily dividing $2\Delta t$ by 2 for this time step only. This is done so that formally the code and the centered prognostic equations of section 4 also describe this first forward step and no additional code is needed for this special step. The model loops through as indicated sequentially in section 4. The time step $2\Delta t$ is set to its original value before beginning the second time step.

b. Boundary Data

In addition to the initial grid–point values described in the previous section, the model also requires lower boundary conditions. The required data are surface temperature (T_s) at each ocean point, the surface geopotential at each point, and a flag at each point to indicate whether the point is land, ocean, or sea ice. The land surface model requires its own boundary data, as described by Bonan (1996a). A surface temperature and three subsurface temperatures must also be provided at non-ocean points.

The sea–surface temperatures, and sea–ice locations are changed to reflect the seasonal changes. The sea–surface temperatures and sea–ice distributions are specified from the monthly mean analyses of Shea *et al.*, (1990). The mean monthly sea–surface temperature and sea ice distribution are assigned the mid–month date and updated every time step at each grid point using linear interpolation.

The radiation parameterization requires monthly mean ozone volume mixing ratios to be specified as a function of the latitude grid, 23 vertical pressure levels, and time. The ozone path lengths are evaluated from the mixing–ratio data. The path lengths are interpolated to the model η–layer interfaces for use in the radiation calculation. As with the sea–surface temperatures, the seasonal version assigns the monthly averages to the mid–month date and updates them every 12 hours via linear interpolation. The actual mixing ratios used in the standard version were derived by Chervin (1986) from analyses of Dütsch (1978).

The sub-grid scale standard deviation of surface orography was specified in the following manner. The variance is first evaluated from the global Navy $10'$ topographic height data over $2^\circ \times 2^\circ$ grid for T42 and lower resolutions, $1.67^\circ \times 1.67^\circ$ for T63, and $1.0^\circ \times 1.0^\circ$ for T106 resolution, and is assumed to be isotropic. Once computed on the appropriate grid, the standard deviations are binned to the CCM2 Gaussian grid (*i.e.,* all values whose latitude and longitude centers fall within each Gaussian grid box are averaged together). Finally, the standard deviation is smoothed twice with a 1–2–1 spatial filter. Values over ocean are set to zero.

8. STATISTICS CALCULATIONS

At each time step, selected global average statistics are computed for diagnostic purposes. Let $\int_3$ denote a global and vertical average and $\int_2$ a horizontal global average. For an arbitrary variable ψ, these are defined by

$$\int_3 \psi dV = \sum_{k=1}^{K} \sum_{j=1}^{J} \sum_{i=1}^{I} \psi_{ijk} w_j \left(\frac{\Delta p_k}{\pi} \right) \Big/ 2I, \tag{8.a.1}$$

and

$$\int_2 \psi dA = \sum_{j=1}^{J} \sum_{i=1}^{I} \psi_{ijk} w_j / 2I, \tag{8.a.2}$$

where recall that

$$\sum_{j=1}^{J} w_j = 2. \tag{8.a.3}$$

The quantities monitored are:

$$\text{global rms } (\zeta + f)(\mathrm{s}^{-1}) = \left[\int_3 (\zeta^n + f)^2 dV \right]^{1/2}, \tag{8.a.4}$$

$$\text{global rms } \delta(\mathrm{s}^{-1}) = \left[\int_3 (\delta^n)^2 dV \right]^{1/2}, \tag{8.a.5}$$

$$\text{global rms } T \text{ (K)} = \left[\int_3 (T^r + T'^n)^2 dV \right]^{1/2}, \tag{8.a.6}$$

$$\text{global average mass times } g \text{ (Pa)} = \int_2 \pi^n dA \, , \tag{8.a.7}$$

$$\text{global average mass of moisture } (\mathrm{kg\ m}^{-2}) = \int_3 \pi^n q^n / g dV. \tag{8.a.8}$$

APPENDIX A—Terms in Equations

The terms of $(3.b.18)$ are

$$\underline{V} = \underline{(\zeta + f)}^{n-1}, \tag{A1}$$

$$\underline{V}_{\lambda} = 2\Delta t\, \underline{n}_V^n, \tag{A2}$$

$$\underline{V}_{\mu} = 2\Delta t\, \underline{n}_U^n. \tag{A3}$$

The terms of $(3.b.19)$ are

$$\underline{D} = \underline{\delta}^{n-1}, \tag{A4}$$

$$\underline{D}_{\lambda} = 2\Delta t\, \underline{n}_U^n, \tag{A5}$$

$$\underline{D}_{\mu} = 2\Delta t\, \underline{n}_V^n, \tag{A6}$$

$$\begin{aligned} \underline{D}_{\nabla} &= 2\Delta t \left[\underline{E}^n + \Phi_s \underline{1} + R\mathbf{H}^r \underline{T}^{'n} \right] \\ &+ \Delta t \left[R\mathbf{H}^r \left((\underline{T}^{'})^{n-1} - 2(\underline{T}')^n \right) + R\left(\underline{b}^r + \underline{h}^r\right) \left(\Pi^{n-1} - 2\Pi^n\right) \right] . \end{aligned} \tag{A7}$$

The terms of $(3.b.20)$ are

$$\underline{T} = \left(\underline{T}'\right)^{n-1} + 2\Delta t\, \underline{\Gamma}^n \; - \Delta t \mathbf{D}^r \left[\underline{\delta}^{n-1} - 2\underline{\delta}^n\right] \;, \tag{A8}$$

$$\underline{T}_{\lambda} = 2\Delta t \underline{(UT')}^n, \tag{A9}$$

$$\underline{T}_{\mu} = 2\Delta t \underline{(VT')}^n. \tag{A10}$$

The nonlinear term in (3.b.21) is

$$\begin{aligned} \underline{PS} = \Pi^{n-1} - 2\Delta t \frac{1}{\pi^n} \left[(\underline{\delta}^n)^T \left(\underline{\Delta p}^n\right) + (\underline{\mathbf{V}}^n)^T \nabla\Pi^n \pi^n \underline{\Delta B} \right] \\ - \Delta t \left[\left(\underline{\Delta p}^r\right)^T \frac{1}{\pi^r} \right] \left[\underline{\delta}^{n-1} - 2\underline{\delta}^n\right] \;. \end{aligned} \tag{A11}$$

The spectral transformation of the terms in the vorticity equation $(3.b.33)$ is given by

$$\underline{VS}_n^m = \sum_{j=1}^{J} \left[\underline{V}^m(\mu_j) P_n^m(\mu_j) + im \underline{V}_{\lambda}^m(\mu_j) \frac{P_n^m(\mu_j)}{a(1-\mu_j^2)} + \underline{V}_{\mu}^m(\mu_j) \frac{H_n^m(\mu_j)}{a(1-\mu_j^2)} \right] w_j. \tag{A12}$$

The spectral transformation of the explicit terms in the divergence equation (3.b.34) is

$$\underline{DS}_n^m = \sum_{j=1}^{J} \Bigg\{ \left[\underline{D}^m(\mu_j) + \frac{n(n+1)}{a^2} \underline{D}_\nabla^m(\mu_j) \right] P_n^m(\mu_j) \tag{A13}$$

$$+ im\underline{D}_\lambda^m(\mu_j) \frac{P_n^m(\mu_j)}{a(1-\mu_j^2)} - \underline{D}_\mu^m(\mu_j) \frac{H_n^m(\mu_j)}{a(1-\mu_j^2)} \Bigg\} w_j.$$

The spectral transformation of the explicit term of the thermodynamic equation (3.b.35) is

$$\underline{TS}_n^m = \sum_{j=1}^{J} \left[\underline{T}^m(\mu_j) P_n^m(\mu_j) - im\underline{T}_\lambda^m(\mu_j) \frac{P_n^m(\mu_j)}{a(1-\mu_j^2)} + \underline{T}_\mu^m(\mu_j) \frac{H_n^m(\mu_j)}{a(1-\mu_j^2)} \right] w_j. \tag{A14}$$

The spectral transformation of the explicit terms of the surface pressure tendency equation (3.b.36) is

$$PS_n^m = \sum_{j=1}^{J} PS^m(\mu_j) P_n^m(\mu_j) w_j. \tag{A15}$$

APPENDIX B—Physical Constants

Following the American Meteorological Society convention, the model uses the International System of Units (SI) (see August 1974 *Bulletin of the American Meteorological Society,* **Vol. 55,** No. 8, pp. 926–930).

a	=	6.37122×10^6 m	Radius of earth
g	=	9.80616 m s^{-2}	Acceleration due to gravity
Ω	=	7.292×10^{-5} s^{-1}	Earth's angular velocity
σ_B	=	5.67×10^{-8} W m^{-2} K^{-4}	Stefan–Boltzmann constant
R	=	287.04 J kg^{-1} K^{-1}	Gas constant for dry air
c_p	=	1.00464×10^3J kg^{-1} K^{-1}	Specific heat capacity of dry air at constant pressure
κ	=	R/c_p	
ϵ	=	.622	Ratio of molecular weight of water vapor to that of dry air
L_v	=	2.5104×10^6 J kg^{-1}	Latent heat of vaporization
L_i	=	3.336×10^5 J kg^{-1}	Latent heat of fusion
R_v	=	4.61×10^2 J kg^{-1} K^{-1}	Gas constant for water vapor
ρ_{H_2O}	=	1.0×10^3 kg m^{-3}	Density of liquid water
c_{p_v}	=	1.81×10^3 J kg^{-1} K^{-1}	Specific heat capacity of water vapor at constant pressure
T_{melt}	=	273.16°K	Melting point of ice

The model code defines these constants to the stated accuracy. We do not mean to imply that these constants are known to this accuracy nor that the low–order digits are significant to the physical approximations employed.

APPENDIX C—Constants for Slab Ocean Themodynamic Sea Ice Model

Temperatures

$T_{of} = -1.9\ \ ^{\circ}C$

$T_{sm} = 0\ \ ^{\circ}C$

Ocean

$\rho_o = 1.026 \times 10^3\ \ kgm^{-3}$

$C_o = 3.93 \times 10^3\ \ Jkg^{-1}K^{-1}$

Ice

$\rho_i = 920\ \ kgm^{-3}$

$C_i = 2.07 \times 10^3\ \ Jkg^{-1}K^{-1}$

$L_i = 3.014 \times 10^8 Jm^{-3}$

$\kappa_i = 2.03\ \ Wm^{-1}K^{-1}$

$k_i = 1.5\ \ m^{-1}$

$h_i^{min} = 0.25\ \ m$

Snow

$\rho_s = 330\ \ kgm^{-3}$

$C_s = 2.09 \times 10^3\ \ Jkg^{-1}K^{-1}$

$L_s = 1.097 \times 10^8\ \ Jm^{-3}$

$\kappa_s = 0.31\ \ Wm^{-1}K^{-1}$

ACKNOWLEDGMENTS

The authors wish to acknowledge other members of the Climate Modeling Section, Tom Acker, Lawrence Buja, Brian Eaton, Jerry Olson, Jim Rosinski, John Truesdale, and Mariana Vertenstein for all their contributions to the development of the CCM3. We also wish to thank Paula Drager for her invaluable help in the preparation of this document.

a

REFERENCES

Acker, T. L., L. E. Buja, J. M. Rosinski, and J. E. Truesdale, 1996: *Users' Guide to NCAR CCM3.* NCAR Technical Note NCAR/TN–421+IA, Boulder, Colorado, 210 pp..

Allison, I., R.E. Brandt, and S.G. Warren, 1992: East Antarctic Sea Ice: Albedo, thickness distribution and snow cover. *J. Geophys. Res.*, submitted.

Anthes, R. A., 1986: Summary of workshop on the NCAR community climate/forecast models 14–26 July 1985, Boulder, Colorado. *Bull. Amer. Meteor. Soc.,* **67,** 94–198.

Asselin, R., 1972: Frequency filter for time integrations. *Mon. Wea. Rev.,* **100,** 487–490.

Baede, A. P. M., M. Jarraud, and U. Cubasch, 1979: *Adiabatic formulation and organization of ECMWF's model.* ECMWF Technical Report No. 15, 40 pp.

Bath, L. M., M. A. Dias, D. L. Williamson, G. S. Williamson, and R. J. Wolski, 1987: *Users' Guide to NCAR CCM1.* NCAR Technical Note NCAR/TN–286+IA, Boulder, Colorado, 173 pp..

——, J. Rosinski, and J. Olson, 1992: *User's Guide to CCM2.* NCAR Technical Note/TN–379+IA, Boulder, Colorado, 127 pp.

Battisti, D.S., D.L. Williamson, and R.E. Moritz 1992: Simulation of the Arctic climatology with the NCAR CCM2. Preprints, *Third Conf. Polar Meterology and Oceanography*, Portland, OR, Amer. Meteor. Soc., 130–136.

Beljaars, A. C. M., and A. A. M. Holtslag, 1991: Flux parameterization over land surfaces for atmospheric models. *J. Appl. Meteorol.*, **30**, 327–341.

Betts, A. K., 1975: Parametric interpretation of trade-wind cumulus budget studies. *J. Atmos. Sci.*, **32**, 1934–1945.

Bhumralkar, C.M., 1975: Numerical Experiments on the Computation of Ground Surface Temperature in an Atmospheric General Circulation Model. *J. Appl. Meteorol.*, 14, 1246–1258.

Bonan, G.B., 1993: Comparison of the land surface climatology of the NCAR CCM2 at R15 and T42 resolutions with implications for sub-grid land surface heterogeneity. submitted to *J. Geophys. Res.*.

——, 1995a: Land-atmosphere CO_2 exchange simulated by a land surface process model coupled to an atmospheric general circulation model. *J. Geophys. Res.*, **100**, 2817–2831.

——, 1995b: Sensitivity of a GCM simulation to inclusion of inland water surfaces. *J. Climate***8**,2691–2704.

——, 1996a: *A land surface model (LSM version 1.0) for ecological, hydrological, and atmospheric studies: technical description and user's guide.* NCAR Technical Note NCAR/TN-417+STR. National Center for Atmospheric Research, Boulder, Colorado. 150 pp.

——, 1996b: Sensitivity of a GCM simulation to subgrid infiltration and surface runoff. *Clim. Dynamics*, in press.

Bourke, R.H., and R.P. Garrett, 1987: Sea ice thickness distribution in the Arctic Ocean. *Cold Regions Science and Technology*, **13**, 259–280.

Bourke, W., B. McAvaney, K. Puri, and R. Thurling, 1977: Global modeling of atmospheric flow by spectral methods. *Methods in Computational Physics,* **17,** Academic Press, 267–324.

Briegleb, B. P., 1992: Delta-Eddington approximation for solar radiation in the NCAR Community Climate Model. *J. Geophys. Res.*, **97**, 7603–7612.

——, and V. Ramanathan, 1982: Spectral and diurnal variations in clear sky planetary albedo. *J. Climate Appl. Meteor.*, **21**, 1160–1171.

——, P. Minnis, V. Ramanathan, and E. Harrison, 1986: Comparison of regional clear–sky albedos inferred from satellite observations and model computations. *J. Climate Appl. Meteor.,* **25,** 214–226.

Bryan, F.O., B.G. Kauffman, W.G. Large and P.R. Gent, 1996: *The NCAR CSM Flux Coupler.* NCAR Technical Note NCAR/TN-424+STR, Boulder, Colorado, 58 pp.

Budd, W.F., 1986: The southern hemisphere circulation of atmosphere ocean and sea ice. In Second International Conference of Southern Hemisphere Meterology, Dec 1-5, 1986, Wellington, New Zealand. Proceedings. Boston, MA. American Meteorological Society. pp 101–106.

——, I. Simmonds, and X. Wu, 1991: The physical basis for a dynamic Antarctic sea ice model for use with an atmospheric GCM. *Ann. Glaciol.*, **15**, 196–203.

Budyko, M. I., 1956: *Heat Balance of the Earth's Surface.* Gidrometeozidat, Leningrad, 255 pp.

Cess, R.D., 1985: Nuclear war: Illustrative effects of atmospheric smoke and dust upon solar radiation. *Clim. Change*, **7**, 237-251.

Chervin, R. M., 1986: Interannual variability and seasonal climate predictability. *J. Atmos. Sci.,* **43,** 233–251.

Coakley, J.A., R.D. Cess and F.B. Yurevich, 1983: The effect of tropospheric aerosols on the Earth's radiation budget: A parameterization for climate models. *J. Atmos. Sci.*, **40**, 116-138.

Daley, R., C. Girard, J. Henderson, and I. Simmonds, 1976: Short–term forecasting with a multi–level spectral primitive equation model. Part I—Model formulation. *Atmosphere,* **14,** 98–116.

Deardorff, J. W., 1972: Parameterization of the planetary boundary layer for use in general circulation models. *Mon. Wea. Rev.,* **100,** 93–106.

Dickinson, R.E., A. Henderson-Sellers, and P.J. Kennedy, 1993: *Biosphere-Atmosphere Transfer Scheme (BATS) Version 1e as coupled to the NCAR Community Climate Model.* NCAR Technical Note, in preparation.

———, ———, ———, and M.S. Wilson, 1986: *Biosphere-Atmosphere Transfer Scheme (BATS) for the NCAR Community Climate Model.* NCAR Technical Note NCAR/TN-275+STR, Boulder, Colorado, 69 pp.

Dütsch, H. V., 1978: Vertical ozone distribution on a global scale. *Pure Appl. Geophys.,* **116,** 511–529.

Duynkerke, P.G., 1988: Application of the $E - \epsilon$ turbulence closure model to the neutral and stable atmospheric boundary layer. *J. Atmos. Sci.*, **45**, 865–880.

Dyer, A.J., 1974: A review of flux-profile relationships. *Boundary-Layer Meteor.*, **7**, 363–372.

Errico, R.M., 1986: *A Description of Software for Determination of Normal Modes of the NCAR Community Climate Model.* NCAR Tech. Note, NCAR/TN-217+STR, National Center for Atmospheric Research, Boulder, Colo., 86 pp.

———, and B.E. Eaton, 1987: *Nonlinear Normal Mode Initialization of the NCAR CCM.* NCAR Tech. Note, NCAR/TN-303+IA, National Center for Atmospheric Research, Boulder, Colo., 106 pp.

Forderhase, K., W.M. Washington, R.M. Chervin, V. Ramanathan, D.L. Williamson, and D.J. Knight, 1980: *Lower boundary conditions for the NCAR Global Circulation Model: Ocean surface temperatures, sea ice, snow cover, continental surface albedos and surface emissivity, subsurface continental temperatures and mountain heights*. NCAR Tech. Note, NCAR/TN–157+STR, National Center for Atmospheric Research, Boulder, Colo., 58 pp.

Geleyn, J. F., 1988: Interpolation of wind, temperature and humidity values from model levels to the height of measurement. *Tellus*, **40A**, 347–351.

Griffith, K. T., S. K. Cox, and R. G. Knollberg, 1980: Infrared radiative properties of tropical cirrus clouds inferred from aircraft measurements. *J. Atmos. Sci.,* **37,** 1077–1087.

Hack, J. J., 1994: Parameterization of moist convection in the National Center for Atmospheric Research Community Climate Model (CCM2). *J. Geophys. Res.*, **99**, 5551–5568.

____, L. M. Bath, G. W. Williamson and B. A. Boville, 1989: *Modifications and Enhancements to the NCAR Community Climate Model (CCM1).* NCAR Technical Note NCAR/TN-336+STR, NTIS PB89–215594/AS, 97 pp.

____, B. A. Boville, B.P. Briegleb, J. T. Kiehl, P. J. Rasch, D.L. Williamson, 1993: *Description of the NCAR Community Climate Model (CCM2).* NCAR Technical Note NCAR.TN-336+STR, 108pp.

____, ____, J. T. Kiehl, P. J. Rasch, and D. L. Williamson, 1994: Climate statistics from the NCAR Community Climate Model (CCM2). *J. Geophys. Res.*, **99**, 20785–20813.

Hansen, J., A. Lacis, D. Rind, G. Russell, P. Stone, I. Fung, R. Ruedy, and J. Lerner, 1983: Climate sensitivity: analysis of feedback mechanisms in climate processes and climate sensitivity. *Geophysical Monograph*, **29**, 130.

Hibler, W.D. III., 1979: A dynamic thermodynamic sea ice model. *J. Phys. Oceanogr.***9**, 815–846.

Hildebrand, F. B., 1956: *Introduction to Numerical Analysis.* McGraw-Hill, New York, 511 pp.

Holloway, J. L., Jr., and S. Manabe, 1971: Simulation of climate by a global general circulation model. 1. Hydrologic cycle and heat balance. *Mon. Wea. Rev.,* **99,** 335–370.

Holtslag, A.A.M., and A. C. M. Beljaars, 1989: Surface flux parameterization schemes: Developments and experiences at KNMI.Proceedings of the ECMWF workshop on Parameterization of fluxes over land surface, ECMWF Reading UK, 121–147 (Also available as KNMI Sci. Rep. 88–06, De Bilt NL, 27p.).

____, and B.A. Boville, 1993: Local versus nonlocal boundary–layer diffusion in a global climate model, *J. Climate*, **6**, 1825-1842.

____, and C.-H. Moeng, 1991: Eddy diffusivity and countergradient transport in the convective atmospheric boundary layer. *J. Atmos. Sci.*, **48**, 1690–1698.

____, E.I.F. de Bruijn, and H.-L. Pan, 1990: A high resolution air mass transformation model for short-range weather forecasting. *Mon. Wea. Rev.*, **118**, 1561-1575

Jacka, T.H., I. Allison, and R. Thwaites, 1987: Characteristics of the seasonal sea ice of east Antarctica and comparisons with satellite observations. *Ann. Glaciol.*, **9**, 85–91.

Joseph, J.H., W.J. Wiscombe and J.A. Weinman, 1976: The delta-Eddington approximation for radiative flux transfer. *J. Atmos. Sci.*, **33**, 2452-2459.

Kasahara, A., 1974: Various vertical coordinate systems used for numerical weather prediction. *Mon. Wea. Rev.*, **102**, 509–522.

Kiehl, J. T., 1991: Modelling and validation of clouds and radiation in the NCAR Community Climate Model. *Proc. ECMWF/WCRP Workshop on Clouds, Radiative Transfer and the Hydrological Cycle*, Reading, *12-15 November 1990*, 413-450.

____, and B.P. Briegleb, 1991: A new parameterization of the absorptance due to the 15 μm band system of carbon dioxide. *J. Geophys. Res.*, **96**, 9013-9019.

____, and V. Ramanathan, 1983: CO_2 radiative parameterization used in climate models: Comparison with narrow band models and with laboratory data. *J. Geophys. Res.*, **88**, 5191-5202.

____, and ____, 1990: Comparison of cloud forcing derived from the earth radiation budget experiment with that simulated by the NCAR Community Climate Model. *J. Geophys. Res.*, **95**, 11679–11698.

____, J. J. Hack, and B.P. Briegleb, 1994: The simulated earth radiation budget of the NCAR CCM2 and Comparisons with the Earth Radiation Budget Experiment (ERBE). *J. Geophys. Res.*, **99**, 20815–20827.

———, R. J. Wolski, B. P. Briegleb, and V. Ramanathan, 1987: *Documentation of Radiation and Cloud Routines in the NCAR Community Climate Model (CCM1).* NCAR Technical Note NCAR/TN–288+IA, Boulder, Colorado.

Levitus, S., 1982: Climatological Atlas of the World Ocean. NOAA Professional paper 13.

Machenhauer, B., 1979: The spectral method. *Numerical Methods Used in Atmospheric Models. GARP Publication Series 17,* 121–275, World Meteorological Organization, Geneva, Switzerland.

Manabe, S., 1969: Climate and ocean circulation. 1. The atmosphere circulation and the hydrology of the earth's surface. *Mon. Wea. Rev.,* **97,** 739–773.

———, J. Smagorinsky, and R. F. Strickler, 1965: Simulated climatology of a general circulation model with a hydrologic cycle. *Mon. Wea. Rev.,* **93,** 769–798.

Matthews, E., 1983: Global vegetation and land use: New high–resolution data bases for climate studies. *J. Clim. Appl. Meteor.,* **22,** 474–487.

Maykut, G.A., 1982: Large scale heat exchange and ice production in the central Arctic. *J. Geophys. Res.***87**, 7971–7984.

McAvaney, B. J., W. Bourke, and K. Puri, 1978: A global spectral model for simulation of the general circulation. *J. Atmos. Sci.,* **35,** 1557–1583.

McFarlane, N.A., 1987: The effect of orographically excited wave drag on the general circulation of the lower stratosphere and troposphere. *J. Atmos. Sci.*, **44**, 1775-1800.

Moeng, C.-H. and P. P. Sullivan, 1994: A comparison of shear- and bouyancy-driven planetary boundary layer flows. *J. Atmos. Sci.*, **51**, 999-1022.

Moritz, R.E., 1992: Seasonal and regional variability of sea ice thickness distribution. AMS Third Conference on Polar Meteorology and Oceanography, 29 September-2 October, 1992.

Moritz, R.E., and K. Runciman-Moore, 1992: Climate Modelling and sea ice thickness distribution. ACRSS Workshop, Monterey, CA, 13 July 1992.

Nieuwstadt, F.T.M., 1984: Some aspects of the turbulent stable boundary layer. *Boundary-Layer Meteor.*, **30**, 31–55.

Orszag, S. A., 1974: Fourier series on spheres. *Mon. Wea. Rev.,* **106,** 405–412.

Paltridge, G.W. and C.M.R. Platt, 1976: *Radiative Processes in Meteorology and Climatology*, Elsevier Scientific Publishing Co., Amsterdam, Oxford-New York, 318pp.

Pitcher, E. J., R. C. Malone, V. Ramanathan, M. L. Blackmon, K. Puri, and W. Bourke, 1983: January and July simulations with a spectral general circulation model. *J. Atmos. Sci.,* **40,** 580–604.

Ramanathan, V., and R. E. Dickinson, 1979: The role of stratospheric ozone in the zonal and seasonal radiative energy balance of the earth–troposphere system. *J. Atmos. Sci.,* **36,** 1084–1104.

_____, and P. Downey, 1986: A nonisothermal emissivity and absorptivity formulation for water vapor. *J. Geophys. Res.,* **91,** 8649–8666.

_____, R. J. Cicerone, H.B. Singh and J. T. Kiehl, 1985: Trace gas trends and their potential role in climate change. *J. Geophys. Res.*, **90**, 5547–5566.

_____, E. J. Pitcher, R. C. Malone, and M. L. Blackmon, 1983: The response of a spectral general circulation model to refinements in radiative processes. *J. Atmos. Sci.,* **40,** 605–630.

Rasch, P. J., and D. L. Williamson, 1990: On shape-preserving interpolation and semi-Lagrangian transport. *SIAM J. Sci. Stat. Comput.*, **11**, 656–687.

_____, B. A. Boville, and G. P. Brasseur, 1995: A Three-Dimensional General Circulation Model with Coupled Chemistry for the Middle Atmosphere, *J. Geophys. Res.*, **100**, 9041-9071.

Richtmeyer, R. D., and K. W. Morton, 1967: *Difference Methods for Initial–Value Problems,* Second Edition. Interscience Publishers, New York, 405 pp.

Robert, A. J., 1966: The integration of a low order spectral form of the primitive meteorological equations. *J. Meteor. Soc. Japan,* **44,** 237–245.

Roberts, R. E., J. E. A. Selby, and L. M. Biberman, 1976: Infrared continuum absorption by atmospheric water vapor in the 8-12 μm window. *Appl. Opt.*, **15**, 2085–2090.

Sato, R. K., L. M. Bath, D. L. Williamson, and G. S. Williamson, 1983: *User's Guide to NCAR CCMOB.* NCAR Technical Note NCAR/TN–211+IA, Boulder, Colorado, NTIS No. PB83 263988, 133 pp.

Sellers, W.D., 1965: *Physical Climatology*, The University of Chicago Press, Chicago and London, 272 pp.

Semtner, A.J. Jr., 1987: A numerical study of sea ice and ocean circulation in the Arctic, *J. Phys. Oceanogr.*, **17**, 1077–1099.

Semtner, A.J. Jr., 1976: A model for the thermodynamic growth of sea ice in numerical investigations of climate. *J. Phys. Oceanogr.*, **6**, 379-389.

Shea, D.J., K.E. Trenberth, R.W. Reynolds, 1990: *A Global Monthly Sea Surface Temperature Climatology.* NCAR Technical Note NCAR/TN–345+STR, Boulder, Colorado, 167 pp.

Simmons, A. J., and R. Strüfing, 1981: *An energy and angular-momentum conserving finite-difference scheme, hybrid coordinates and medium-range weather prediction.* ECMWF Technical Report No. 28, 68pp.

_____, B. J. Hoskins, and D. M. Burridge, 1978: Stability of the semi–implicit method of time integration. *Mon. Wea. Rev.,* **106,** 405–412.

Slingo, A., 1989: A GCM parameterization for the shortwave radiative properties of water clouds. *J. Atmos. Sci.*, **46**, 1419–1427.

Slingo, J.M., 1987: The development and verification of a cloud prediction scheme for the ECMWF model. *Quart. J. Roy. Meteor. Soc.*, **113**, 899-927.

Smagorinsky, J., 1963: General circulation experiments with the primitive equations, 1. The basic experiment. *Mon. Wea. Rev.,* **91,** 98–164.

_____, S. Manabe, and J. L. Holloway, Jr., 1965: Numerical results from a nine–level general circulation model of the atmosphere. *Mon. Wea. Rev.,* **93,** 927–768.

Smith, G.D., 1965: *Numerical Solution of Partial Differential Equations*, Oxford University Press, New York and London, 179 pp.

Sundqvist, H., 1988: Parameterization of condensation and associated clouds in models for weather prediction and general circulation simulation. In *Physically Based Modelling and Simulation of Climate and Climatic Change*, Schlesinger, Ed., Kluwer Academic, pp 433-461. Troen, I., and L. Mahrt, 1986: A simple model of the atmospheric boundary layer; Sensitivity to surface evaporation. *Boundary-Layer Meteor.*, **37**, 129-148.

Verstraete, M.M., 1988: *Defining the Thermal Properties of Continental Surfaces in GCMs*, unpublished manuscript (NCAR MS. 8076/88–1), pp. 12.

Vogelezang, D.H.P., and A.A.M. Holtslag, 1996: Evaluation and model impacts of alternative boundary-layer height formulations. *Boundary Layer Meteorology*, in press.

Wadhams, P., M.A. Lange, and S.F. Ackley, 1987: The ice thickness - distribution across the Atlantic sector of the Antarctic Ocean in mid-winter. *J. Geophys. Res.*, **92**, 14535–14552.

Walsh, J.E., W.D.Hibler III., and B. Ross, 1985: Numerical simulation of northern hemisphere sea ice variability, 1951-1980. *J. Geophys. Res.*, **90**, 4847–4865.

Washington, W. M., 1982: *Documentation for the Community Climate Model (CCM), Version ∅.* NCAR report, Boulder, Colorado, NTIS No. PB82 194192.

____, and C.L. Parkinson, 1986: *An Introduction to Three Dimensional Climate Modeling.* University Science Books, Mill Valley, CA. 422 pp.

____, and L. VerPlank, 1986: *A Description of Coupled General Circulation Models of the Atmosphere and Oceans Used for Carbon Dioxide Studies.* NCAR Technical Note, NCAR/TN–271+EDD, National Center for Atmospheric Research, Boulder, Colo., 29 pp.

Williamson, D.L., 1983: *Description of NCAR Community Climate Model (CCM0B).* NCAR Technical Note NCAR/TN–210+STR, Boulder, Colorado, NTIS No. PB83 231068, 88 pp.

____, and J.G. Olson, 1994: Climate simulations with a semi-Lagrangian version of the NCAR Community Climate Model. *Mon. Wea. Rev.*, **122**, 1594-1610.

____, and P.J. Rasch, 1989: Two-dimensional semi-Lagrangian transport with shape preserving interpolation. *Mon. Wea. Rev.*, **117**, 102-129.

____, and ____, 1994: Water vapor transport in the NCAR CCM2. *Tellus*, **46A**, 34-51.

____, and G. S. Williamson, 1984: *Circulation Statistics from January and July Simulations with the NCAR Community Climate Model (CCM0B).* NCAR Technical Note NCAR/TN–224+STR, Boulder, Colorado, NTIS No. PB85 165637/AS, 112 pp.

____, L.M. Bath, R.K. Sato, T.A. Mayer, and M.L. Kuhn, 1983: *Documentation of NCAR CCM0B Program Modules.* NCAR Technical Note NCAR/TN–212+IA, Boulder, Colorado, NTIS No. PB83 263996, 198 pp.

____, J.T. Kiehl, V. Ramanathan, R.E. Dickinson and J.J Hack, 1987: *Description of NCAR Community Climate Model (CCM1).* NCAR Tech. Note, NCAR/TN–285+STR, National Center for Atmospheric Research, Boulder, Colo., 112 pp.

Williamson, G.S., 1993: *CCM2 Datasets and Circulation Statistics.* NCAR Technical Note NCAR/TN-391+STR, Boulder, Colorado, 85 pp.

Williamson, G.S., and D.L. Williamson, 1987: *Circulation Statistics from Seasonal and Perpetual January and July Simulations with the NCAR Community Climate Model (CCM1):R15.* NCAR Tech. Note, NCAR/TN-302+STR, National Center for Atmospheric Research, Boulder, Colorado., 199 pp.

Xu, K.-M., S. K. Krueger, 1991: Evaluation of cloud models using a cumulus ensemble model. *Mon. Wea. Rev.*, **119**, 342-367.

Yanai, M., S. Esbensen and J.-H. Chu, 1973: Determination of bulk properties of tropical cloud clusters from large-scale heat and moisture budgets. *J. Atmos. Sci.*, **30**, 611–627.

Zwally, H.J., J.C. Comiso, C.L. Parkinson, W.J.Campbell, F.D.Carsey, and P. Gloersen, 1983: *Antarctic Sea Ice, 1973-1976 Satellite Passive Microwave Observations.* NASA Publication 206pp.